

JOURNAL *of the* MEXICAN



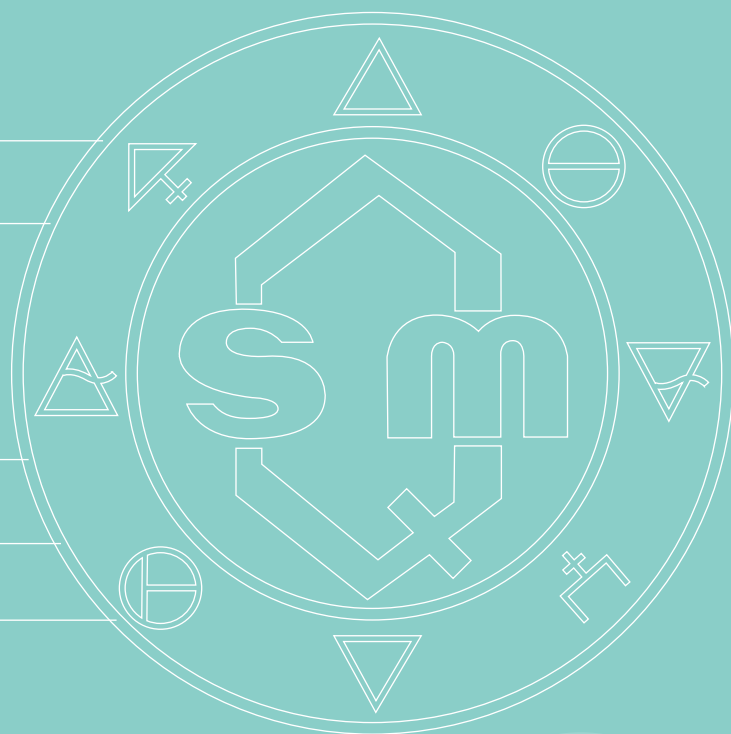
CHEMICAL SOCIETY

JULY - SEPTIEMBER - 2015

(J. Mex. Chem. Soc.)

REVISTA de la SOCIEDAD QUÍMICA de MÉXICO
former

(Rev. Soc. Quím. Méx.)



J. Mex. Chem. Soc. 2015, 59(3)

Pages 173-228
Quarterly publication
www.jmcs.org.mx
Mexico City



JOURNAL of the MEXICAN CHEMICAL SOCIETY

(*J. Mex. Chem. Soc.*)

The *Journal of the Mexican Chemical Society* (former *Revista de la Sociedad Química de México*) is a peer reviewed trimonthly journal which publishes original contributions and critical reviews in all areas of chemical sciences. It will publish fundamental work on physical, organic, inorganic, theoretical, analytical and biological chemistry, as well as aspects of supramolecular chemistry, electrochemistry, polymer chemistry, natural products chemistry, oil chemistry, organometallic chemistry, medical chemistry, biochemistry, chemical ecology, green chemistry, environmental chemistry, macromolecular chemistry, nuclear chemistry, chemistry of materials, and catalysis, among other topics. Full details on how to submit material to publication are given in Instructions for Authors on the printed journal, on the website: www.jmcs.org.mx or via e-mail to: editor.jmcs@gmail.com

EDITORIAL BOARD 2015

Ignacio González (Editor); igm@xanum.uam.mx

Associated Editors

Miguel Antonio Costas Basín; costasmi@unam.mx
Gabriel Eduardo Cuevas González Bravo; gecgb@unam.mx
Guillermo Delgado; delgado@unam.mx
Bernardo Frontana Uribe; bafrontu@unam.mx
Annia Galano Jiménez; annia.galano@gmail.com
Enrique Lima Muñoz; lima@iim.unam.mx
Víctor Loyola Vargas; vmloyola@cicy.mx
Antonio Martínez Richa; richa@ugto.mx
José L. Medina-Franco; jose.medina.franco@gmail.com
Mercedes Teresita Oropeza-Guzmán; oropeza1@yahoo.com
Gerko Oskam; oskam@mda.cinvestav.mx
Armando Salinas Rodríguez; armando.salinas@cinvestav.edu.mx
Joaquín Tamariz Mascarúa; jtamarizm@gmail.com
Hugo Torrens Miquel; torrens@unam.mx
Alberto Vela Amieva; avela@cinvestav.mx
Carlos Velazquez Martínez; velazque@ualberta.ca
Margarita Viniegra Ramírez; mvr@xanum.uam.mx
Katarzyna Wrobel; katarzyn@ugto.mx
Francisco Yuste López; yustef@unam.mx

EDITORIAL ASSISTANCE

Adriana Vázquez Aguirre; editor.jmcs@gmail.com

ADVISORY EDITORIAL BOARD 2015

Francisco Bolívar; bolivar@ibt.unam.mx
Guillermina Burillo; burillo@nucleares.unam.mx
Luis Echegoyen; luis@clemsun.edu
Nikolaus H. Fischer; nfischer@advantexmail.net
Eusebio Juaristi; juaristi@relaq.mx
Pedro Joseph Nathan; pjoseph@nathan.cinvestav.mx
Mario J. Molina; mmolina@mit.edu
Heinrich Nöth; H.Noeth@lrz.uni-muenchen.de
Keith Pannell; kpannell@utep.edu
Ratnasamy Somanathan; somanathan@sundown.sdsu.edu

FORMER EDITORS

José I. Bolívar Goyanes, Manuel Ulacia Esteve, Elvira Santos de Flores, Federico García Jiménez, Guillermo Delgado Lamas, Joaquín Tamariz Mascarúa, Juvencio Robles García

TECHNICAL EDITOR

Formas e Imágenes; formaseimagenes@gmail.com

ISSN 1870-249X

www.jmcs.org.mx

Journal of the Mexican Chemical Society (*J. Mex. Chem. Soc.*) Quarterly publication.
Editor-in-Chief: Ignacio González

Indexed Journal

Certificate of reserved rights granted by the Instituto Nacional del Derecho de Autor (INDAUTOR): 04-2005-052710530600-102
Certificate of lawful title and content: Under procedure
Postal registration of printed matter deposited by editors or agents granted by SEPOMEX: IM09-0312

Copyright © Sociedad Química de México, A.C. Total or partial reproduction is prohibited without written permission of the right holder.

Edited and distributed by Sociedad Química de México, A.C.

Barranca del Muerto 26, Col. Crédito Constructor, Del. Benito Juárez, C.P. 03940, Mexico City. Phone: +5255 56626837; +5255 56626823 Contact: soquimex@sqm.org.mx <http://www.sqm.org.mx>

Printed by Formas e Imágenes, Av. Universidad 1953, Edif. 2 local E, Col. Copilco el Bajo, México, D.F. Phone: +5255 55501784; +5255 56167117 Contact: formaseimagenes@gmail.com

Print run: 300 copies.

ISSN 1870-249X

JOURNAL *of the* MEXICAN



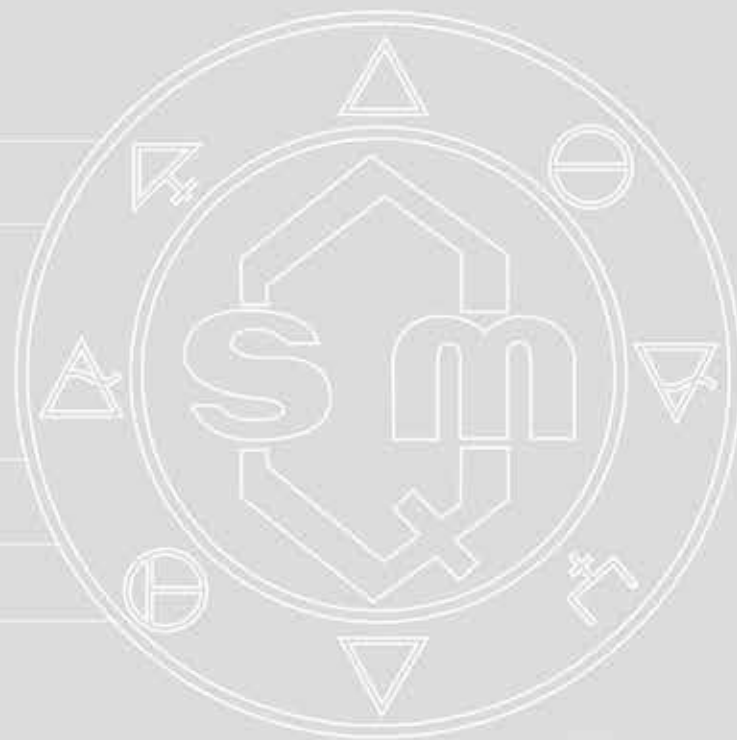
CHEMICAL SOCIETY

JULY - SEPTEMBER - 2015

(*J. Mex. Chem. Soc.*)

REVISTA de la SOCIEDAD QUÍMICA de MÉXICO
former

(*Rev. Soc. Quím. Méx.*)



J. Mex. Chem. Soc. 2015 59(3)

Pages 173-228
Quarterly publication
www.jmcs.org.mx
Mexico City

Sociedad Química de México, A.C.

Barranca del Muerto 26,
Col. Crédito Constructor,
Del. Benito Juárez, C.P. 03940, Mexico City.
Phone: +5255 56626837; +5255 56626823
Contact: soquimex@sqm.org.mx
www.sqm.org.mx

The *Sociedad Química de México* was founded in 1956 as a non-profit association to promote the development of the professionals and students of chemistry in education, research, services and industry, and for the diffusion of chemical knowledge. The *Sociedad Química de México* organizes annually the *Mexican Congress of Chemistry* and the *National Congress of Chemical Education*, both congresses include activities of current interest for professionals and students of the chemical sciences. It grants annually the "Andrés Manuel del Río" National Award of Chemistry in the Academic area (field of research and field of education) and in the Technological area (field of technological development). It also grants each year the *Rafael Illescas Frisbie Best Bachelor, Master and Doctoral Thesis in Chemical Sciences Awards* and the biennial Award of the *Sociedad Química de México in honor of the Doctor Mario J. Molina, directed to the professionals in Chemistry Sciences*.

The *Journal of the Mexican Chemical Society (J. Mex. Chem. Soc.)* is the official journal of the *Sociedad Química de México*, it was published as *Revista de la Sociedad Química de México (Rev. Soc. Quím. Mex.)* from 1957 to 2003, changing its name in 2004. The *Journal of the Mexican Chemical Society* is a quarterly publication, devoted to the advancement of the understanding of chemistry by means of publication of research papers and critical reviews; the instructions for authors appear in each issue. The *Sociedad Química de México* also publishes since 2007 articles of general interest in the *Boletín de la Sociedad Química de México*.

La *Sociedad Química de México* fue fundada en 1956 como una agrupación sin fines de lucro para promover el desarrollo de los profesionales y estudiantes de la química en las áreas educativa, investigación, servicios e industria, y para difundir el conocimiento de la química. La *Sociedad Química de México* organiza anualmente el *Congreso Mexicano de Química* y el *Congreso Nacional de Educación Química*, en los cuales se desarrollan diversas actividades de interés para los profesionales y estudiantes de las ciencias químicas. Asimismo, otorga anualmente el *Premio Nacional de Química "Andrés Manuel del Río"* en el área Académica (campos de docencia e investigación) y en el área Tecnológica (campo de Desarrollo Tecnológico). También otorga anualmente el *Premio a las Mejores Tesis de Licenciatura, Maestría y Doctorado en Ciencias Químicas, Rafael Illescas Frisbie*. De manera bienal otorga el *Premio de la Sociedad Química de México en Honor al Doctor Mario J. Molina, dirigido a los profesionistas de las Ciencias Químicas*.

El *Journal of the Mexican Chemical Society (J. Mex. Chem. Soc.)*, es la revista oficial de la *Sociedad Química de México*. Desde 1957 y hasta 2003 fue publicada como *Revista de la Sociedad Química de México (Rev. Soc. Quím. Mex.)*, cambiando su nombre en 2004. Es una publicación trimestral que tiene como objetivo coadyuvar al avance del entendimiento de la química; las instrucciones para los autores aparecen en cada fascículo. La *Sociedad Química de México* también publica desde 2007 artículos de interés general en el *Boletín de la Sociedad Química de México*.

Journal of the Mexican Chemical Society

(*J. Mex. Chem. Soc.*)

ISSN 1870-249X

former

Revista de la Sociedad Química de México

(*Rev. Soc. Quím. Mex.*)

ISSN 0583-7693

Journal of the Mexican Chemical Society (J. Mex. Chem. Soc.)

Quarterly publication.

Editor-in-Chief: Ignacio González

Indexed Journal

Certificate of reserved rights granted by the Instituto Nacional del Derecho de Autor (INDAUTOR): 04-2005-052710530600-102

Certificate of lawful title and content: Under procedure

Postal registration of printed matter deposited by editors or agents granted by SEPOMEX: IM09-0312

Copyright © Sociedad Química de México, A.C.

Total or partial reproduction is prohibited without written permission of the right holder.

Edited and distributed by Sociedad Química de México, A.C.

Barranca del Muerto 26, Col. Crédito Constructor,

Del. Benito Juárez, C.P. 03940, Mexico City.

Phone: +5255 56626837; +5255 56626823

Contact: soquimex@sqm.org.mx http: www.sqm.org.mx

Printed by Formas e Imágenes

Av. Universidad 1953, Edif. 2, local E, Col. Copilco el Bajo, México, D.F.

Phone: +5255 55501784; +5255 56167117

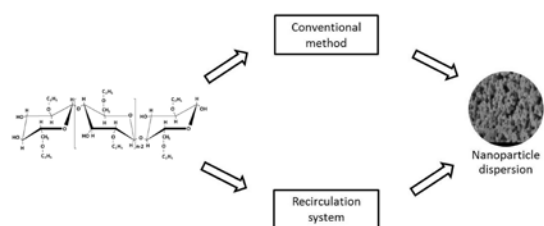
Contact: formaseimagenes@gmail.com



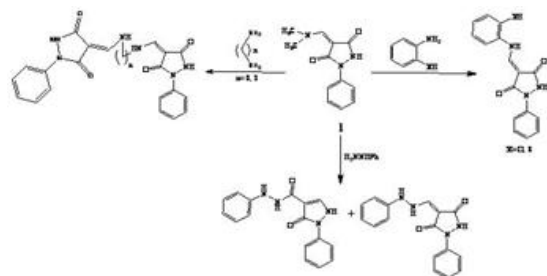
Table of Contents

Articles

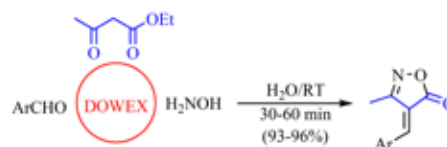
- 173-180 **Preparation of Ethyl Cellulose Nanoparticles by Solvent-Displacement Using the Conventional Method and a Recirculation System**
Zaida Urbán-Morlán, Susana E. Mendoza-Elvira, Ricardo S. Hernández-Cerón, Sergio Alcalá-Alcalá, Humberto Ramírez-Mendoza, Abel Ciprián-Carrasco, Elizabeth Piñón-Segundo and David Quintanar-Guerrero*



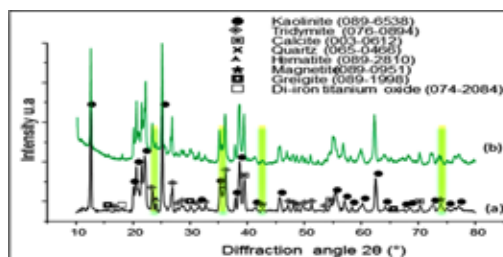
- 181-190 **Convenient Synthesis and Biological Activity of 4-Aminomethylene 1-phenylpyrazolidine-3,5-diones**
Eman A. Ahmed



- 191-197 **DOWEX(R)50WX4/H2O: A Green System for a One-pot and Three-Component Synthesis of isoxazol-5(4H)-one Derivatives**
*Davood Setamdideh**



- 198-202 **Kaolin Bleaching by Leaching Using Phosphoric Acid Solutions**
Román A. Hernández Hernández, Felipe Legorreta García, Leticia E. Hernández Cruz and Arnoldo Bedolla Jacuinde*



*The asterisk indicates the name of the author to whom inquiries about the paper should be addressed

Table of Contents

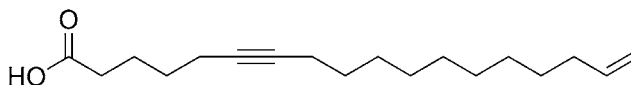
- 203-210 **Application of Wavelet and Genetic Algorithms for QSAR Study on 5-Lipoxygenase Inhibitors and Design New Compounds**

*Fatemeh Bagheban Shahri**, *Ali Niazi*
and *Ahmad Akrami*



- 211-214 **Cytotoxic Constituents from the Stem Bark of *Alvaradoa amorphoides***

Carlos Quintal-Novelo, *Luis W. Torres-Tapia*,
Rosa Moo-Puc and *Sergio R. Peraza-Sanchez**



- 215-228 **Removal of Direct Dyes with Alginic Acid**

Juan Antonio Lozano-Alvarez, *Virginia-Francisca Marañón-Ruiz**, *Juan Jáuregui-Rincón*,
Iliana Medina-Ramírez, *Claudio Frausto-Reyes*
and *Rogelio Salinas-Gutiérrez*



Preparation of Ethyl Cellulose Nanoparticles by Solvent-Displacement Using the Conventional Method and a Recirculation System

Zaida Urbán-Morlán,^{1*} Susana E. Mendoza-Elvira,² Ricardo S. Hernández-Cerón,¹ Sergio Alcalá-Alcalá,¹ Humberto Ramírez-Mendoza,³ Abel Ciprián-Carrasco,² Elizabeth Piñón-Segundo,⁴ David Quintanar-Guerrero¹

¹ Laboratorio de Investigación y Posgrado en Tecnología Farmacéutica, Facultad de Estudios Superiores Cuautitlán, Universidad Nacional Autónoma de México. Av. 1° de Mayo s/n, Santa María las Torres, Cuautitlán Izcalli, Estado de México, México, C.P. 54740.

² Laboratorio de Microbiología y Virología de las Enfermedades Respiratorias del Cerdo, Facultad de Estudios Superiores Cuautitlán, Universidad Nacional Autónoma de México. Av. 1° de Mayo s/n, Santa María las Torres, Cuautitlán Izcalli, Estado de México, México, C.P. 54740.

³ Facultad de Medicina Veterinaria y Zootecnia, Departamento de Microbiología e Inmunología, Universidad Nacional Autónoma de México, Ciudad Universitaria, C.P. 04510, México, D.F.

⁴ Laboratorio de Sistemas Farmacéuticos de Liberación Modificada, L13, Unidad de Investigación Multidisciplinaria, Facultad de Estudios Superiores Cuautitlán, Universidad Nacional Autónoma de México, Km 2.5 Carretera Cuautitlán-Teoloyucan, San Sebastián Xhala, Cuautitlán Izcalli, Estado de México, México, C.P. 54714.

* Corresponding author: Av. 1° de Mayo s/n, Santa María las Torres, Cuautitlán Izcalli, Estado de México, México, C.P. 54766. Tel +52 55 5623 20 65; Fax + 52 55 5623 20 43; mzum_1212@hotmail.com

Received April 1st, 2015; Accepted July 20th, 2015

Abstract. Ethyl cellulose polymeric nanoparticles (NPs) were prepared using the solvent-displacement technique with ethanol as the solvent. Optimization of the method included evaluating stirring rate and stabilizer type. NPs of 142.1 to 226.5 nm were obtained in a reproducible and efficient way (95% process efficiency) and with good stability (at room temperature). Moreover, a recirculation device was used in order to obtain concentrated NPs dispersions by a continuous process with potential scale-up. This method was challenged to encapsulate a hydrophilic antiviral model molecule (glycyrrhizinic acid) resulting in low entrapment efficiencies (approximately 1%).

The results indicate that NPs are obtained using this simple, economical process that offers the possibility to transport different agents for applications in food-processing, cosmetics production or pharmaceutical products.

Key words: ethyl cellulose, polymeric nanoparticles, solvent-displacement method, optimization, recirculation device.

Resumen. Se prepararon nanopartículas poliméricas (NPs) de etilcelulosa por la técnica de desplazamiento de disolvente usando etanol como disolvente. La optimización del método incluyó evaluación de la velocidad de agitación y el tipo de estabilizante. Se obtuvieron NPs de 142.1 a 226.5 nm en un modo reproducible y eficiente (95% eficiencia del proceso) y con buena estabilidad (a temperatura ambiente). Además, se utilizó un dispositivo de recirculación con la finalidad de obtener dispersiones concentradas por un proceso continuo con potencial de escalamiento. Este método se retó para encapsular una molécula hidrofílica antiviral modelo (ácido glicirricínico) teniendo como resultado bajas eficiencias de encapsulamiento (aproximadamente 1%).

Los resultados indican que se obtienen NPs de etilcelulosa por este método simple y económico que ofrece la posibilidad de transportar diferentes agentes para su aplicación en alimentos, cosméticos o productos farmacéuticos.

Palabras clave: Etilcelulosa, nanopartículas poliméricas, método de desplazamiento de solvente, optimización, dispositivo de recirculación.

Introduction

For at least the past three decades, polymeric NPs have been extensively studied as carriers for drugs and other substances. The preferred polymers are biodegradable, but some non-biodegradable ones also have important pharmaceutical characteristics that can be exploited according to the route of administration.

In 1987, Fessi et al., developed and patented a method to prepare nanoparticles called solvent-displacement, or nanoprecipitation [1]; which has the advantages of being simple, economical, reproducible and fast [2, 3]. Moreover, the amounts of

organic solvent and surface-active agents needed are small, and the resulting particles are also small, generally with narrow polydispersity indexes. Furthermore, mechanical or thermal stress is minimal because prolonged shearing/stirring times, sonication, or very high temperatures are not required, which lowers energy consumption. Additionally, solvents with low toxic potential could be used [1, 2, 3].

In general, this method requires two miscible phases: one solvent, the other non-solvent. The polymer and the drug selected are dissolved in the solvent phase (eg. acetone, ethanol, methylene chloride, etc.), while a stabilizer is incorporated into

the non-solvent phase (usually water). The injection of the organic phase into the aqueous phase under magnetic stirring leads to immediate formation of NPs due to displacement of the solvent. The pre-formed polymers most commonly used in this technique are biodegradable polyesters (eg. poly (ϵ -caprolactone), poly (D-lactic-*co*-D-glycolic) acid) and, to a lesser extent, cellulose derivatives; however, the first are quite expensive. Another option to form polymeric nanoparticles is ethyl cellulose, a water-insoluble, non-biodegradable, ether cellulose polymer that forms strong, tough films with good adhesion at low concentrations [4].

Different studies have proposed using ethyl cellulose as the matrix polymer to formulate drug NPs. Tachaprutinun *et al.* (2009) [5] attempted to encapsulate astaxanthin in ethyl cellulose NPs using the solvent-displacement method through a dialysis bag, but their results were disappointing, since using this modality to obtain NPs makes process scale-up very difficult. A high-loading encapsulation of six fragrances was achieved with a polymer blend (ethyl cellulose, hydroxypropyl methyl cellulose and polyvinyl alcohol) using the solvent-displacement method. Because all the fragrances were lipophilic, high encapsulation efficiency was achieved; but, once again, the dialysis bag system was an important drawback in terms of obtaining and encapsulating the oils efficiently [6]. Arias *et al.* [7] developed a magnetic colloid with iron in the core of the particle, surrounded by a polymeric shell of ethyl cellulose. The process followed to prepare the magnetic NPs was emulsion solvent evaporation. In addition, two methods of drug-loading were studied: addition and adsorption. High drug-loading was obtained with both methods, but the main drawback of this research was the use of benzene and decane in the process, since both substances are toxic (ICH Class 1).

On the other hand, Piñón-Segundo *et al.*, [8] proposed a novel recirculation system (Fig. 1b) to prepare poly(ϵ -caprolactone) NPs by solvent-displacement to obtain dispersions with high polymer concentrations. This device represents a considerable industrial advantage and offers the possibility of scaling-up the solvent-displacement method, while also helping to improve efficiency and avoid polymer-aggregation as the ethanol diffuses. The device they designed permits constant changes of water after first contact with the organic solution.

In the literature, there are two mechanisms to explain NP formation by this technique. The first one proposed that the interfacial turbulence at the interface of the solvent and non-solvent phases (which are governed by the Marangoni effect) [3] together with diffusion and flow phenomena, lead to polymer aggregation from stabilized emulsion droplets. As the two solvents are mutually miscible, when they are mixed a violent spreading occurs because of the difference in surface tension between them. Thus, a constant formation of eddies of solvent at the interface of the two phases causes the polymer present in the solvent droplets to aggregate and form NPs as a consequence of the lack of a non-solvent medium and continuous solvent diffusion which are rapidly stabilized by the surfactant [2, 9, 10, 11]. Fig. 1a shows the process of nanoparticle formation using this mechanism.

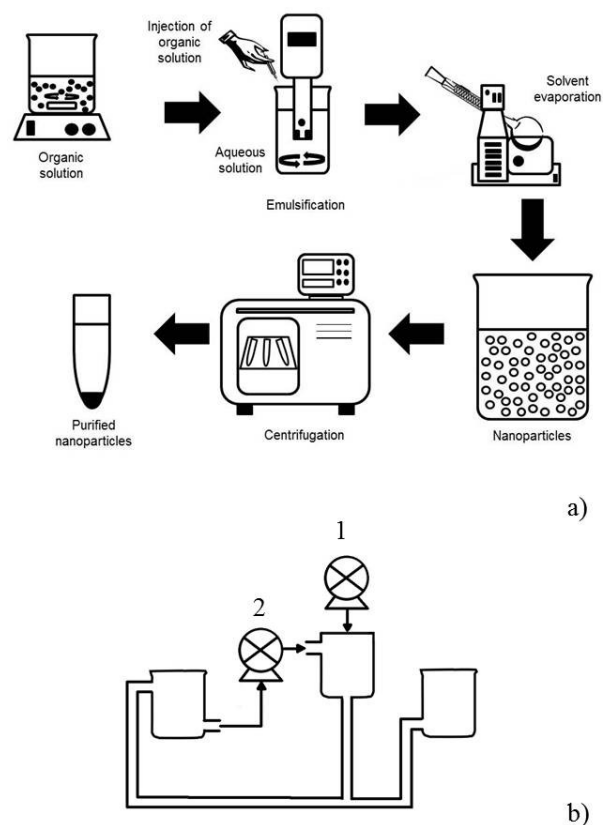


Fig. 1. Solvent-displacement method to obtain EthocelTM nanoparticles. a) conventional method; b) recirculation system; pump 1 controls the organic solution injection rate (ethyl cellulose/ethanol), and pump 2 controls the recirculation rate.

More recently, some publications have explained nanoparticle formation based on the “ouzo effect” [12, 13], which occurs in a ternary system composed of a hydrophobic solute, a solvent, and a non-solvent; specifically in the so-called ouzo region between the bimodal (miscibility-limit) and spinodal (stability-limit) curves, called the metastable region where the hydrophobic solute is introduced rapidly to cause super-saturation and then nuclei formation [3, 12, 14]. The small particles that form then increase in size due to Ostwald ripening (nucleation and growth process). In this process, polymer molecules act as the hydrophobic solute molecule with the ability to grow and generate polymeric NPs (Fig. 2). This is why droplet or particle size will depend on the polymer concentration in the organic solution [15]. On the right side of the ouzo boundary (spinodal curve) the polymer precipitates spontaneously because of solution instability and large fluctuations in the solute concentration, yielding macroscopic aggregates [16].

One issue with the solvent-displacement technique is that it is limited to water-miscible solvents and, as a result, only drugs that are soluble in these solvents can be incorporated. Then, one of the goals of this research was to encapsulate a model drug (specifically, glycyrrhizic acid, GA, in its non-ionized form) by the solvent-displacement method to challenge this system which is usually used to carry lipophilic

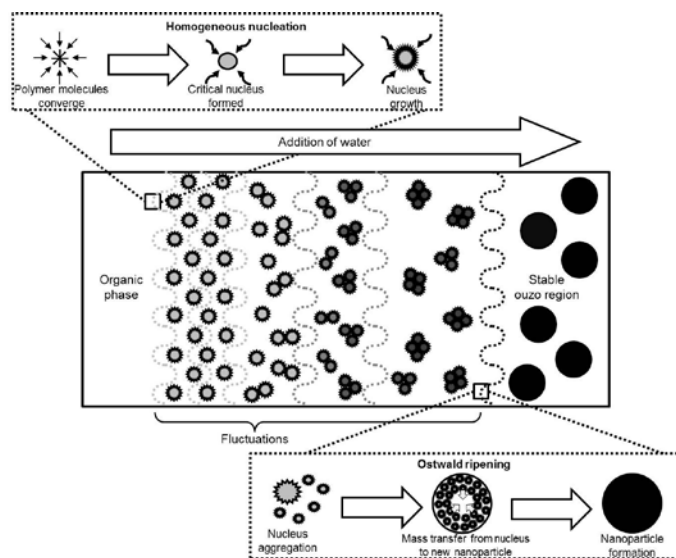


Fig. 2. Mechanism of the formation of nanoparticles explained by the ouzo effect.

drugs, but holds the appealing potential of being able to transport water-soluble drugs as well.

GA is a water-soluble molecule comprised of a hydrophilic part (two moieties of glucuronic acid) and a hydrophobic fragment (a moiety of glycyrrhetic acid, known as the aglycone moiety) (Fig. 3) [17]. The acid form is easily soluble in alcohol (methanol and ethanol). This drug is a weak acid with five hydroxyl and three carboxyl groups and presents three pK_a values ($pK_{a1}= 2.76$; $pK_{a2}= 2.81$; $pK_{a3}= 4.71$) [18]. FDA has included this molecule in the list of GRAS (*Generally Recognized as Safe*) substances [19]. For many years, glycyrrhizic acid (GA) has been used as anti-ulcer, anti-inflammatory, anti-tumor, and anti-viral [17, 20] and is the most important saponin of licorice root.

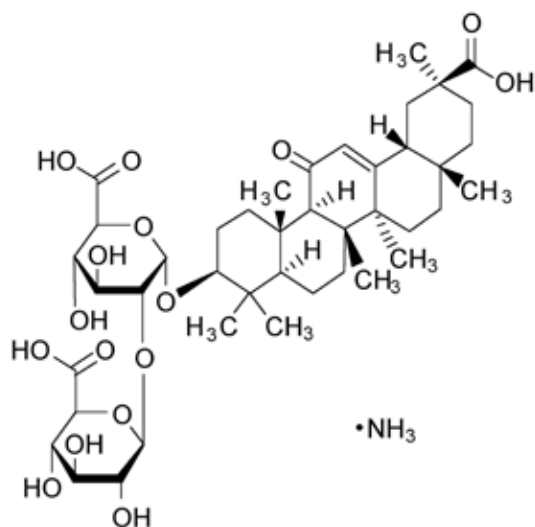


Fig. 3. Molecular structure of glycyrrhizic acid (GA) (ammonium salt).

Finally, the main objective of this research was to produce NPs of ethyl cellulose in a reproducible way by the solvent-displacement technique using ethanol as solvent, and following the conventional method or the recirculation system, in order to determine if NPs can be formed efficiently and with the desired characteristics of size and electrical charge. The selection of this particular polymer (Ethocel™ Std 4 Premium or Std 10 Premium FP) was based on its lower cost compared to biodegradable polymers; also, since it is pharmaceutical grade, it is already approved and accepted worldwide; furthermore they present different viscosity ranges (3-5.5 and 9-11 cP), which is a feature that impacts nanoparticle formation. The use of ethanol as a solvent has additional advantages, since it is classified as ICH Class 3, has low toxic potential, and is relatively inexpensive and polar, which could allow it to encapsulate polar drugs. Therefore, the solvent-displacement technique proposed in this research is a simple, economical, one-step process for producing nanoparticles. Stirring rates and stabilizer type were examined as the main preparative variables. The recirculation system was evaluated in order to obtain a continuous process which helps produce concentrated nanoparticle dispersions. No homogenization process was required in either case, which means additional savings in energy and other costs for industrial applications.

Results and Discussion

As expected, mean particle size was inversely- proportional to stirring rate: *i.e.*, the higher the stirring rate, the smaller the particle size (Fig. 4).

The reduction in particle size at higher velocities is explained due to the increase in kinetic energy on the solvent front that caused a higher degree of polymer/solvent-droplet dispersion in the aqueous phase, thus reducing local saturation of the polymer/solvent droplets in the aqueous phase [3].

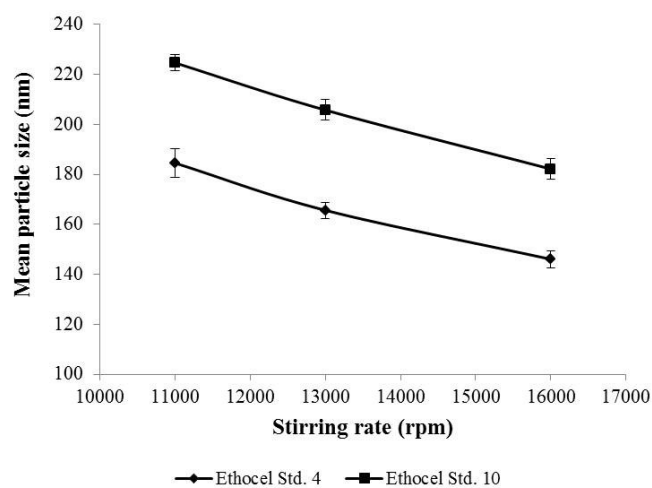


Fig. 4. Mean particle size of batches prepared with Ethocel™ Std 4-PVAL at 5% w/v and Ethocel™ Std 10-SLS at 2% w/v as a function of stirring rate. The bars show the standard deviation, $n= 3$.

Table 1. Mean particle size and Z-potential of Ethocel™ Std 4 and Ethocel™ Std 10 NPs obtained by the conventional method.

Batch	Ethocel™ Std 4, PVAL at 5%						Ethocel™ Std 10, LSS at 2%					
	11,000 rpm		13,000 rpm		16,000 rpm		11,000 rpm		13,000 rpm		16,000 rpm	
	MPS (nm) ^a	Z-Pot (mV) ^a	MPS (nm) ^a	Z-Pot (mV) ^a	MPS (nm) ^a	Z-Pot (mV) ^a	MPS (nm) ^a	Z-Pot (mV) ^a	MPS (nm) ^a	Z-Pot (mV) ^a	MPS (nm) ^a	Z-Pot (mV) ^a
1	191.3 ± 3.9 [0.254]	-27.9 ± 0.5	168.6 ± 1.2 [0.201]	-28.1 ± 1.7	149.4 ± 1.2 [0.214]	-29.7 ± 0.1	226.5 ± 2.4 [0.168]	-48.1 ± 1.0	209.8 ± 2.0 [0.235]	-48.0 ± 0.8	183.9 ± 1.7 [0.326]	-50.3 ± 0.7
2	180.1 ± 1.1 [0.183]	-27.9 ± 0.6	166.8 ± 1.1 [0.213]	-28.2 ± 1.4	142.7 ± 2.7 [0.230]	-29.8 ± 0.2	226.3 ± 1.8 [0.177]	-48.2 ± 1.0	202.1 ± 1.5 [0.208]	-48.2 ± 0.6	177.7 ± 4.2 [0.196]	-50.1 ± 0.7
3	182.3 ± 2.3 [0.249]	-28.0 ± 0.6	161.7 ± 0.5 [0.156]	-28.3 ± 2.0	146.1 ± 2.2 [0.175]	-29.6 ± 0.2	221.2 ± 2.4 [0.123]	-48.1 ± 1.3	205.5 ± 4.5 [0.312]	-48.0 ± 0.6	185.0 ± 1.2 [0.269]	-50.3 ± 0.5

^a Reported as mean ± standard deviation; n = 3. Numbers in square brackets indicate polydispersity indexes.

With all stirring rates it was possible to obtain sub-micron sizes for both polymers; ranging from 180-226 nm, 160-209 nm, and 142-185 nm at 11,000, 13,000 and 16,000 rpm, respectively (Table 1); with no need for a homogenization process (a factor of economic interest for industry as it allows energy and money savings).

According to the mechanism of particle formation due to interfacial turbulences (Marangoni effect), when globules of the emulsion are finer and homogeneous, the polymer-saturated region becomes thinner; thus facilitating the stabilization and formation of smaller particles [21, 22, 23]. The process of mixing the organic phase that contains the polymer with the aqueous phase is an important factor that strongly impacts final particle size.

We found that the particle size obtained with Ethocel™ Std 4 was smaller than that produced with Ethocel™ Std 10 at the same stirring rates. This can be explained by the higher viscosity achieved with the latter due to the higher number of ethoxy groups in its structure. The higher the viscosity of the polymer solution, the lower the solvent diffusion rate, but the NPs formed from the turbulent flow of the solvent will be larger [3, 23, 24]. Upon analyzing the “ouzo effect”, we found that Ostwald ripening has a great impact on final particle size, mainly due to the diffusive transport of dissolved matter through the dispersion medium. Thus, it is to be expected that in more viscous solutions the rate of diffusion will be lower and will exert an effect on final nanoparticle size. In addition to the viscosity of the phase containing the polymer, that of the solvent *per se* also plays an important role in nanoparticle formation.

According to some experiments, increasing the rate of diffusion allow obtaining smaller particles. In this regard, upon studying three different solvents (acetone, acetonitrile and tetrahydrofuran, with diffusion coefficients in water of 1.28, 1.26 and 1.08 x10⁻⁵ cm²/s, respectively) size decreased in the following order: acetone < acetonitrile < tetrahydrofuran [3] for PLGA nanoparticles. Ethanol has a diffusion coefficient of 1.21 x10⁻⁵ cm²/s but, as can be seen in Table 1, some batches would fix in size between the sizes reported using acetonitrile and tetrahydrofuran.

However, size depends not only on diffusion velocity but also, as explained above, on the polymer concentration and stirring rate [3, 22].

Two types of stabilizers were tested, PVAL and SLS with both it was possible to obtain stable dispersions with Ethocel™ Std 4 and PVAL at 5% w/v and Ethocel™ Std 10 and SLS at 2% w/v. Two different concentrations of SLS were tested (1.5% and 2% w/v), and the best results were obtained with 2% of SLS, because an absence of agglomerates or sediment characterized these systems during at least 15 days. Also, particle size was under 300 nm. According to the mechanism of NP-formation under the method used, when solvent-displacement occurs because of the miscibility between ethanol and water, droplets of the solvent are rapidly stabilized by the surfactant when they are torn from the solvent's interface. Hence, if there are more molecules of the stabilizing agent at the interface, the resulting particle will be protected against aggregation more efficiently than in a system that contains a lower concentration of stabilizer [22, 23]. SLS is an ionic surfactant, while PVAL is non-ionic. In this respect, SLS exerts its function through charge repulsion, while PVAL acts as a barrier among NPs [9, 23]. Quintanar-Guerrero *et al.* concluded that PVAL chains are strongly-attached to the NP surface, forming a stable layer which exerts sufficient steric stabilization-producing dispersions that remain stable for long periods of time [25].

For practical purposes, the following batches were prepared at a constant stirring rate of 11,000 rpm because while particles of nanometric size were obtained at all stirring rates tested (Table 1), the separation procedure proved to be quite difficult with smaller sizes as they required longer ultracentrifugation times.

Table 1 shows the results of mean particle size and Z-potential for Ethocel™ Std 4 and 10 NPs. Z-potential suggests that stable dispersions were obtained with SLS at 2% w/v (Table 1) because the value of those batches was above |30 mV| [26]. Colloids in aqueous media present an electrical charge, and their stability is determined by adding the contribution of van der Waals attractive forces and electrical double-layer

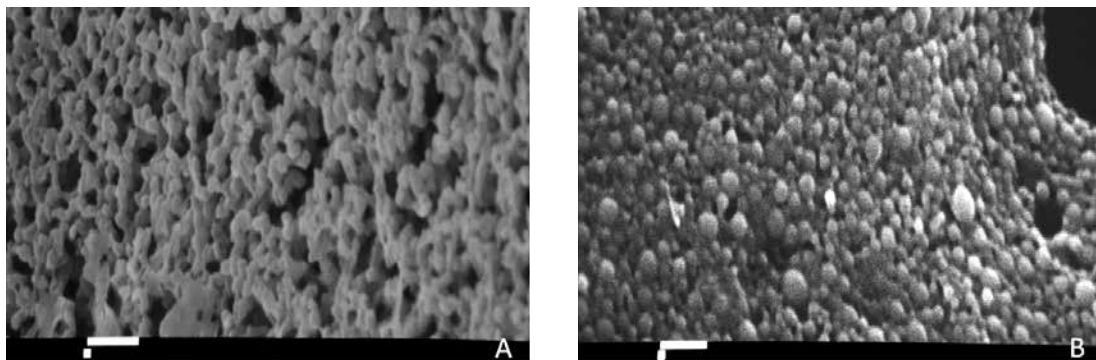


Fig. 5. Scanning electron micrographs of: A) Ethocel™ Std. 4 Premium-PVAL at 5%; and, B) Ethocel™ Std. 10 Premium FP-SLS at 2% (bar = 1 μm).

repulsive forces. SLS is an anionic surfactant that provides a negative charge to the nanoparticle which acts as an energy barrier that prevents two particles from adhering or coalescing. Batches with PVAL had a Z-potential close to 30 mV. Although these values are not as high as those obtained for NPs with SLS, they are also considered stable due to the steric repulsion that PVAL exerts, as discussed above.

With respect to mean particle size, findings indicate that the particles obtained were of the desired size, and these results were corroborated by micrographs (Fig. 5). Microscopic observation revealed spherical particles with a diameter of 250 nm that corresponded to the results obtained by dynamic light-scattering. SEM also revealed spherical particles with a solid matrix structure, but no crystal formation on the surface.

In the conventional solvent-displacement method and in the recirculation system the same polymer and stabilizer concentrations in the organic phase were used. However, in the recirculation system, consecutive injections of 20 mL of organic solution were carried out. The mean sizes obtained with the recirculation system were very similar to those produced by the conventional method (ranged from 160 to 197 nm for both polymers) (Table 2). It is important to point out that after the third injection of the organic phase into the aqueous phase of the device; particle size did not change; suggesting that polymer aggregation take place in the aqueous phase with no deposition on the dispersed particles. This behavior changed with the ensuing injections, when size increased quickly to micrometer range. The recirculation of the aqueous phase into the device allows to continually changing the water having first contact with the organic solution during the process of nanoparticles preparation. For that reason, recirculation system would

avoid a possible saturation of the medium as ethanol diffuses, so the process of nanoparticle formation would be more efficient than the traditional process, and a higher quantity of polymer would be transformed into nanoparticles. In this case, the maximum concentration of nanoparticles dispersion was 70 mg/ml.

The batches prepared with the drug increased their particle size (227 nm and 262 nm for Ethocel™ Std 4 and 10, respectively), while Z-potential remained virtually identical (no statistically-significant difference, $p < 0.05$). Additionally, the freeze dried NPs were easily re-suspended and showed a physical stability for 15 days at room temperature.

However, our attempt to encapsulate GA in its non-ionized form resulted in low entrapment efficiency for both polymers (approximately 1%), as determined by HPTLC, *High Performance Thin Layer Chromatography* (data not shown). The reason of modifying the ammonium salt of GA to obtain the molecular form (neutral and more hydrophobic) of it obeys to the fact that as having any electrical charge on the molecule, it will be more easily entrapped. The non-ionized form of GA was obtained under strong acidic conditions, this means at pH values lower than the first pKa of the molecule ($\text{pK}_{a1} = 2.76$) [18] and has the same therapeutic properties as the ionized form. In contrast, our group encapsulated 4.3% of the same drug using the double-emulsion technique [21]. This was due to the high solubility of the drug in the aqueous phase, which led to diffusion from the water-miscible organic phase into the external aqueous phase. We are currently attempting to enhance drug entrapment by decreasing water-drug solubility through the formation of an ion-pair between GA and a salt which acts as a counter-ion under certain conditions, such as pH and the

Table 2. Mean particle size and Z-potential of NPs prepared with Ethocel™ Std 4 and Ethocel™ Std 10 using the recirculation system.

Batch	Ethocel™ Std 4-PVAL at 5%		Ethocel™ Std 10- LSS at 2%	
	Mean particle size (nm) ^a	Z-potential (mV) ^a	Mean particle size (nm) ^a	Z-potential (mV) ^a
1	159.8 \pm 2.4; [0.892]	-27.3 \pm 0.649	197.2 \pm 1.5; [1.894]	-49.8 \pm 0.736
2	160.3 \pm 1.4; [0.267]	-29.6 \pm 0.910	195.2 \pm 0.7; [0.734]	-48.6 \pm 0.866
3	160.8 \pm 1.4; [1.329]	-26.8 \pm 0.472	194.9 \pm 1.8; [1.211]	-49.3 \pm 0.614

^a Reported as mean \pm standard deviation, n=3. Numbers in parentheses indicate polydispersity indexes.

concentration of this salt. Preliminary results show an improvement in this characteristic.

Ethyl cellulose NPs were obtained using the solvent-displacement method that has the advantages of being a fast and economical technique that employs an affordable, non-toxic polymer. The conventional method and the recirculation system produced NPs successfully; the latter with the attractive potential for scale-up. Additionally, the recirculation system permits the continue production of NPs, the polymer is completely transformed into NPs with no apparent aggregation, the efficiency would be higher than the conventional method, the polydispersity indexes are lower resulting in more homogeneous particle sizes and the scaling-up for an industrial application is simple. Results showed that it is possible to obtain submicronic dispersions up to a maximum concentration of 70 mg/ml without aggregation (size less than 200 nm and Z-potential indicating good stability) for both polymers used. To the best of our knowledge, this is the first time that ethyl cellulose (Ethocel™) NPs have been obtained with good physical and chemical characteristics by this method. The attempt to encapsulate a hydrophilic model drug resulted in very low encapsulation; however, these carriers may have a wide variety of applications in such areas as food-processing, cosmetics production and pharmaceuticals. Also, they can be used as a coating or film-forming material.

Experimental

Materials

Ethyl cellulose polymers (Ethocel™ Std 4 Premium and Ethocel™ Std 10 Premium FP) (Fig. 5) were donated by Colorcon de México, S. de R.L. de C.V. Poly(vinyl alcohol) (PVAL) with a molecular mass of 31,000 (Mowiol® 4-88) was obtained from Hoechst (Frankfurt-am-Main, Germany). Sodium lauryl sulphate (SLS) was provided by Hycel de México, S.A. de C.V. Glycyrrhizinic acid (GA, ammonium salt, ≥95% purity) was purchased from Sigma Aldrich (St. Louis, MO, USA). Absolut Ethanol ACS was supplied by Fermont (Monterrey, Mexico), and the distilled water was obtained from a Milli-Q station (Milli-Q, USA). All other reagents were at least of analytical grade and used without further purification.

Glycyrrhizinic acid in its non-ionized form

Briefly, 5 g of ammonium salt of GA was dissolved in distilled water under magnetic stirring. Then a solution 0.1 N of HCl was added until the formation of a rigid gel. After removing the water from this gel in an oven at 50°C, the precipitate was filtered and washed with distilled water. Finally, a fine white powder was obtained after drying in a desiccator.

Nanoparticle preparation using the solvent-displacement method

The conventional solvent-displacement method was used [5, 6] to prepare the NPs. An initial screening of the main parameters that commonly have impact on NP formation was performed as the first step of the study. The studied parameters were stirring rate, time of stirring, type and concentration of stabilizer. Briefly, 400 mg of Ethocel™ Std 4 Premium or Std 10 Premium FP were dissolved in 20 ml of ethanol. When the model drug was included, 30 mg were dissolved in this phase. This solution was placed in a syringe and injected into 40 ml of a solution of the stabilizing agent during 4 min under high-speed stirring at room temperature (Ultraturrax® T25, IKA; NC, USA). Finally, the residual ethanol was eliminated by vacuum distillation at 25°C and 70 mmHg. The remaining stabilizer and un-encapsulated drug was then removed by ultracentrifugation at 35,000 rpm for 40 min (Beckman® Optimal LE-80K, CA, USA).

To determine the effect of the process conditions, NPs were prepared at different stirring rates: 11,000, 13,000, and 16,000 rpm, with a high-speed stirrer (Ultraturrax®, T25, IKA, NC, USA) and two types of stabilizers, PVAL (5% w/v) and SLS (1.5% and 2% w/v). Batches were prepared in triplicate.

Freeze-drying of some batches was performed after removing the excess of stabilizer in a Freezone 6 (Labconco®, United Kingdom) lyophilizer for 24 h at -40 °C and 100 x 10⁻³ mbar.

Recirculation system

The device used was the one proposed by Piñón-Segundo [16] (Fig. 1b). The organic/aqueous phase ratio and polymer and stabilizer concentrations were kept at the same proportions used in

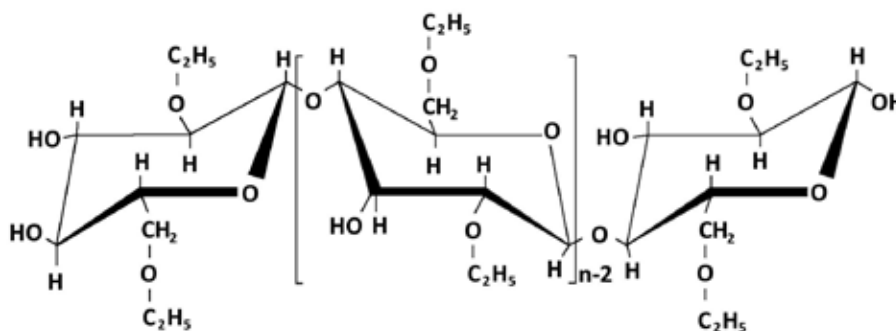


Fig. 6. Chemical structure of ethyl cellulose.

the conventional solvent-displacement method. The organic phase was injected directly into the circulating distilled water at a fixed injection rate of 25 ml/min, using a Masterflex® L/S 7518 pump (Cole Parmer, USA), and the recirculation rate at 55 ml/min was controlled by a Watson Marlow 502 S pump (New Brunswick Scientific, USA). Successive injections of the organic solution were poured into the circulating aqueous phase (three times in total), allowing solvent evaporation between each injection at room temperature. NPs and polymer aggregates were recovered in the recirculated water and were then separated using a mesh (US Std No. 100) and dried in a desiccator until reaching a constant weight.

Particle size analysis

Measurements were performed in triplicate using the dynamic light-scattering technique (Coulter N4, CA, USA) at a 90°C fixed-angle for 180 s at 25°C. The laser light wavelength (He/Ne, 10 mW) was set at 678 nm. A digital correlator was used to analyze the scattering intensity data under a unimodal analysis mode.

Z-potential

The electrophoretic mobility of the dispersions was measured and then transformed into Z-potential in triplicate by applying the Smoluchowski approximation (Malvern Instruments NS ZEN 3600, Worcestershire, UK) at 25°C in a capillary cell. Samples were analyzed in triplicate.

Scanning electron microscopy

After removing the excess stabilizer from the sample by two centrifugations (30,000 rpm/50 min) and following re-suspension in distilled water, a few drops of the dispersion were placed on a glass coverslip and dried at room temperature. The dried samples were then coated with gold (~20 nm thickness) using a Sputter Coater JFC-1100 (JEOL, Tokyo, Japan).

Entrapment efficiency

In order to evaluate the performance of the proposed method, a highly hydrophilic drug (glycyrrhizinic acid, solubility in water = 1 mg/ml) was encapsulated in NPs by both processes. Once lyophilized, 20 mg of the nanoparticles were added to 5 ml of ethanol and stirred for 24 h. This sample was filtered (Millipore® 0.22 µm), and the filtrate was assayed by HPTLC [11]. Fifty microliters of the filtrate were applied on a normal phase plate by means of an Automated TLC Sampler III (ATS3, CAMAG, Muttenz, Switzerland) and developed with a mobile phase composition of ethyl acetate-methanol-acetic acid-water (67:8:8:17). The chamber was equilibrated with 10 ml of mobile phase for 15 min prior to inserting the plate. Then the plate was scanned and measured in the absorbance-reflection mode at $\lambda = 254$ nm with a densitometer (CAMAG TLC-Scanner 3, Muttenz, Switzerland). Results were interpolated in a calibra-

tion curve which was linear within a range of 56-280 ng, $R^2 = 0.998$. Entrapment efficiency expressed as a percentage was calculated from the percent of drug-loading [amount of drug in NPs x 100/amount of NPs] x 100, divided by the percent of initial drug content in the formulation.

Acknowledgements

Zaida Urbán Morlán thanks CONACyT for funding through grant number 168259. The authors acknowledge the financial support from PAPIIT/UNAM IT201914-3, CONACyT CB221629, INFRA251940 y PIAPI001.

References

1. Minost, A.; Delaveau, J.; Bolzinger, M.A.; Fessi, H.; Elaissari, A. *Recent Pat. Drug Deliv. Formul.* **2012**, *6*, 250-258.
2. Kulterer, M. R.; Reischl, M.; Reichel, V. E.; Hribernik, S.; Wu, M.; Köstler, S.; Kargl, R.; Ribitsch, V. *Colloids Surf. A: Physicochem. Eng. Aspects.* **2011**, *375*, 23-29.
3. Beck-Broichsitter, M.; Rytting, E.; Lehardt, T.; Wang, X.; Kissel, T. *Eur. J. Pharm. Sci.* **2010**, *41*, 244-253.
4. www.dow.com/dowwolff/en/pdf/192-00818.pdf Ethocel, Ethylcellulose polymers, Technical Handbook, accessed in July, 2014.
5. Tachaprutinun, A.; Udomsup, T.; Luadthong, Ch.; Wanichwecharungruang, S. *Int. J. Pharm.* **2009**, *374*, 119-124.
6. Sansukcharearnpon, A.; Wanichwecharungruang, S.; Leepipatpaiboon, N.; Kercharoen, T.; Arayachukeat, S. *Int. J. Pharm.* **2010**, *391*, 267-273.
7. Arias, J.L.; López-Viota, M.; López-Viota, J.; Delgado, A.V. *Int. J. Pharm.* **2009**, *382*, 270-276.
8. Piñón-Segundo, E.; Ganem-Quintanar, A.; Garibay-Bermúdez, J.R.; Escobar-Chávez, J.J.; López-Cervantes, M.; Quintanar-Guerrero, D. *Pharm. Dev. Technology.* **2006**, *11*, 493-501.
9. Quintanar-Guerrero, D.; Allémann, E.; Fessi, H.; Doelker, E. *Drug Dev. Ind. Pharm.* **1998**, *24*, 1113-1128.
10. Mendoza-Muñoz, N.; Quintanar-Guerrero, D.; Alléman, E. *Recent Pat. Drug Deliv. Formul.* **2012**, *6*, 236-249.
11. Bilati, U.; Allémann, E.; Doelker, E. *Eur. J. Pharm. Sci.* **2005**, *24*, 67-75.
12. Vitale, S.A.; Katz, J.L. *Langmuir.* **2003**, *19*, 4105-4110.
13. Ganachaud, F.; Katz, J.L. *Chem. Phys. Chem.* **2005**, *6*, 209-216.
14. Mora-Huertas, C.E.; Fessi, H.; Elaissari, A. *Adv. Colloid Interface Sci.* **2011**, *163*, 90-122.
15. Aschenbrenner, E.; Bley, K.; Koynov, K.; Makowski, M.; Kappl, M.; Landfester, K.; Weiss, C.K. *Langmuir.* **2013**, *29*, 8845-8855.
16. Aubry, J.; Ganachaud, F.; Cohen Addad, J-P.; Cabane, B. *Langmuir.* **2009**, *25*, 1970-1979.
17. Obolentseva, G.V.; Litvinenko, V.I.; Ammosov, A.S.; Popova, T.P.; Sampiev, A.M. *Pharmaceut. Chem. J.* **1999**, *33*, 24-31.
18. Sun, Ch.; Xie, Y.; Tian, Q.; Liu, H. *Colloids Surf. A.* **2007**, *305*, 42-47.
19. Kvasnička, F.; Voldřich, M.; Vyhánek, J. *J. Chromatogr. A.* **2007**, *1169*, 239-242.
20. Fenwick, G.R. *Food Chem.* **1990**, *38*, 119-143.
21. Hernández Cerón, R. S. Bachelor's Thesis, Facultad de Estudios Superiores Cuautitlán, Universidad Nacional Autónoma de México, Estado de México; 2013.

22. Quintanar-Guerrero, D.; Tamayo-Esquivel, D.; Ganem-Quintanar, A.; Allémann, E.; Doelker, E. *Eur. J. Pharm. Sci.* **2005**, 26, 211-218.
23. Noriega-Peláez, E.K.; Mendoza-Muñoz, N.; Ganem-Quintanar, A.; Quintanar-Guerrero, D. *Drug Dev. Ind. Pharm.* **2011**, 37, 160-166.
24. Galindo-Rodríguez, S.; Allémann, E.; Fessi, H.; Doelker, E. *Pharm. Res.* **2004**, 21, 1428-1439.
25. Quintanar-Guerrero, D.; Ganem-Quintanar, A.; Allémann, E.; Fessi, H.; Doelker, E. *J Microencapsulation.* **1998**, 15, 107-119.
26. Heurtault, B.; Saulnier, P.; Pech, B.; Proust, J-E.; Benoit, J-P. *Biomaterials.* **2003**, 24, 4283-4300.

Convenient Synthesis and Biological Activity of 4-Aminomethylene 1-phenylpyrazolidine-3,5-diones

Eman A. Ahmed

Chemistry Department, Faculty of Science, Sohag University, 82524 Sohag, Egypt

E-mail:abdala_15@yahoo.com. Tel.: +20934601159

Received April 1st, 2015; Accepted August 3rd, 2015

Abstract. Reaction of (*Z*)-4-((dimethylamino)methylene)-1-phenylpyrazolidine-3,5-dione (**1**) with different nucleophiles is described. Treatment of enaminone **1** with phenylhydrazine led to 3-oxo-*N'*,2-diphenyl-2,3-dihydro-1*H*-pyrazole-4-carbohydrazide **7**. New enaminone derivatives **2–6** and **12–14** were conveniently obtained in high yields via nucleophilic substitution of the dimethylamino group in enaminone **1** when reacted with *o*-aminophenol, *o*-aminothiophenol, ethanolamine, cysteamine hydrochloride, piperidine, morpholine, 2-aminopyridine and glycine. Reaction of enaminone **1** with diaza-nucleophiles, such as hydrazine hydrate, ethylenediamine and *o*-phenylenediamine, afforded the corresponding *bis*-enaminones **9–11**. Anti-inflammatory and antimicrobial activities of some new products were evaluated. Compounds **1**, **2**, **4**, **7**, **12a**, and **12b** showed high anti-inflammatory activity compared with indomethacin as the reference, while the highest antimicrobial effect was observed in the case of compound **3**.

Key words: pyrazolidine-3,5-diones, enaminones, nucleophiles, anti-inflammatory activity, antimicrobial activity.

Resumen. Se describe la reacción de (*Z*)-1-fenil-4-((dimetilamino)metileno)pirazolidin-3,5-diona (**1**) con diferentes nucleófilos. El tratamiento de la enaminona **1** con fenilhidrazina condujo a la *N'*,2-difenil-2,3-dihidro-3-oxo-1*H*-pirazol-4-carbohidrazida **7**. Los nuevos derivados enaminónicos **2–6** y **12–14** se obtuvieron convenientemente en elevados rendimientos vía sustitución nucleofílica del grupo dimetilamino en la enaminona **1** cuando reaccionó con *o*-aminofenol, *o*-aminotiofenol, etanolamina, clorhidrato de cisteamina, piperidina, morfolina, 2-aminopiridina y glicina. La reacción de **1** con diaza-nucleófilos, tales como hidrato de hidrazina, etilendiamina y *o*-fenildiamina, proporcionó las *bis*-enaminonas correspondientes **9–11**. Se evaluó la actividad anti-inflamatoria y antimicrobiana de algunos productos nuevos. Los compuestos **1**, **2**, **4**, **7**, **12a** y **12b** mostraron elevada actividad anti-inflamatoria en comparación a la indometacina como compuesto de referencia, mientras que se observó la más elevada actividad antimicrobiana para el compuesto **3**.

Palabras clave: pirazolidin-3,5-dionas, enaminonas, nucleófilos, actividad anti-inflamatoria, actividad antimicrobiana.

Introduction

The synthesis of β -enaminones has received much attention in recent times due to their chemical and biological activities. It is known that, β -enaminone derivatives are push-pull electron systems which represent versatile synthetic intermediates. These category of compounds showed significant reactivity in a wide variety of nucleophilic and electrophilic substitution [1,2], photochemical [3], reduction and oxidation reactions [4,5]. Also, they have been employed as synthons of a wide variety of biologically and medicinally active compounds [6,7], as well as of pharmaceutical compounds having anti-epileptic [8], antibacterial [9,10], anti-inflammatory [10], anti-convulsant [11], antitumor [12] and anti-parasitic activities [13]. In addition to this wide spectrum of activity, enaminones revealed good stability under simulated physiological pH conditions and low toxicity [14]. On the other hand, *N*-arylpyrazoles possess significant medicinal applications, such as antitumor [15], antiviral [16] and anti-inflammatory agents [17]. Building on above chemical and biological activity of enaminones and *N*-arylpyrazoles, the present work describes new derivatives in which both enaminone moiety and *N*-arylpyrazole nucleus are gathered in one-molecular frame. Thus, the biological activity of these new derivatives were test-

ed in the hope of obtaining novel anti-inflammatory and/or antimicrobial agents.

Results and Discussion

Chemistry

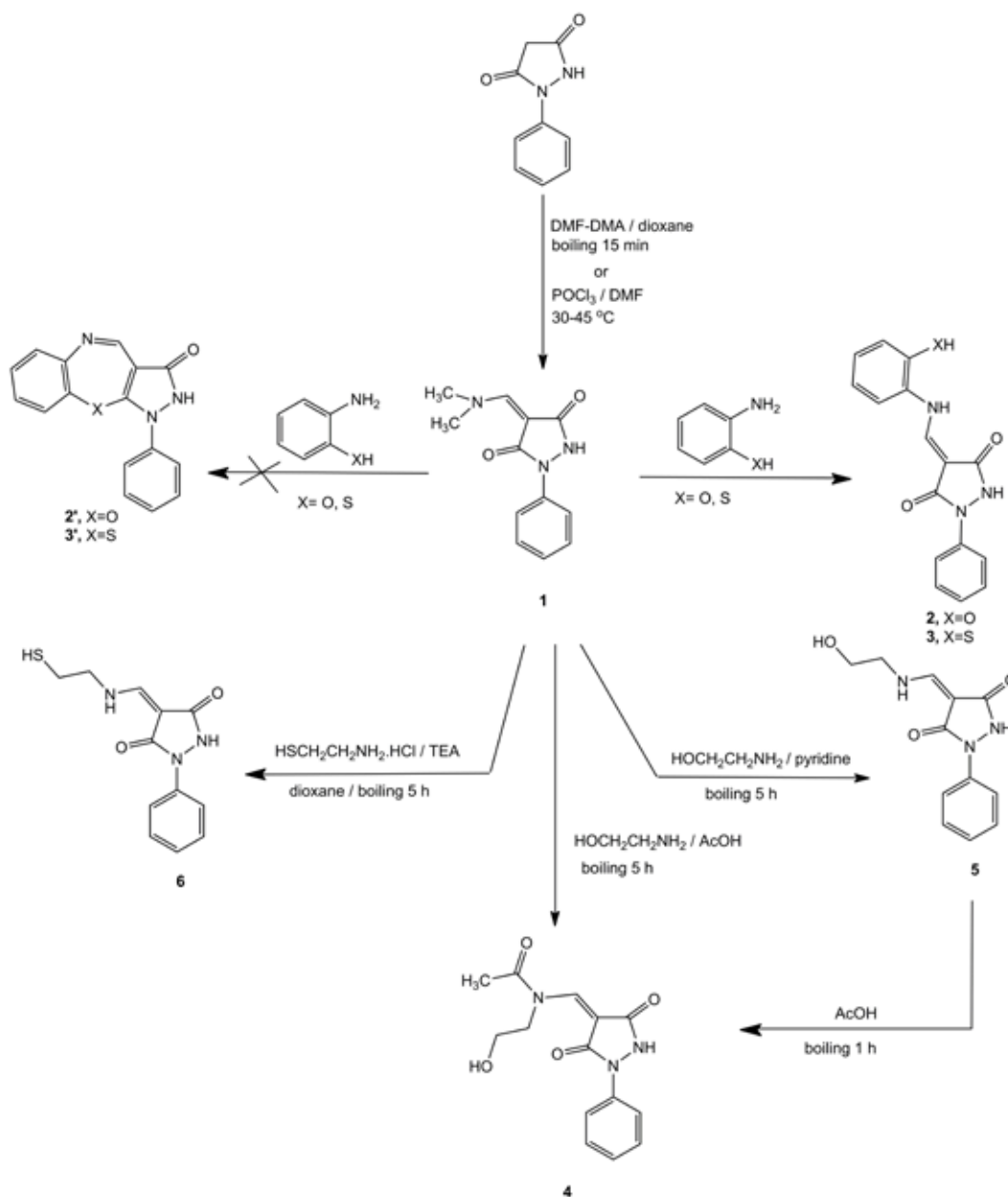
As depicted in Scheme 1, the starting compound; 4-((dimethylamino)methylene)-1-phenylpyrazolidine-3,5-dione (**1**) was obtained via two convenient synthetic routes. Condensation of 1-phenylpyrazolidine-3,5-dione with dimethylformamide-dimethyl acetal (DMF-DMA) in boiling dioxane gave enaminone **1** in 90% yield. When 1-phenylpyrazolidine-3,5-dione was subjected to Vilsmeier-Haack reaction using phosphorus oxychloride and dimethylformamide the same enaminone **1** was afforded in 75% yield. Even when the last route leads to a relatively lower yield, it was economically favored because DMF-DMA is expensive compared to POCl_3 and DMF. ^1H NMR spectrum of **1** revealed a singlet signal at δ 9.55 assignable to N–H proton, a singlet signal at δ 7.09 due to the olefinic proton, and two singlet signals due to the dimethylamino group at δ 3.35 and 3.72. Mass spectrum revealed the molecular ion (M^+) at m/z 231 as the base peak. IR spectrum showed the existence

of two strong stretching vibrations at ν 1645 and 1695 cm^{-1} due to two carbonyl functions of the pyrazolidione nucleus.

Enaminone **1** was treated with some 1,4-bisnucleophiles such as *o*-aminophenol and *o*-aminothiophenol. Thus, treatment with *o*-aminophenol, in boiling glacial acetic acid, gave (4*E*)-4-(((2-hydroxyphenyl)amino)methylidene)-1-phenylpyrazolidine-3,5-dione (**2**). Similarly, when *o*-aminothiophenol was reacted with **1**, in boiling dioxane, led to (4*E*)-4-(((2-mercaptophenyl)amino)methylene)-1-phenylpyrazolidine-3,5-dione (**3**). Neither the expected cyclized products pyrazolobenzoxazepinone **2'** nor pyrazolobenzothiazepinone **3'** were obtained at any ratio (Scheme 1).

The structure of compounds **2** and **3** was established on the basis of their spectral and analytical data. In addition, X-ray single crystal technique was employed to explore the geometry of compound **2** (Fig. 1)[19]. The products were formed via initial addition of the amino group of *o*-aminophenol or *o*-aminothiophenol to the enaminone double bond, followed by elimination of dimethylamine. As shown in Fig. 1, compound **2** has the (*E*)-geometry in which intramolecular cyclocondensation is not allowed. This accounts for the obtained open-chain compounds **2** and **3** but not the cyclized products.

Reaction of enaminone **1** with some aliphatic *bis*-nucleophiles was also studied. Thus, by heating **1** with ethanolamine in



Scheme 1. Synthesis of enaminone **1** and its reactions with *o*-aminophenol, *o*-aminothiophenol, ethanolamine and cysteamine hydrochloride.

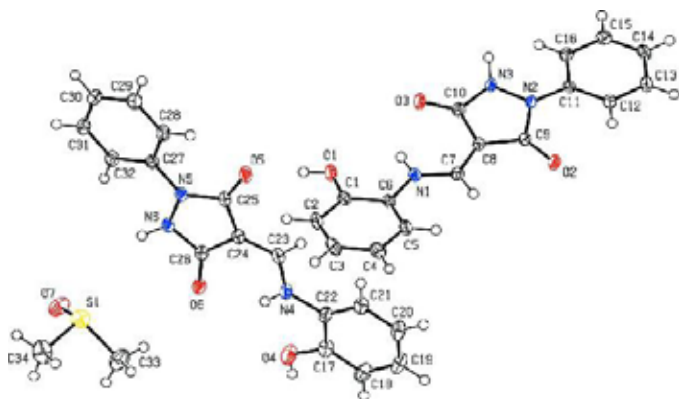


Fig. 1. X-ray molecular structure of compound 2.

pyridine afforded 4-(((2-hydroxyethyl)amino)methylene)-1-phenylpyrazolidine-3,5-dione (**5**) in 79% yield. Interestingly, during attempts to recrystallize compound **5** from glacial acetic acid, *N*-acetylation took place leading to *N*-[(3,5-dioxo-1-phenylpyrazolidin-4-ylidene)methyl]-*N*-(2-hydroxyethyl)-acetamide (**4**) (Scheme 1). So that the same reaction of enaminone **1** with ethanolamine have been carried out in boiling glacial acetic acid to afford the expected acetamide **4**, in 88% yield (Scheme 1). Obviously, this product was formed via initial *N*-nucleophilic replacement of dimethylamine group, followed by *N*-acetylation. Similarly, when enaminone **1** was reacted with cysteamine hydrochloride in dioxane under reflux in presence of triethylamine, the corresponding 4-(((2-mercaptoethyl)amino)methylene)-1-phenylpyrazolidine-3,5-dione (**6**) was afforded (Scheme 1).

In addition, when enaminone **1** was subjected to react with phenylhydrazine in boiling dioxane, afforded a mixture of 3-oxo-*N*',2-diphenyl-2,3-dihydro-1*H*-pyrazole-4-carbohydrazide (**7**) in 84% and 1-phenyl-4-((2-phenylhydrazino)methyl)

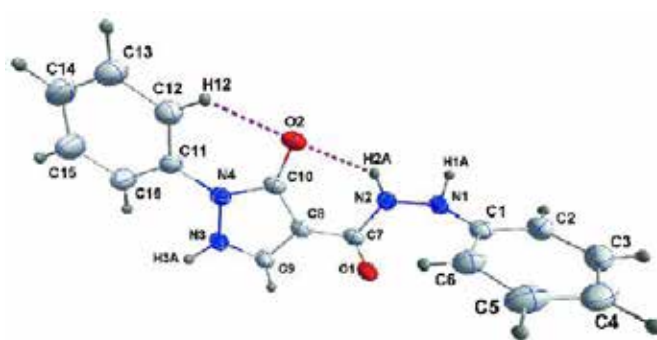
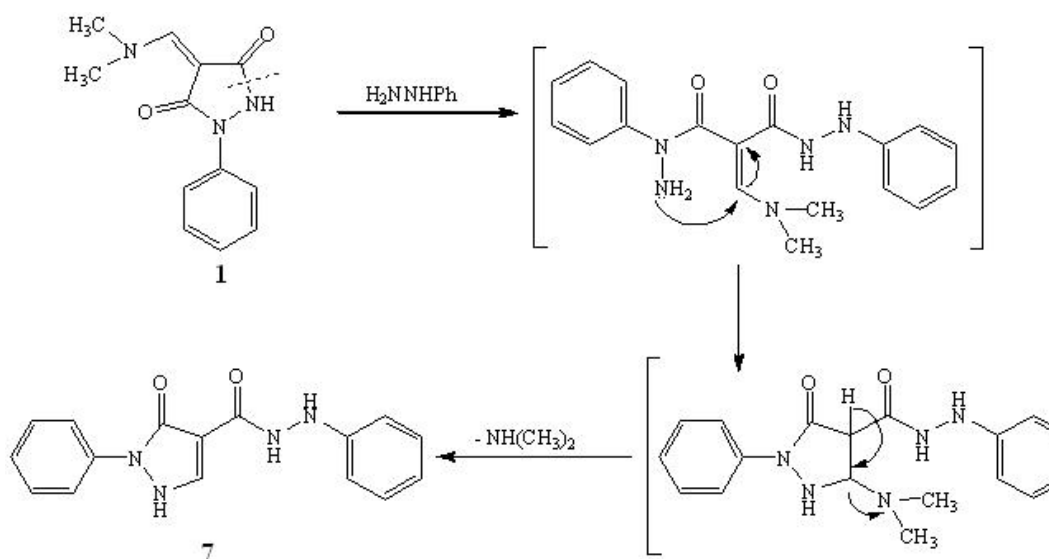


Fig. 2. X-ray molecular structure of compound 7.

lene) pyrazolidine-3,5-dione (**8**) in 12% (Schemes 2-3). The structure of these products was established on the basis of their spectral and analytical data. X-ray single crystal technique was employed to confirm the structure of compound **7** (Fig. 2)[20]. The suggested reaction mechanism for compound **7** was assumed to be as described in Scheme 2.

Enaminone **1** was then allowed to react with diamines, such as hydrazine hydrate, ethylenediamine and *o*-phenylenediamine with the hope to obtain pyrazoles with an additional five or seven-membered heterocycles annulated at the [*c*] or [*e*] face or new pyrazoles carbohydrazides as like in the case of compound **7**. Remarkably, the reaction of enaminone **1** with the aforementioned diamines gave neither the open chain enaminones nor cyclized products. Interpretations of analytical and spectral data of the products confirmed that *bis*-enaminones were formed (Scheme 3). Reaction with hydrazine hydrate in boiling dioxane afforded *N,N'*-disubstituted hydrazine derivative **9**, in 89% yield. ¹H NMR spectrum (DMSO-*d*₆) exhibited chemical shifts at δ 9.31 and 7.97 which were exchangeable with deuterium on addition of deuterium oxide and were assigned to N–H

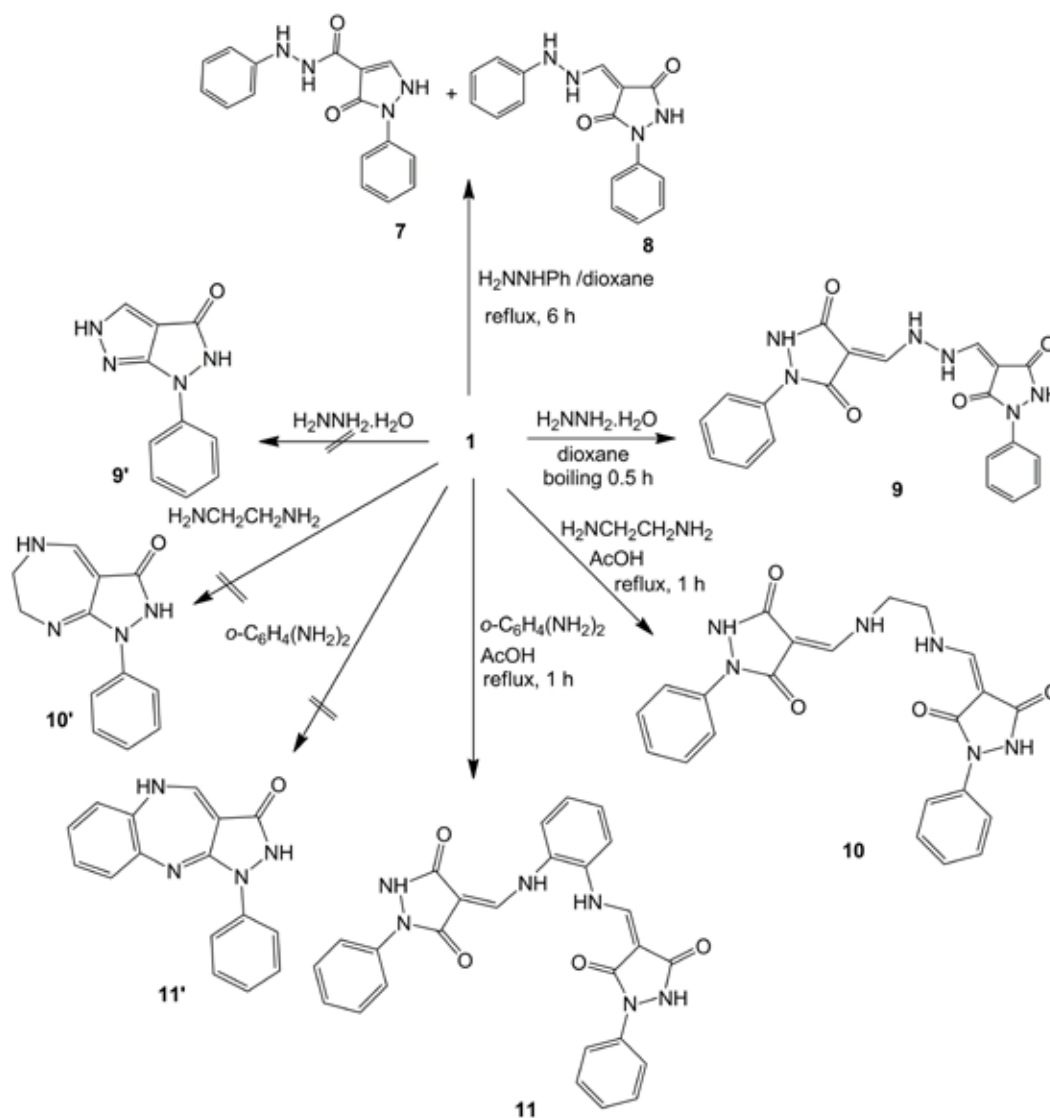


Scheme 2. Reaction of compound **1** with phenylhydrazine to yield compound **7**.

protons. Additionally, a singlet signal at δ 6.7 for two olefinic protons was observed. Elemental microanalysis of product **9**, for C, H, and N elements (within \pm 0.4%) supported the proposed molecular formula $C_{20}H_{16}N_6O_4$ (MW 404.37).

The structure of the *N,N'*-disubstituted ethylenediamine **10** was proven on basis of its 1H NMR and ^{13}C NMR, in addition to elemental microanalysis. NMR spectra showed the presence of (N-CH₂-CH₂-N) grouping. A set of singlet signal appeared at δ 3.7 due to four protons of two (N-CH₂), while ^{13}C NMR spectrum showed signals of two aliphatic *sp*³-carbons at δ 50 and two olefinic *sp*²-carbons at δ 90, in addition to aromatic *sp*²-carbons appeared at δ 118–138. 1H NMR spectrum of *N,N'*-disubstituted *o*-phenylenediamine **11** revealed integration of aromatic protons, in the range of δ 7.1–8.1, corresponding to 14 protons. Mass spectrum as well as C, H, and N microanalysis (within \pm 0.4%) strongly supported the proposed molecular

formula $C_{26}H_{20}N_6O_4$ (MW 480.47). Quantum mechanics calculations were performed to confirm the structure of the obtained products and validate the spectral analysis data. For this purpose, DFT calculations were carried out for enaminone **1**, diamines and proposed products using hybrid functional B3LYP with polarized basis set 6-311G (d,p) as implemented in Gaussian03 program package [21]. This method is considered as most suitable for organic systems with reasonable computational time [22]. Stability of compounds **9**, **9'**, **10**, **10'**, **11**, and **11'** were evaluated from energetic point of view, more specifically the reaction energies were calculated using the formula ($\Delta E = EP - ER$), where EP is the sum of products energy and ER is the sum of reactants energy. Table 1 lists the calculated reaction energies for all products. According to these values, it is clear that (*bis*-products) **9-11** are more stable than cyclized products **9'-11'**.



Scheme 3. Reactions of enaminone **1** with phenylhydrazine, hydrazine hydrate, ethylenediamine and *o*-phenylenediamine.

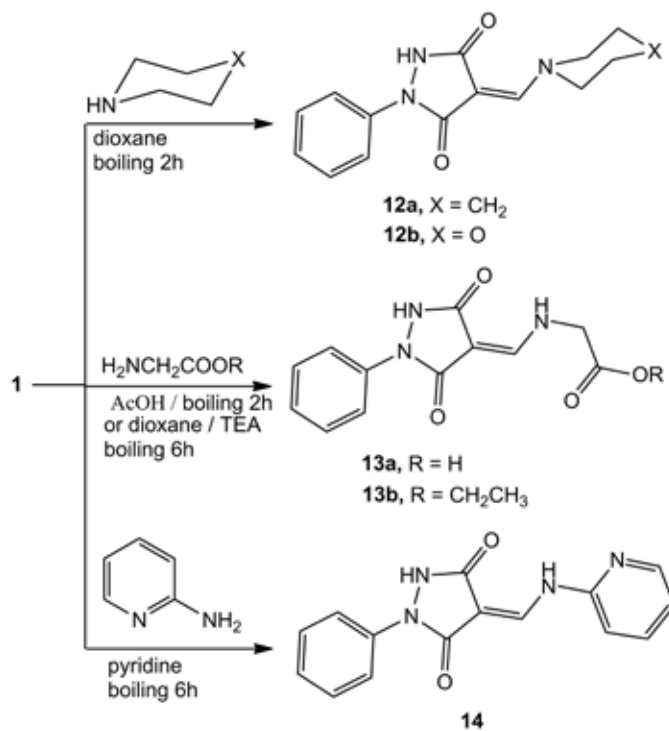
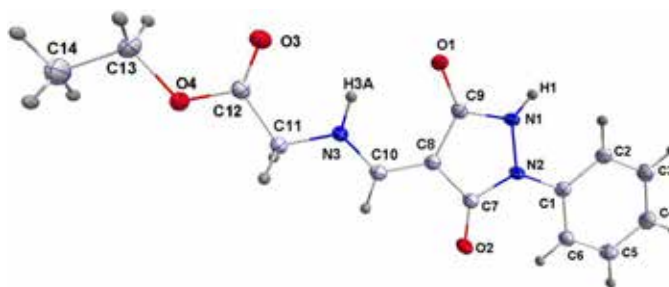
Table 1. The calculated formation energies for 9, 9', 10, 10', 11 and 11' according to the reactions in Scheme 3.

Reaction Energy	ΔE (Kcal/mol)
Compound 9'	0.92
Compound 9	-7.34
Compound 10'	9.33
Compound 10	-14.62
Compound 11'	21.07
Compound 11	-0.92

Reactions of enaminone **1** with some selected primary and secondary amines were carried out to obtain new enaminones of biological interest. Thus, reacting **1** with piperidine and/or morpholine, in boiling dioxane, led to 4-[(1-piperidyl)/(4-morpholinyl)]methylene-pyrazolidinediones **12a** and **12b**, in 95-98% yields (Scheme 4). IR of piperidinyl derivative **12a** showed the presence of absorption vibrations for two different (C=O) at ν 1695 and 1648 cm^{-1} . ^1H NMR spectrum exhibited characteristic set of chemical shifts due to *N*-substituted piperidine moiety. This spectrum revealed a multiplet signal at δ ~1.65 due to six protons ($\text{CH}_2\text{-CH}_2\text{-CH}_2$) and two triplets at δ 3.71 and 4.44 due to four protons ($\text{CH}_2\text{-N-CH}_2$). Nevertheless, ^{13}C NMR spectrum of piperidinyl derivative **12a** gave a good evidence for its structure in which the chart showed chemical shift signals at δ 57, 52, 27, 25, and 23 due to sp^3 -carbons, due to two (NCH_2) and three (CH_2) methylenes, in addition to a characteristic signal at δ 90 corresponding to sp^2 -carbon of enamine. Mass spectrum revealed the molecular ion (M^+) as the base peak at m/z 271 along with (M^++1) ion m/z 272 (relative intensity 19%), which supported the proposed molecular formula. Similarly, the structure of morpholinyl derivative **12b** was evidenced utilizing IR, ^1H NMR, ^{13}C NMR, and mass spectra.

When enaminone **1** was reacted with glycine, in boiling acetic acid, white crystalline product of *N*-substituted glycine derivative **13a** was obtained in 98% yield (Scheme 4). IR spectrum showed presence of both O-H and N-H functional groups appeared as medium broad bands at ν 3433, 3257, and 3150 cm^{-1} , in addition to three strong stretching vibrations at ν 1740, 1690, 1638 cm^{-1} due to (C=O) of the carboxylic acid, and pyrazolidinedione, respectively. ^1H NMR and ^{13}C NMR spectral data of compound **13a** are coincident with the suggested structure. When enaminone **1** was reacted with ethyl glycinate hydrochloride, in boiling dioxane in presence of triethyl amine, a yellowish white crystalline product of ethyl (((*Z*)-(3,5-dioxo-1-phenylpyrazolidin-4-ylidene)methyl)amino)acetate **13b** was obtained in 90% yield (Scheme 4). IR spectra of compounds **13b** showed new absorption bands corresponding to the NH and (C=O)-ester groups at 3296 and 1745 cm^{-1} , respectively. Its ^1H NMR spectrum showed new signals corresponding to the NH glycinate group at 9.32 ppm, 2CH_2 at 4.32, 4.19-4.14 ppm and CH_3 at 1.22 ppm, respectively. X-ray single crystal technique confirmed the structure of compound **13b** (Fig. 3)[23].

Condensation of enaminone **1** with 2-aminopyridine was attempted in different solvent media and reaction conditions.

**Scheme 4.** Reaction of enaminone **1** with piperidine, morpholine, glycine, ethyl glycinate hydrochloride and 2-aminopyridine.**Fig. 3.** X-ray molecular structure of compound **13b**.

Thus, when the reaction was carried out in acetic acid or ethanol or DMF low yields were obtained. Interestingly, a high yield (91%) of 4-(2-pyridinylaminomethylene)pyrazolidinedione **14** was achieved when the reaction was carried out in boiling pyridine. The structure of product **14** was evidenced utilizing spectral and analytical data.

Biological Results

Antimicrobial Activity

The newly synthesized products **1**, **2**, **3**, **4**, **6**, **7**, **12a**, **12b**, **13a** and **13b** were tested for their antimicrobial activities using six bacterial species, namely *Staphylococcus aureus*, *Bacillus*

Table 2. Antimicrobial activity of compounds **1**, **2**, **3**, **7** and **13a**.

Tested Microorganism	Inhibition zone diameter					
	1	2	3	7	13a	Stand.*
<i>Staphylococcus aureus</i> (+ve) AUMC No. B-54	16	0	12	0	10	24
<i>Bacillus cereus</i> (+ve) AUMC No. B-52	16	11	12	12	0	30
<i>Escherichia coli</i> (-ve) AUMC No. B-53	22	10	11	11	11	25
<i>Micrococcus luteus</i> (+ve) AUMC No. B-112	0	0	13	12	11	23
<i>Pseudomonas aeruginosa</i> (-ve) AUMC No. B-53	0	0	15	12	0	15
<i>Serratia marcescens</i> (-ve) AUMC No. B-55	15	0	12	8	0	34
<i>Candida albicans</i> AUMC No. 1299	0	0	30	20	0	24
<i>Geotrichum candidum</i> AUMC No. 226	0	0	26	20	0	24
<i>Trichophyton rubrum</i> AUMC No. 1804	0	0	42	28	0	36
<i>Fusarium oxyspoum</i> AUMC No. 5119	0	0	40	26	0	25
<i>Scopulariopsis brevicaulis</i> AUMC No. 361	0	0	30	20	0	28
<i>Aspergillus flavus</i> AUMC No. 1276	0	0	15	20	0	26

p.i

* Chloramphenicol was used as a standard antibacterial agent and clotrimazole was used as a standard antifungal agent.

AUMC: Assuit University Mycological Center

p.i: Partial Inhibition

cerus, *Escherichia coli*, *Micrococcus luteus*, *Pseudomonas aeruginosa* and *Serratia marcescens*, in addition to six species of fungi, namely *Candida albicans*, *Geotrichum candidum*, *Trichophyton rubrum*, *Fusarium oxyspoum*, *Scopulariopsis brevicaulis* and *Aspergillus flavus*. The organisms were tested against the activity of solutions of 50 mg/mL of each compound and using inhibition zone diameter (IZD) in mm as criterion for the antimicrobial activity. The bactericide chloramphenicol and the fungicide clotrimazole were used as the references to evaluate the potency of the tested compounds under the same conditions. The results, depicted in Table 2, revealed that compounds **3** and **7** exhibited high degree of inhibition against *Pseudomonas aeruginosa*, *Candida albicans*, *Geotrichum candidum*, *Trichophyton rubrum*, *Fusarium oxyspoum*, *Scopulariopsis brevicaulis* and *Aspergillus flavus*, more than the fungicide reference. Compound **1** had high inhibition effect against *Esch-*

erichia coli and *Staphylococcus aureus*. Compounds **1**, **2**, **3**, and **7** also exhibited moderate inhibition effect against *Bacillus cereus*. Compounds **4**, **6**, **12a-b**, and **13b** were reflecting no inhibition of growth against all the tested microorganisms.

Anti-inflammatory Activity

The anti-inflammatory effects of compounds **1**, **2**, **3**, **4**, **6**, **7**, **12a**, **12b**, and **13a** were evaluated by the Kataoka *et al* method [24,25]. Male rats weighing 200–250 g were purchased from animal house of Assuit University. All animals were maintained with a balanced diet and water *ad libitum*, rats were divided into 11 groups, each of three animals. One group left as a control group, 9 groups received the tested compounds and one group received the reference standard. Paw oedema was induced by injecting single dose of Carrageenan that was dissolved in

Table 3. The anti-inflammatory activity of products **1**, **2**, **3**, **4**, **6**, **7**, **12a**, **12b**, **13a** (50 mg/mL) and indomethacin (50 mg/mL).

(I) Treatment Indomethacin	(J) Treatment	Mean Difference (I-J)	Std. Error	Sig.	95% Confidence Interval	
					Lower Bound	Upper Bound
	treatment 1	-.03333	.02789	.246	-.0915	.0248
	treatment 2	-.03333	.02789	.246	-.0915	.0248
	treatment 3	-.10000*	.02789	.002	-.1582	-.0418
	treatment 4	.00000	.02789	1.000	-.0582	.0582
	treatment 6	-.11667*	.02789	.001	-.1748	-.0585
	treatment 7	.00000	.02789	1.000	-.0582	.0582
	treatment 12a	.00000	.02789	1.000	-.0582	.0582
	treatment 12b	-.01667	.02789	.557	-.0748	.0415
	treatment 13a	-.20000*	.02789	.001	-.2582	-.1418

* The mean difference is significant at the 0.05 level.

physiological saline solution (500 μl of 1% v/v) in the right paw. The tested compounds (60 mg/kg body weight) were administered. The thickness of the paw was measured after administration of the compounds at 0.5, 1, 2, 3, 4 and 5 h by using micrometer. The effect of the tested compounds and indomethacin, as the reference, was measured before and 0.5, 1, 2, 3, 4 and 5 h after carrageenan injection. Edema inhibition was calculated as a regard to saline control group, as depicted in Table 3 and Fig. 4. The results indicated that:

- Compounds **1**, **2**, **4**, **7**, **12a**, and **12b** showed high anti-inflammatory activity compared with indomethacin.
- Compounds **3**, **6** and **13a** showed moderate anti-inflammatory activity compared with indomethacin.

Statistical analysis

The results were analyzed by one way analysis of variance (ANOVA) followed by Newman-Keuls Multiple Comparison Test as a post-Test. These analyses were carried out using computer prism program for windows, version 3.0 (Graph pad software, Inc, San Diego CA. USA). The significance difference between groups was accepted at $p < 0.05$, 0.001^* , and the data were expressed as mean \pm Standard error (SE) after 5 hour as shown in Table 3

Conclusion

It was found that 4-[(dimethylamino)methylene]-1-phenylpyrazolidine-3,5-dione is good precursor for the synthesis of biologically important heterocyclic enaminone derivatives. This compound shows significant chemical reactivity towards different nucleophilic reagents, in which dimethylamino group acts as good leaving group even against low-reactive nucleop-

hiles such as glycine and 2-aminopyridine. Many new enaminone derived from this compound exhibited moderate to high anti-inflammatory and antimicrobial activities.

Experimental Section

General

All melting points were determined on a Melt-Temp-II apparatus and are uncorrected. IR spectra were taken on a Nicolet 710 Fourier Transform (FT) instrument in potassium bromide discs. ^1H NMR and ^{13}C NMR spectra were recorded at 400 and 100 MHz, respectively, on a Bruker Bio spin AG-400 spectrometer, using $\text{DMSO-}d_6$ as solvent and TMS as an internal reference. Mass spectra were measured on a Shimadzu Qp-2010 plus spectrometer (70 eV). Elemental analyses were carried out at the Microanalytical Center of Cairo University. X-ray was measured on Bruker APEX2; cell refinement: Bruker SAINT; program(s) used to solve structure: SHELXS97; program(s) used to refine structure: SHELXL97; molecular graphics: XSEED. Anti-inflammatory and Antimicrobial activities were evaluated at Faculty of Medicine and Mycological Center, Assuit University, respectively.

4-[(Dimethylamino)methylene]-1-phenylpyrazolidine-3,5-dione (1). **Method a.** A mixture of 1-phenylpyrazolidine-3,5-dione (1.76 g, 0.01 mol) and dimethylformamide dimethylacetal (DMF-DMA) (1.19 g, 0.01 mol) in anhydrous dioxane (10 mL) was refluxed for 15 min., the solid product was precipitated on hot, collected by filtration and recrystallized from dimethyl sulfoxide to give white crystals, yield 2.08 g, 90%. **Method b.** To phosphorous oxychloride (10 mL, 0.1 mol), in a conical flask with magnetic stirrer, dry dimethylformamide (35 mL) was added drop-wise with stirring at temperature did not exceed 30–35 $^\circ\text{C}$ for 30 min. Then a solution of 1-phenylpyrazolidine-3,5-dione (8.8 g, 0.05 mol), in dimethylformamide (15 mL), was drop-wise added with continuous stirring at temperature did not exceed 45 $^\circ\text{C}$. The reaction mixture was left overnight, poured onto crushed ice. The solid product was collected by filtration and recrystallized from dimethylsulfoxide to give white crystals, yield 8.66 g, 75%, m. p. 260–262 $^\circ\text{C}$ (248 – 250 $^\circ\text{C}$).¹⁸ IR (KBr) ν : 3118 (N–H), 1695 (C=O), 1645 (C=O) cm^{-1} . ^1H NMR ($\text{DMSO-}d_6$) δ : 9.55 (s, 1H, N–H disappeared on addition of D_2O), 7.63–7.37 (m, 5H, H_{arom}), 7.09 (s, 1H, N– $\text{CH}_{\text{olefin}}$), 3.72 (s, 3H, N– CH_3), 3.35 (s, 3H, N– CH_3). ^{13}C NMR ($\text{DMSO-}d_6$) δ : 169, 167 (CONPh), 166 (CONH), 163, 159.29 (=CH–N), 138 (C), 130 (CH), 123 (CH), 118 (CH), 117 (CH), 92 (C-4), 47 (N– CH_3), 43 (N– CH_3). MS, m/z (%) 232 ($\text{M}^+ + 1$, 16), 231 (M^+ , 100), 139 (26), 105 (42), 97 (22), 80 (29), 69 (26). Anal. Calcd. for $\text{C}_{12}\text{H}_{13}\text{N}_3\text{O}_2$ (231.25): C, 62.33; H, 5.67; N, 18.17. Found: C, 62.40; H, 5.51; N, 17.77.

4-[(2-Hydroxyphenyl)amino]methylene}-1-phenylpyrazolidine-3,5-dione (2). A mixture of enaminone **1** (0.23 g, 0.001 mol) and *o*-aminophenol (0.11 g, 0.001 mol) in anhydrous acetic acid (15 mL) was refluxed for 1 h. The solid product was precipitated on hot, collected by filtration, washed with

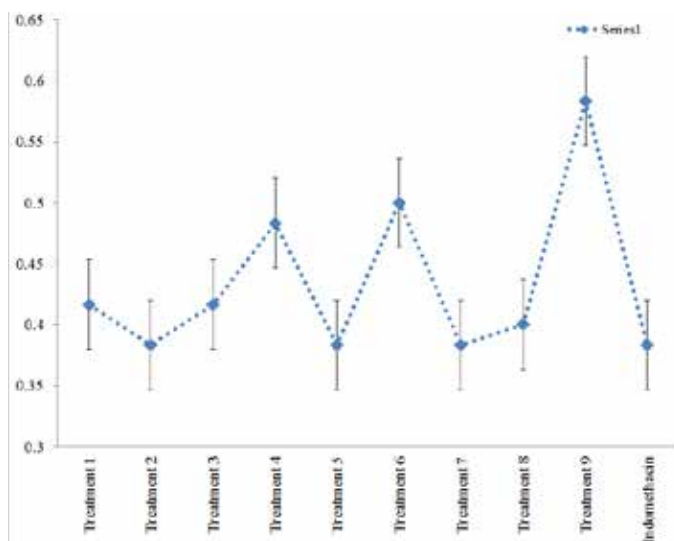


Fig. 4. Anti-inflammatory of the tested compounds and indomethacin.

water and recrystallized from dimethyl sulfoxide to give colorless crystals, yield 0.28 g, 97%, m.p. 268–269 °C. IR (KBr) ν : 3414 (OH), 3290 (N–H), 3152 (N–H), 1690 (C=O), 1640 (C=O) cm^{-1} . $^1\text{H-NMR}$ (DMSO- d_6) δ : 10.70–10.30 (br, 3H, OH+2N–H disappeared on addition of D_2O), 8.56 (s, 1H, CH=), 7.73–6.86 (m, 9H, H_{arom}). $^{13}\text{C-NMR}$ (DMSO- d_6) δ : 169, 165 (CONPh), 163 (CONH), 147 (=CH), 146 (CH), 145 (C), 138 (C), 130 (CH), 126 (CH), 120 (CH), 119 (CH), 118 (CH), 116 (CH), 93 (C-4). MS, m/z (%) ($\text{M}^+ + 1$, 17), 295 (M^+ , 80), 187 (55), 162 (20), 133 (11), 119 (59), 91(36), 80 (100), 64(68). Anal. Calcd. for $\text{C}_{16}\text{H}_{13}\text{N}_3\text{O}_3$ (295.29): C, 65.08; H, 4.44; N, 14.23. Found: C, 65.48; H, 4.61; N, 14.03.

4-[(2-mercaptophenyl)amino]methylene}-1-phenylpyrazolidine-3,5-dione (3). A mixture of enaminone **1** (0.23 g, 0.001 mol) and o-aminothiophenol (0.125 g, 0.001 mol) in anhydrous dioxane (50 mL) was refluxed for 4 h. After cooling, the solid product was collected by filtration and recrystallized from ethanol to give yellow crystals, yield 0.25 g, 80%, m.p. 280 °C. IR (KBr) ν : 3200 (N–H), 1689 (C=O), 1641 (C=O) cm^{-1} . $^1\text{H-NMR}$ (DMSO- d_6) δ : 9.35 (s, 1H, N–H disappeared on addition of D_2O), 7.94–7.11 (m, 11H, N–H+ H_{arom} + H_{olefin}). $^{13}\text{C-NMR}$ (DMSO- d_6) δ : 169 (CONPh), 166 (CONH), 145 (=CH), 140 (C), 138 (C), 130 (CH), 126 (CH), 119 (CH), 118 (CH), 92 (C-4). Anal. Calcd. for $\text{C}_{16}\text{H}_{13}\text{N}_3\text{O}_2\text{S}$ (311.36): C, 61.72; H, 4.21; N, 13.50; S, 10.30. Found: C, 61.49; H, 3.91; N, 13.35; S, 10.66.

N-[(3,5-Dioxo-1-phenylpyrazolidin-4-ylidene)methyl]-N-(2-hydroxyethyl)-acetamide (4).

Method a. A mixture of enaminone **1** (0.23 g, 0.001 mol) and ethanolamine (0.06 g, 0.001 mol) in anhydrous acetic acid (15 mL) was refluxed for 4 h. After cooling, the reaction mixture was poured onto ice cold water, the solid product was collected by filtration and recrystallized from ethanol. White crystals yield 0.254 g, 88%, m. p. 207–208 °C. IR (KBr) ν : 3428 (OH), 3264 (N–H), 1725 (C=O), 1693 (C=O), 1641 (C=O) cm^{-1} . $^1\text{H-NMR}$ (DMSO- d_6) δ : 10 (s, 1H, OH disappeared on addition of D_2O), 9.30 (s, 1H, N–H disappeared on addition of D_2O), 7.80–7.10 (m, 6H, H_{arom} + H_{olefin}), 4.19 (s, 2H, CH_2OH), 3.69 (s, 2H, CH_2N), 2.02 (s, 3H, CH_3). $^{13}\text{C-NMR}$ (DMSO- d_6) δ : 171 (COCH_3), 169, 167 (CONPh), 164 (CONH), 163, 157 (=CH), 138 (C), 145(130 (CH), 123 (CH), 118 (CH), 90 (C-4), 63 (CH_2O), 49 (CH_2N), 21 (CH_3). MS, m/z (%) 290 ($\text{M}^+ + 1$, 7), 289 (M^+ , 38), 230 (15), 187 (13), 114 (24), 96(14), 80 (100), 64(42). Anal. Calcd. for $\text{C}_{14}\text{H}_{15}\text{N}_3\text{O}_4$ (289.29): C, 58.13; H, 5.23; N, 14.53. Found: C, 57.9; H, 4.86; N, 14.2. **Method b.** Boiling of compound **5** (0.5 g, 0.002) in glacial acetic acid (5 mL) for 1 h gave white crystals of the same compound **4**, 0.526 g, yield 90%.

4-[(2-Hydroxyethyl)amino]methylene}-1-phenylpyrazolidine-3,5-dione (5). A mixture of enaminone **1** (0.23 g, 0.001 mol) and ethanolamine (0.06 g, 0.001 mol) in anhydrous pyridine (15 mL) was refluxed for 4 h. After cooling, the reaction mixture was concentrated. The solid product was collected by filtration and recrystallized from ethanol to give green crystals, yield 0.195 g, 79%, m.p. 194–196 °C. IR (KBr) ν : 3408 (OH), 3284 (N–H), 1693 (C=O), 1647 (C=O) cm^{-1} . $^1\text{H-NMR}$

(DMSO- d_6) δ : 10 (s, 1H, OH disappeared on addition of D_2O), 9.37 (s, 1H, N–H disappeared on addition of D_2O), 7.87–7.08 (m, 7H, N–H+ H_{arom} + H_{olefin}), 3.56 (s, 2H, CH_2OH), 3.48 (s, 2H, CH_2N -H). $^{13}\text{C-NMR}$ (DMSO- d_6) δ : 169, 167 (CONPh), 164 (CONH), 163, 156 (=CH), 138 (C), 129 (CH), 123 (CH), 118 (CH), 90 (C-4), 60 (CH_2O), 52 (CH_2N). Anal. Calcd. for $\text{C}_{12}\text{H}_{13}\text{N}_3\text{O}_3$ (247.25): C, 58.29; H, 5.30; N, 16.99. Found: C, 58.69; H, 5.44; N, 16.62.

4-[(2-Mercaptoethyl)amino]methylene}-1-phenylpyrazolidine-3,5-dione (6). A mixture of enaminone **1** (0.23 g, 0.001 mol), cysteamine hydrochloride (0.113 g, 0.001 mol) and triethylamine (1.01 g, 0.001 mol) in anhydrous dioxane (50 mL) was refluxed for 4 h. The solid product was precipitated on hot, collected by filtration, washed with water, dried and recrystallized from DMF to give white crystals, yield 0.244 g, 93%, m.p. 285–287 °C. IR (KBr) ν : 3265 (N–H), 1695 (C=O), 1639 (C=O) cm^{-1} . $^1\text{H-NMR}$ (DMSO- d_6) δ : 10.02 (s, 1H, N–H disappeared on addition of D_2O), 9.44 (s, 1H, N–H disappeared on addition of D_2O), 7.89–7.09 (m, 6H, H_{arom} + H_{olefin}), 3.75 (s, 2H, CH_2N -H), 3.05 (s, 2H, CH_2SH), 2.75 (s, 1H, SH). $^{13}\text{C-NMR}$ (DMSO- d_6) δ : 169, 167 (CONPh), 164 (CONH), 163, 156 (=CH), 138 (C), 129 (CH), 123 (CH), 118 (CH), 90 (C-4), 49 (CH_2N), 38 (CH_2S). Anal. Calcd. for $\text{C}_{12}\text{H}_{13}\text{N}_3\text{O}_2\text{S}$ (263.32): C, 54.74; H, 4.98; N, 15.96; S, 12.18. Found: C, 54.9; H, 4.68; N, 15.8; S, 12.46.

1-Phenyl-4-[(2-phenylhydrazino)methylene]pyrazolidine-3,5-dione (8). A mixture of enaminone **1** (0.23 g, 0.001 mol) and phenyl hydrazine (0.108 g, 0.001 mol) in anhydrous dioxane (50 mL) was refluxed for 6 h, small amount of yellow precipitate was formed, filtered on hot, recrystallized from DMF to give yellowish white crystals, yield 0.035 g, 12%, m.p. 270–272 °C. IR (KBr) ν : 3420, 3255, 3150 (3NH), 1700, 1642 (2C=O) cm^{-1} . $^1\text{H-NMR}$ (DMSO- d_6) δ : 11.05 (s, 1H, N–H disappeared on addition of D_2O), 10.35, 9.45 (br, 2H, 2NH disappeared on addition of D_2O), 8.44 (s, 1H, =CH), 7.73–7.14 (m, 10H, H_{arom}). $^{13}\text{C-NMR}$ (DMSO- d_6) δ : 168 (CONPh), 165 (CONH), 164, 148 (=CH), 147 (C), 130 (C), 129 (CH), 125 (CH), 124 (CH), 118 (CH), 93 (C-4). Anal. Calcd. For $\text{C}_{16}\text{H}_{14}\text{N}_4\text{O}_2$ (294.31): C, 65.30; H, 4.79; N, 19.04. Found: C, 65.6; H, 4.63; N, 18.72.

3-Oxo-N',2-diphenyl-2,3-dihydro-1H-pyrazole-4-carbohydrazide (7). The filtrate of the compound **8** was cooled, the solid product was collected by filtration and recrystallized from ethanol, yield 0.246 g, 84%, m. p. 210–211 °C. IR (KBr) ν : 3400, 3252, 3150 (3NH), 1695, 1642 (2C=O) cm^{-1} . $^1\text{H-NMR}$ (DMSO- d_6) δ : 11.00, 10.00 (s, 2H, NH disappeared on addition of D_2O), 8.22 (s, 1H, $\text{H}_{\text{pyrazole}}$), 7.74–6.71 (m, 10H, H_{arom}). $^{13}\text{C-NMR}$ (DMSO- d_6) δ : 170 (CONH), 164 (CONPh), 158 (C), 150 (C), 140 (CH-5), 138 (CH), 130 (CH), 128 (CH), 122 (CH), 119 (CH), 112 (CH), 98 (C-4). Anal. Calcd. For $\text{C}_{16}\text{H}_{14}\text{N}_4\text{O}_2$ (294.31): C, 65.30; H, 4.79; N, 19.04. Found: C, 65.7; H, 4.75; N, 18.71.

4,4'-[Hydrazine-1,2-diylidimethylidene]bis(1-phenylpyrazolidine-3,5-dione) (9). A mixture of enaminone **1** (0.23 g, 0.001 mol) and hydrazine hydrate (0.05 g, 0.001 mol) in anhydrous dioxane (50 mL) was refluxed for 30 min, the solid

product was precipitated on hot, collected by filtration and recrystallized from dioxane to give yellow crystals, yield 0.18 g, 89%, m.p. >300 °C. IR (KBr) ν : 3150 (N–H), 1645 (C=O) cm^{-1} . $^1\text{H-NMR}$ (DMSO- d_6) δ : 9.31 (s, 2H, 2N–H disappeared on addition of D_2O), 7.97 (s, 2H, 2N–H disappeared on addition of D_2O), 7.78–6.70 (m, 12H, $\text{H}_{\text{arom}}+\text{H}_{\text{olefin}}$). Anal. Calcd. for $\text{C}_{20}\text{H}_{16}\text{N}_6\text{O}_4$ (404.37): C, 59.40%; H, 3.99%; N, 20.78%. Found: C, 59.27; H, 3.75; N, 21.21%.

4,4'-[Ethane-1,2-diylbis(iminomethylidene)]bis(1-phenylpyrazolidine-3,5-dione) (10). A mixture of enaminone **1** (0.23 g, 0.001 mol) and ethylenediamine (0.06 g, 0.001 mol) in anhydrous acetic acid (15 mL) was refluxed for 2 h, the solid product was precipitated on hot, collected by filtration and recrystallized from dimethylsulfoxide to give white crystals, yield 0.18 g, 90%, m.p. >300 °C. IR (KBr) ν : 3290, 3150 (2N–H), 1695, 1649 (2C=O) cm^{-1} . $^1\text{HNMR}$ (DMSO- d_6) δ : 9.60–9.20 (br, 4H, 4N–H disappeared on addition of D_2O), 7.86–7.08 (m, 12H, $\text{H}_{\text{arom}}+\text{H}_{\text{olefin}}$), 3.70 (s, 4H, 2 CH_2). $^{13}\text{CNMR}$ (DMSO- d_6) δ : 164 (CONPh), 163 (CONH), 157 (=CH), 156 (=CH), 138 (C), 129 (CH), 125 (CH), 118 (CH), 90 (C), 50 (2 CH_2). Anal. Calcd. for $\text{C}_{22}\text{H}_{20}\text{N}_6\text{O}_4$ (432.43): C, 61.10%; H, 4.66%; N, 19.43%. Found: C, 61.16; H, 4.35; N, 19.57%.

4,4'-[1,2-Phenylenebis(iminomethylidene)]-bis(1-phenylpyrazolidine-3,5-dione) (11). A mixture of enaminone **1** (0.23 g, 0.001 mol) and *o*-phenylenediamine (0.108 g, 0.001 mol), in anhydrous acetic acid (15 mL), was refluxed for 1 h. The solid product was precipitated on hot, collected by filtration, washed with water and recrystallized from dimethylsulfoxide to give white crystals, yield 0.204 g, 85%, m.p. 300 °C. IR (KBr) ν : 3149 (N–H), 1644 (C=O) cm^{-1} . $^1\text{HNMR}$ (DMSO- d_6) δ : 11.25 (s, 2H, 2N–H disappeared on addition of D_2O), 10.45 (s, 2H, 2N–H disappeared on addition of D_2O), 8.10–7.10 (m, 16H, $\text{H}_{\text{arom}}+\text{H}_{\text{olefin}}$). Anal. Calcd. for $\text{C}_{26}\text{H}_{20}\text{N}_6\text{O}_4$ (480.47): C, 64.99%; H, 4.20%; N, 17.49%. Found: C, 65.32; H, 3.98; N, 17.70%.

1-Phenyl-4-(piperidin-1-ylmethylene)pyrazolidine-3,5-dione (12a). A mixture of enaminone **1** (0.23 g, 0.001 mol) and piperidine (0.85 g, 0.001 mol) in anhydrous dioxane (50 mL) was refluxed for 2 h. The solid product was precipitated on hot, collected by filtration and recrystallized from dioxane to give white crystals, yield 0.257 g, 95%, m.p. 245–247 °C. IR (KBr) ν : 3145 (N–H), 1695 (C=O), 1648 (C=O) cm^{-1} . $^1\text{HNMR}$ (DMSO- d_6) δ : 9.91 (s, 1H, N–H disappeared on addition of D_2O), 7.63–7.34 (m, 5H, H_{arom}), 7.07 (s, 1H, H_{olefin}), 4.44 (t, 2H, CH_2N), 3.71 (t, 2H, CH_2N), 1.65 (m, 6H, (CH_2)₃). $^{13}\text{CNMR}$ (DMSO- d_6) δ : 169, 167 (CONPh), 165 (CONH), 162, 152 (=CH), 138 (C), 129 (CH), 124 (CH), 118 (CH), 90 (C-4), 57 (CH_2), 52 (CH_2), 27 (CH_2), 25 (CH_2), 23 (CH_2). MS, m/z (%) 272 (M^++1 , 19), 271 (M^+ , 100), 231 (15), 198 (18), 179 (47), 136(22), 108 (27), 93(17), 83(64), 80(85), 69(15), 64(32), 53(18). Anal. Calcd. for $\text{C}_{15}\text{H}_{17}\text{N}_3\text{O}_2$ (271.31): C, 66.40; H, 6.32; N, 15.49. Found: C, 66.09; H, 5.98; N, 15.4.

4-(Morpholin-4-ylmethylene)-1-phenylpyrazolidine-3,5-dione (12b). A mixture of enaminone **1** (0.23 g, 0.001 mol) and morpholine (0.87 g, 0.001 mol) in anhydrous dioxane (50 mL) was refluxed for 2 h. The solid product was precipitated

on hot, collected by filtration and recrystallized from DMF. To give white crystals, yield 0.267 g, 98%, m.p. 280–282 °C. IR (KBr) ν : 3125 (N–H), 1695 (C=O), 1650 (C=O) cm^{-1} . $^1\text{HNMR}$ (DMSO- d_6) δ : 10.10 (s, 1H, N–H disappeared on addition of D_2O), 7.61–7.09 (m, 6H, $\text{H}_{\text{arom}}+\text{H}_{\text{olefin}}$), 4.57 (s, 2H, CH-O), 3.80–3.60 (br, 6H, (CH-O + 2 $\text{CH}_2\text{-N}$)). $^{13}\text{CNMR}$ (DMSO- d_6) δ : 169, 167 (CONPh), 162 (CONH), 152 (=CH), 138 (C), 129 (CH), 124 (CH), 118 (CH), 89 (C-4), 67 (CH_2), 66 (CH_2), 56 (CH_2), 53 (CH_2); MS, m/z (%) 274 (M^++1 , 15), 273 (M^+ , 100), 231 (27), 187 (19), 181 (25), 138(14), 105 (15), 93(17), 85(38), 80(40), 77(38), 64(20), 53(23). Anal. Calcd. for $\text{C}_{14}\text{H}_{15}\text{N}_3\text{O}_3$ (273.29): C, 61.53; H, 5.53; N, 15.38. Found: C, 61.2; H, 5.34; N, 15.7.

{[(3,5-Dioxo-1-phenylpyrazolidin-4-ylidene)methyl]amino}acetic acid (13a). A mixture of enaminone **1** (0.23 g, 0.001 mol) and glycine (0.75 g, 0.001 mol) in anhydrous acetic acid (15 mL) was refluxed for 2 h. The solid product was precipitated on hot, collected by filtration, washed with water, dried and recrystallized from dimethylformamide to give white crystals, yield 0.256 g, 98%, m.p. 290–291 °C. IR (KBr) ν : 3433 (O–H), 3257, 3150 (2NH), 1740, 1690, 1638 (3C=O) cm^{-1} . $^1\text{HNMR}$ (DMSO- d_6) δ : 11.0 (s, 1H, COOH disappeared on addition of D_2O), 9.35 (s, 1H, N–H disappeared on addition of D_2O), 7.91–7.10 (m, 7H, N–H + $\text{H}_{\text{arom}}+\text{H}_{\text{olefin}}$), 4.26 (s, 2H, $\text{NCH}_2\text{CO}_2\text{H}$). $^{13}\text{CNMR}$ (DMSO- d_6) δ : 171 (COOH), 169, 167 (CONPh), 165 (CONH), 164, 163, 157 (=CH), 156, 128 (CH), 124 (CH), 118 (CH), 90 (C-4), 50 (CH_2). Anal. Calcd. for $\text{C}_{12}\text{H}_{11}\text{N}_3\text{O}_4$ (261.23): C, 55.17; H, 4.24; N, 16.09. Found: C, 55.1; H, 4.26; N, 15.69.

Ethyl {(Z)-(3,5-dioxo-1-phenylpyrazolidin-4-ylidene)methyl}amino}acetate (13b). A mixture of enaminone **1** (0.23 g, 0.001 mol), ethyl glycinate hydrochloride (0.139 g, 0.001 mol) and triethylamine (0.101 g, 0.001 mol) in anhydrous dioxane (50 mL) was refluxed for 6 h. The solid product was precipitated on hot, collected by filtration, washed with water, dried and recrystallized from DMSO to give white crystals, yield 0.26 g, 90%, m.p. 216–218 °C. IR (KBr) ν : 3296, 3150 (2NH), 1740, 1693, 1637 (3C=O) cm^{-1} . $^1\text{HNMR}$ (DMSO- d_6) δ : 10.15 (s, 1H, NH disappeared on addition of D_2O), 9.35 (s, 1H, N–H disappeared on addition of D_2O), 7.92–7.08 (m, 6H, $\text{H}_{\text{arom}}+\text{H}_{\text{olefin}}$), 4.32 (s, 2H, $\text{NCH}_2\text{CO}_2\text{Et}$), 4.19–4.14 (q, 2H, CH_2CH_3), 1.24–1.2 (t, 3H, CH_2CH_3). $^{13}\text{CNMR}$ (DMSO- d_6) δ : 170 (COOR), 169, 167 (CONPh), 165 (CONH), 164, 156 (=CH), 155, 138 (C), 129 (CH), 124 (CH), 118 (CH), 90 (C), 62 (OCH_2), 50 (NCH_2), 14 (CH_3). MS, m/z (%) 290 (M^++1 , 14), 289 (M^+ , 78), 216 (20), 199 (10), 187 (14), 156(25), 128 (10), 108(17), 93(27), 82(67), 80(100), 77(57), 64(83), 55(26), 53(33). Anal. Calcd. for $\text{C}_{14}\text{H}_{15}\text{N}_3\text{O}_4$ (289.29): C, 58.13; H, 5.23; N, 14.53. Found: C, 58.43; H, 5.02; N, 14.19.

1-Phenyl-4-[(pyridin-2-ylamino)methylene]pyrazolidine-3,5-dione (14). A mixture of enaminone **1** (0.23 g, 0.001 mol) and 2-aminopyridine (0.094 g, 0.001 mol) in anhydrous pyridine (15 mL) was refluxed for 4 h. After cooling, the solid product was collected by filtration and recrystallized from pyridine to give yellow crystals, yield 0.254 g, 91%, m. p. 268–270 °C. IR (KBr) ν : 3265, 3152 (2N–H), 1690 (C=O), 1650

(C=O) cm^{-1} . ^1H NMR (DMSO- d_6) δ : 11.20(s, 1H, N–H disappeared on addition of D_2O), 8.83 (s, 1H, N–H disappeared on addition of D_2O), 8.41(s, 1H, N–H disappeared on addition of D_2O), 7.88–7.13 (m, 10H, $\text{H}_{\text{arom}} + \text{H}_{\text{olefin}}$). Anal. Calcd. for: $\text{C}_{15}\text{H}_{12}\text{N}_4\text{O}_2$ (280.28): C, 64.28; H, 4.32; N, 19.99. Found: C, 64.6; H, 4.41; N, 19.7.

Acknowledgement

I would like to express my deep thanks and appreciations for Dr. Mohamed Ismael, lecturer of theoretical chemistry, Faculty of Science, Sohag University, Dr. Sabry Younes, lecturer of organic chemistry, Faculty of Science, Sohag University and Dr. Mohamed Abbas, Professor of organic chemistry, Faculty of Education, Ain shams University.

References

- Singh, K.; Singh, J.; Singh, H. *Tetrahedron* **1998**, 54, 935-942.
- Shawali, A. S.; Haboub, A. J. M. *J. Chem. Res.* **2011**, 35, 341-345.
- Al-Awadi, N. A.; Ibrahim, M. R.; Elnagdi, M. H.; John, E.; Ibrahim, Y. A. *Beilstein J. Org. Chem.* **2012**, 8, 441-447.
- Dominguez, E.; Ibeas, E.; de Maigorta, E. M.; Palacios, J. K.; SanMartin, R. A. *J. Org. Chem.* **1996**, 61, 5435-5439.
- Nikolovaa, S.; Kochovskaa, E.; Ivanov, I. *Synth. Commun.* **2013**, 43, 326-336.
- Khodairy, A. *Synth. Commun.* **2011**, 41, 612-621.
- Nagaraju, V.; Purnachander, D.; Rao Mangina, N. S. V. M.; Suresh, S.; Sridhar, B.; Karunakar, G. V. *Org. Biomol. Chem.* **2015**, 13, 3011-3023.
- Khurana, M.; Salama, N. N.; Scott, K. R.; Nemieboka, N. N.; Bauer, K. S. Jr.; Eddington, N. D. *Biopharm. Drug Dispos.* **2003**, 24, 397-407.
- Thumar, N. J.; Patel, M. P. *Saudi Pharm J.* **2011**, 19, 75-83.
- Michael, J. P.; Koning, C. B.; Hosken, G. D.; Stanbury, T. V. *Tetrahedron* **2001**, 57, 9635-9648.
- Jackson, P. L.; Hanson, C. D.; Farrell, A. K.; Butcher, R. J.; Stables, J. P.; Eddington, N. D.; Scott, R. K. *Eur. J. Med. Chem.* **2012**, 5, 42-51.
- Riyadh, S. M. *Molecules* **2011**, 16, 1834-1853.
- El-Shennawy, A. M.; Mohamed, A. H.; Abass, M. *Medscape Gen. Med. J.* **2007**, 9, 15-33.
- Naringrekar, V. H.; Stella, V. J. *J. Pharm. Sci.* **1990**, 79, 138-146.
- El-Deeb, I. M.; Lee, S. H. *Bioorg. Med. Chem.* **2010**, 18, 3961-3973.
- Rashad, A. E.; Hegab, M. I.; Abdel-Megeid, R. E.; Micky, J. A.; Abdel-Megeid, F. M. E. *Bioorg. Med. Chem.* **2008**, 16, 7102-7106.
- El-Hashim, A.; Yousefi, S.; Edafiogho, I.; Raghupathy, R.; Yousif, M.; Simon, H. *Eur. J. Pharm.* **2010**, 632, 73-78.
- Kolle, U.; Kolb, B.; Mannschreck, A. *Chem. Ber.* **1980**, 113, 2545-2565.
- Crystallographic data have been deposited at the Cambridge Crystallographic Data Centre as supplementary publication number CCDC 964084. Akkurt, M.; Mohamed, S. K.; Elremaily, M. A. A.; Ahmed, E. A.; Albayati, M. R. *Acta Crystallogr. E* **2013**, 69, o1408-o1409.
- Crystallographic data have been deposited at the Cambridge Crystallographic Data Centre as supplementary publication number CCDC 1005600. Mague, J. T.; Mohamed, S. K.; Akkurt, M.; Ahmed, E. A.; Albayati, M. R. *Acta Crystallogr. E* **2014**, 70, o819-o820.
- Hay, P. J.; Wadt, W. R. *J. Chem. Phys.* **1985**, 82, 270-283.
- Janoschek, R. *Pure Appl. Chem.* **2001**, 73, 1521-1553.
- Crystallographic data have been deposited at the Cambridge Crystallographic Data Centre as supplementary publication number CCDC 1015152. Mohamed, S. K.; Akkurt, M.; Mague, J. T.; Ahmed, E. A. and Albayati, M. R. *Acta Crystallogr. E* **2014**, 70, o938-o939.
- Kataoka, T.; Teraoka, J.; Sakoda, A.; Nishiyama, Y.; Yamato, K.; Monden, M.; Ishimori, Y.; Nomura, T.; Taguc, T.; Yamaoka, K. *Inflammation* **2012**, 35, 713-722.
- Winter, C. A.; Risley, E. A.; Nuss, G. W. *Experiment. Biol. Med.* **1962**, 111, 544-547.

DOWEX(R)50WX4/H₂O: A Green System for a One-pot and Three-Component Synthesis of isoxazol-5(4*H*)-one Derivatives

Davood Setamdideh*

Department of Chemistry, Mahabad Branch, Islamic Azad University, Mahabad, Iran.

*E-mail: davood.setamdideh@gmail.com; d.setamdideh@iauh-mahabad.ac.ir

Received May 12th, 2015; Accepted August 3rd, 2015

Abstract. A one-pot and three-component synthesis of 3-methyl-4-arylmethyleneisoxazol-5(4*H*)-ones was developed in the presence of DOWEX(R)50WX4 as the catalyst. The products were obtained in high yields (93-96%) and short reaction times (30-60 min). The present method provides an easy and efficient approach for the synthesis of this class of compounds, because of its clean reaction profile and operational simplicity.

Key words: DOWEX(R)50WX4, isoxazol-5(4*H*)-one, one-pot reaction, water, green chemistry.

Resumen. Se describe el desarrollo de una síntesis de 3-metil-4-arilmetilenoisoxazol-5(4*H*)-onas a través de un método tri-componente en un solo matraz y en presencia de DOWEX(R)50WX4 como catalizador. Los productos se obtuvieron en elevados rendimientos (93-96%) y en tiempos de reacción cortos (30-60 min). Este método representa una alternativa fácil y eficiente para la síntesis de esta clase de compuestos, en razón de un perfil de reacción que evita la formación de subproductos y es de gran simplicidad operacional.

Palabras clave: DOWEX(R)50WX4, isoxazol-5(4*H*)-ona, reacción *one-pot*, agua, química sustentable.

Introduction

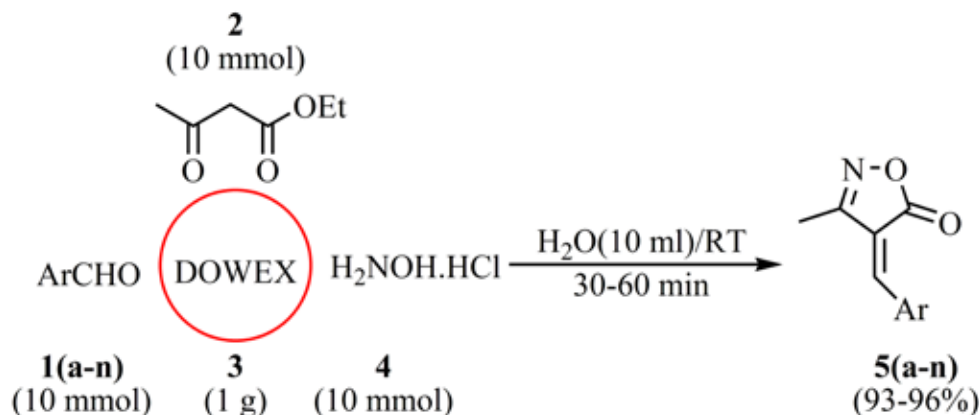
Isoxazole derivatives are a class of heterocyclic compounds featuring a variety of biological activities such as treatment of arthritis [1a], treatment of leishmaniasis [1b], inhibition of protein-tyrosine phosphatase 1B [1c], anti-mycobacterial [1d], anti-convulsing [1e], HDAC inhibitory activity [1f], analgesic [1g-h], nematocidal [1i], anti-oxidant [1j-k], anti-microbial [1l], COX-2 inhibitory [1m], anti-inflammatory [1n], anti-cancer [1o], anti-viral [1p], and anti-tuberculosis [1q]. Furthermore, isoxazolone moieties can also be found in compounds used for the design of liquid crystals [1r], merocyanine dyes in optical research [1s-t], and photochromic components [1u-v]. Literature survey shows that the synthesis of aryl-3-methylisoxazol-5(4*H*)-one derivatives involves a coupling of aromatic aldehydes with ethyl acetoacetate and hydroxylamine. This procedure has been performed by different reagents and catalysts in basic medium such as *via* pyridine [2a], sodium silicate [2b], sodium benzoate [2c], sodium azide [2d], sodium saccharin [2e], sodium citrate [2f], sodium sulfide [2g], sodium ascorbate [2h], and sodium tetraborate [2i]. Also some methods have been carried out at high temperature and long reaction times [2j], with moderate yields [2k], or under unconventional energy sources such as ultrasound irradiation [2k], visible light [2l], and microwave irradiation [2m]. On the other hand, multi-component reactions (MCRs) have been used as very powerful method for the synthesis of a variety of molecules in one-pot reactions. This type of reactions is important in the synthesis of natural products and biologically active compounds, because they have many advantages such as excellent functional group compatibility, minimization of

waste, versatility, atom economy, environmentally friendly, and easy work-up [3].

Recently, we have reported that DOWEX(R)50WX4 (ion-exchange resin) is a strong acid been used for the regioselective synthesis of oximes by using an NH₂OH·HCl/DOWEX(R)50WX4 system [4a], the reduction of a variety of carbonyl compounds such as aldehydes, ketones, α -diketones, acylolins and α,β -unsaturated carbonyl compounds to their corresponding alcohols by applying the NaBH₄/DOWEX(R)50WX4 system [4b], the synthesis of cyanohydrins by NaCN/DOWEX(R)50WX4 [4c], the reductive-amination of a variety of aldehydes and anilines by NaBH₄/DOWEX(R)50WX4 [4d], and for the reductive acylation of aldehydes by borohydrides/Ac₂O/DOWEX(R)50WX4-8 systems [4e-f]. These achievements encouraged us to probe the development of convenient and environmentally benign procedure by DOWEX(R)50WX4 as the catalyst for the synthesis of 4-arylmethylidene-3-substituted-isoxazol-5(4*H*)-ones. Thus, the synthesis of 4-arylmethylidene-3-methyl-isoxazol-5(4*H*)-ones was attempted by using equimolecular quantities of ethyl acetoacetate, hydroxylamine hydrochloride, and a variety of aromatic aldehydes in the presence of DOWEX(R)50WX4 as catalyst in water (Scheme 1).

Results and Discussion

Recognizing the MC-based processes as powerful methods for the synthesis of structurally diverse compounds [3], we conceived the preparation of diverse arylmethylidene-isoxazole-5(4*H*)-ones from the reaction between an aromatic aldehyde, hydroxylamine hydrochloride, and ethyl acetoacetate



Scheme 1. General procedure for the synthesis of (*Z*)-3-methyl-4-arylmethylene-isoxazol-5(4*H*)-ones (**5**) from the corresponding aromatic aldehydes (**1**) with hydroxylamine hydrochloride (**4**) and ethyl acetoacetate (**2**) in the presence of DOWEX(R)50WX4 (**3**) as catalyst in water at room temperature.

(EAA) catalyzed by DOWEX(R)50WX4. In order to determine the optimal reaction conditions, we screened different amounts of DOWEX(R)50WX4 (0-2 g) (Table 1) using benzaldehyde as a model compound. When the amount of DOWEX(R)50WX4 was increased from 0.5 to 1 g, the yield of product was improved from 60 to 95 % (entries 1–2). However, when the amount of DOWEX(R)50WX4 was increased to 2 g, a remarkable increase in the yield of the product was not observed (Table 1, entries 3–4). Consequently, the amount of 1 g for DOWEX(R)50WX4 was selected as the optimized amount of the catalyst for this procedure.

The efficiency of this protocol was examined by the reaction of a variety of aldehydes with electron-donating groups (**5b-e** and **5n**), with electron-withdrawing groups (**5h** and **5k-m**), cinnamaldehyde (**5f**) as an unsaturated aldehyde, and furfural (**5g**) as a heterocyclic aldehyde. In general, aldehydes with donating groups react in shorter times. However, all reactions were completed in appropriate times within 30-60 min in excellent yields (93-96%) (Table 2). The products were characterized by ¹H-NMR spectroscopy, considering the chemical shifts of the olefinic proton of the exocyclic methylene group (Table 2, column 7) and the methyl group (Table 2, column 8), which appear around 7.20-8.40 ppm and

2.21-2.33 ppm, respectively, as singlet signals. The C=O stretching frequency in the FT-IR spectrum of the products appears around 1714-1768 cm⁻¹ (Table 2, column 9). Melting points of the products (Table 2, column 6) were measured and compared with the literature for the known compounds [2]. Two isomeric products the (*E*) and (*Z*)-arylmethylidene moiety are possible in these products. Characterization and comparison of the formed products with suitable references [**2k** and **2l**] supports the selectivity for the formation of the (*Z*)-isomer. Therefore, the products are assumed to have the double bond with the (*Z*) geometry.

Two proposed mechanism for the formation of the products and the influences of DOWEX(R)50WX4 are shown in Schemes 2 and 3. It is likely that the SO₃H groups on DOWEX-(R)50WX4 (as cation-exchange resin and strong acid catalyst) protonate the carbonyl group of ethyl acetoacetate and the aromatic aldehyde. Therefore, DOWEX(R)50WX4 activates aldehyde and ester moieties to produce oxime intermediate (A, scheme 2 and 3). In the first pathway (Scheme 2), the obtained oxime can react with the aromatic aldehyde. Then, the reaction proceeds *via* the intermolecular Knoevenagel addition to give the corresponding adduct (B), which is followed by a ring closure.

Table 1. Optimization reaction condition for the synthesis of (*Z*)-4-benzylidene-3-methylisoxazol-5(4*H*)-one (**5a**) from benzaldehyde (10 mmol), ethyl acetoacetate (10 mmol) and NH₂OH.HCl (10 mmol) in H₂O (10 ml) in the presence of DOWEX(R)50WX4 as shown in scheme 1.

Entry	DOWEX(R)50WX4 (g)	time (min)	conversion (%) ^a	yield (%) ^b
1	0	90	100<	40
2	0.25	90	100<	60
3	0.5	70	100	94
4	1	40	100	95
5	2	30	100	95

^a Conversion refers to TLC monitoring.

^b Yield refers to isolated pure product.

Table 2. Synthesis of (*Z*)-4-arylmethylene-3-methyl-isoxazol-5(4*H*)-ones with DOWEX(R)50WX4/H₂O system as shown in scheme 1.

Entry	Product	Ar	time (min)	yield (%) ^a	mp (°C) ^b	¹ H-NMR (CDCl ₃)/ppm		FT-IR (KBr)/cm ⁻¹
						CH=C	CH ₃	
1 ^c	5a	Ph	40	95	140-142	7.44	2.31	1732
2 ^c	5b	4-MeO-Ph	30	96	177-179	7.34	2.28	1730
3 ^c	5c	2-MeO-Ph	30	95	159-160	8.06	2.31	1732
4 ^c	5d	4-HO-Ph	35	93	214-216	7.80	2.30	1730
5 ^c	5e	2-HO-Ph	35	93	200-202	8.10	2.23	1755
6 ^c	5f	Ph-CH=CH	40	96	180-182	-	2.25	1733
7 ^c	5g	2-furyl	50	93	240-242	7.85	2.32	1748
8 ^d	5h	3-Br-Ph	50	95	141-143	7.35	2.31	1729
9 ^d	5i	4-Me ₂ N-Ph	30	95	206-209	7.27	2.23	1714
10 ^c	5j	4-Me-Ph	40	94	129-131	7.40	2.29	1731
11 ^c	5k	4-F-Ph	50	93	154-156	8.12	2.23	1768
12 ^c	5l	3-F-Ph	50	95	142-144	7.39	2.33	1730
13 ^d	5m	4-O ₂ N-Ph	60	95	163-165	8.25	2.21	1778
14 ^c	5n	4-C ₂ H ₅ O-Ph	60	93	151-153	7.34	2.28	1735

^a Yields refer to isolated pure products after recrystallization in appropriate solvent.

^b The melting points have been compared with the literatures. 5c and 5h are new compounds. [2].

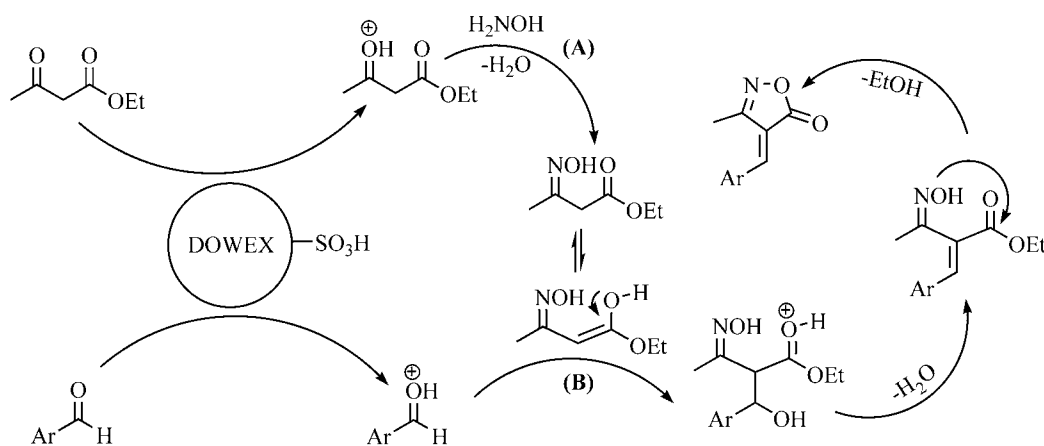
^c The products have been recrystallized in ethanol (96%).

^d The products have been recrystallized in acetone.

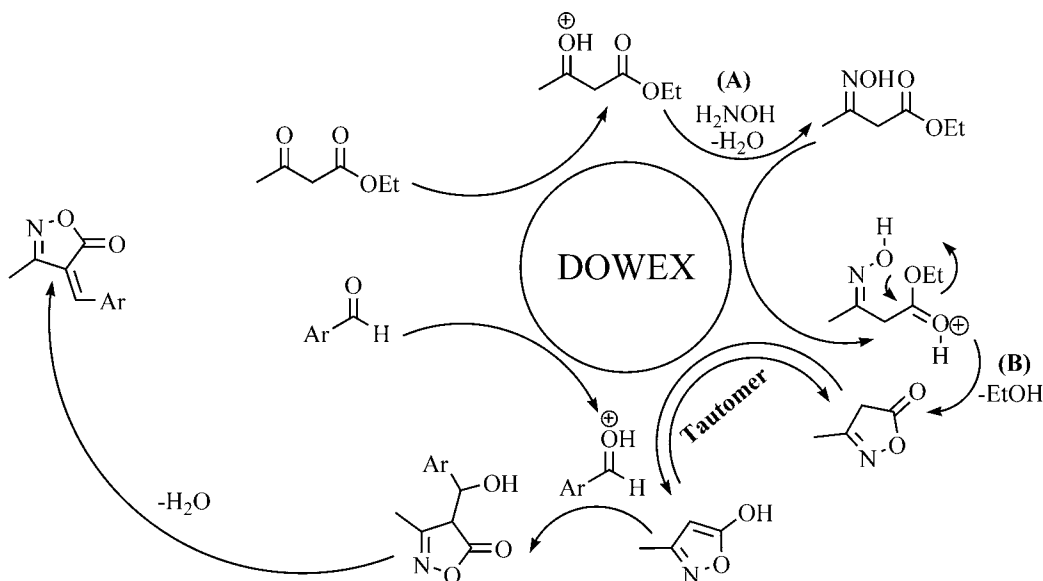
As shown in Scheme 3, an alternative pathway for the mechanism is the formation of the 3-methyl-5(4*H*)-isoxazolone (B) before the alkylidene formation by condensation with the aldehyde. Since the intramolecular attack of the oxime to the ester moiety may be a faster process than the intermolecular Knoevenagel adduct (B, scheme 2), it is expected that the heterocyclic formation were anticipated to the condensation with the aldehyde component.

These mechanisms are supported by carrying the reactions in the absence and presence of the catalyst. As shown in Table 1, without any catalyst, the yields of the products were low even after long periods of time.

In order to show the merit of DOWEX(R)50WX4 in comparison with other catalysts (used for the same reaction), we have tabulated and compared some of the results in Table 3. The comparison shows that the yields and reaction times are improved in the presence of DOWEX(R)50WX4. In addition, the work-up is easier (The ion-exchange resin DOWEX(R)50WX4 is insoluble in H₂O and its removal is very easy), the reaction conditions milder, the catalyst is reused, and by using water as a green solvent, are clear advantages for this new protocol, in comparison with other reported methods, which use more severe conditions and complicate extraction procedures.



Scheme 2. The proposed mechanism for the synthesis of (*Z*)-3-methyl-4-arylmethylene-isoxazol-5(4*H*)-ones in the presence of DOWEX(R)50WX4.



Scheme 3. The another proposed mechanism for the synthesis of (*Z*)-3-methyl-4-arylmethylene-isoxazol-5(*4H*)-ones in the presence of DOWEX(R)50WX4.

Table 3. Comparison of the synthesis of (*Z*)-4-(4-methoxybenzylidene)-3-methylisoxazol-5(*4H*)-one (**5b**) by DOWEX(R)50WX4 and other reported systems.

Entry	Catalyst and conditions	time (min)	yield (%) ^a	Recyclable catalyst	Reference
1	DOWEX(R)50WX4 /H ₂ O/R.T.	30	96	yes	This context
2	Na ₂ S/EtOH/R.T	90	88	no	2g
3	Pyridine/EtOH/reflux	180	71	no	2a
4 ^b	Catalyst free/grinding	48	61	-	2j
5 ^c	Catalyst free/105–110 °C	15	66	-	2j
6	Pyridine/H ₂ O/ultrasound	60	82	no	2k
7	Sodium tetraborate/H ₂ O/R.T.	50	95	no	2i
8	Sodium Benzoate/H ₂ O/R.T.	90	87	no	2c
9	visible light/aq. EtOH/R.T.	10	82	-	2l

^a Isolated yield.

^b The mixture was allowed to stand 12 h after the completion of the reaction.

^c The mixture was allowed to stand overnight after the completion of the reaction.

We have checked the reusability of the catalyst by using the recovered DOWEX(R)50WX4 from the synthesis of (*Z*)-4-benzylidene-3-methylisoxazol-5(*4H*)-one (**5a**) as shown in Table 4. We have observed that the recovered catalyst could be satisfactorily used for the second run without regeneration. Whereas, a third run of the recovered catalyst leads to poor yields and longer reaction times. Likewise, the reaction was also efficient like the first run by carrying out the reaction in the presence of the regenerated DOWEX(R)50WX4 (Table 4, entry 4). Regeneration of the latter was achieved by stirring in HCl 5-10% for 30-60 min, then washed with distilled water.

Conclusion

In conclusion, we have shown that DOWEX(R)50WX4 in water is a convenient catalyst for the preparation of a variety of alkylidene isoxazol-5(*4H*)-ones, using aromatic aldehydes, ethyl acetoacetate, and hydroxylamine hydrochloride precursors in one-pot, three-component condensation reaction at room temperature in excellent yields. High efficiency, shorter reaction times, easy work-up, mild reaction conditions, reuse of catalyst, and using of water as a green solvent make to this new protocol attractive for the synthesis of these heterocycles. Therefore, this

Table 4. Reusability of DOWEX(R)50WX4 in the synthesis of (*Z*)-4-benzylidene-3-methylisoxazol-5(4*H*)-one (**5a**) from benzaldehyde under optimized reaction conditions.

yields (%) ^c	conversion (%) ^b	time (min) ^a	Run Number	Entry
95	100	40	1	1
91	100	50	2	2
60	100<	90	3	3
93	100	40		4 ^d

^a It is the highest time when the reaction ends or dose not further progress.

^b Conversion refers to TLC monitoring (eluent; CH₂Cl₂);

^c Yields refer to isolated pure products (±3%).

^d Regeneration by HCl (5-10%).

new efficient protocol can be added to the list of the currently used methodologies.

Experimental

General. All substrates and reagents were purchased from commercially sources (Merck and Sigma-Aldrich). DOWEX(R)50WX4 (100-200 mesh)(CAS No. 111134-61-4) was prepared from Sigma-Aldrich company. FT-IR, ¹H-NMR, and ¹³C-NMR spectra were recorded on PerkinElmer FT-IR RXI and 300 MHz Bruker spectrometers, respectively. The products were characterized by their FT-IR, ¹H-NMR, and ¹³C-NMR spectra and comparison with authentic samples. Organic layers were dried over anhydrous sodium sulfate. All yields referred to isolated pure products. The purity of products was determinate by ¹H NMR. Also, reactions were monitored over silica gel 60 F₂₅₄ aluminum sheet.

A typical procedure for the synthesis of (*Z*)-4-arylmethylene-3-methyl-isoxazol-5(4*H*)-ones

In a round-bottomed flask (25 mL) equipped with a magnetic stirrer, a mixture of ethyl acetoacetate (1.30 g, 10 mmol), hydroxylamine hydrochloride (0.7 g, 10 mmol), aromatic aldehyde (10 mmol), and DOWEX(R)50WX4 (1 g) in 10 mL of distilled water was prepared and stirred at room temperature for mentioned time in Table 2. After completion of reaction (monitored by TLC), the precipitate was filtered off and washed with cold distilled water. Then products were recrystallized from ethanol or acetone as mentioned in Table 2. Pure (*Z*)-4-arylmethylene-3-methyl-isoxazol-5(4*H*)-ones were obtained as solids after recrystallization from ethanol or acetone and were characterized by ¹H-NMR, ¹³C-NMR, and FT-IR spectroscopy.

Spectral data for prepared compounds:

(*Z*)-4-benzylidene-3-methylisoxazol-5(4*H*)-one (**5a**)

Yellow crystal: mp 140-142 °C (Lit [2k] mp 142-144 °C); ¹H-NMR (300 MHz, CDCl₃): δ 2.31 (s, 3H, CH₃), 7.44 (s, 1H, ArCH=), 7.49-7.59 (m, 3H, Ar), 8.35 (dd, J = 1.3, 7.4 Hz, 2H, Ar); ¹³C-NMR (300 MHz, CDCl₃): δ 11.63 (CH₃), 119.65 (C=, inside

of isoxazolone ring), 129.03 (Ar), 130.47 (Ar), 132.29 (Ar), 134.01 (Ar), 149.98 (ArCH=), 161.16 (C=N), 167.88 (C=O); IR (KBr) v: 1732 (C=O), 1620, 1100, 1216, 879, 763 cm⁻¹.

(*Z*)-4-(4-methoxybenzylidene)-3-methylisoxazol-5(4*H*)-one (**5b**)

Yellow crystal: mp 177-179 °C (Lit [2k] mp 177-178 °C); ¹H-NMR (300 MHz, CDCl₃): δ 2.28 (s, 3H, CH₃), 3.92 (s, 3H, OCH₃), 7.34 (s, 1H, ArCH=), 7.00 (d, J = 8.7 Hz, 2H, Ar), 8.44 (d, J = 8.7 Hz, 2H, Ar); ¹³C-NMR (300 MHz, CDCl₃): δ 11.63 (CH₃), 55.70 (OCH₃), 114.64 (C=, inside of isoxazolone ring), 116.31 (Ar), 125.82 (Ar), 136.96 (Ar), 149.35 (ArCH=), 161.29 (Ar-O), 164.60 (C=N), 168.77 (C=O); IR (KBr) v: 1730 (C=O), 1590, 1267, 1018, 875, 775 cm⁻¹.

(*Z*)-4-(2-methoxybenzylidene)-3-methylisoxazol-5(4*H*)-one (**5c**)

Yellow crystal: mp 159-160 °C; ¹H-NMR (300 MHz, CDCl₃): δ 2.31 (s, 3H, CH₃), 3.95 (s, 3H, OCH₃), 6.96 (d, J = 8.4 Hz, 1H, Ar), 7.09 (t, J = 7.8 Hz, 1H, Ar), 7.56 (t, J = 7.05 Hz, 1H, Ar), 8.06 (s, 1H, ArCH=), 8.92 (d, J = 8.1 Hz, 1H, Ar); ¹³C-NMR (300 MHz, CDCl₃): δ 11.67 (CH₃), 55.47 (OCH₃), 110.70 (C=, inside of isoxazolone ring), 118.32 (Ar), 120.84 (Ar), 121.20 (Ar), 133.37 (Ar), 136.27 (Ar), 143.98 (ArCH=), 159.82 (C=N), 161.52 (C=O); IR (KBr) v: 1732 (C=O), 1590, 1256, 1103, 887, 765 cm⁻¹. IR (KBr) v: 1732 (C=O), 1590, 1256, 1103, 887, 765 cm⁻¹.

(*Z*)-4-(4-hydroxybenzylidene)-3-methylisoxazol-5(4*H*)-one (**5d**)

Yellow crystal: mp 214-216°C (Lit [2k] mp 215-218 °C); ¹H-NMR (300 MHz, CDCl₃): δ 2.30 (s, 3H, CH₃), 6.95 (d, J=9.3 Hz, 2H, Ar), 7.80 (s, 1H, ArCH=), 8.48 (d, J=9.3 Hz, 2H, Ar), 11.06 (s, 1H, OH); IR (KBr) v: 1730 (C=O), 1596, 1556, 1515, 1310, 1234 cm⁻¹.

(*Z*)-4-(2-hydroxybenzylidene)-3-methylisoxazol-5(4*H*)-one (**5e**)

Yellow crystal: mp 200-202 °C (Lit [2f] mp 198-201 °C); ¹H-NMR (300 MHz, CDCl₃): δ 2.23 (s, 3H, CH₃), 6.90 (t, J=6.7 Hz, 1H, Ar), 7.00 (t, J=6.7 Hz, 1H, Ar), 7.48 (t, J=7.4 Hz, 1H, Ar), 8.10 (s, 1H, ArCH=), 8.75 (t, J=7.4 Hz, 1H, Ar); 11.00 (s, 1H, OH); IR (KBr) v: 1755 (C=O), 1590, 1459, 1369, 1312, 1268 cm⁻¹

(*Z*)-3-methyl-4-(3-phenylallylidene)isoxazol-5(4*H*)-one (**5f**)

Yellow crystal: mp 180-182 °C (Lit [2k] mp 179-181 °C); ¹H-NMR (300 MHz, CDCl₃): δ 2.25 (s, 3H, CH₃), 7.28-7.36 (m,

2H, CH=CH), 7.36-7.47 (m, Ar (2H) & ArCH= (1H)), 7.64-7.66 (m, 2H, Ar), 8.26-8.35 (m, 1H, Ar); $^{13}\text{C-NMR}$ (300 MHz, CDCl_3): δ 11.19 (CH_3), 117.86 (C=, inside of isoxazolone ring), 121.34 (Ar), 122.38 (Ar), 129.31 (Ar), 131.53 (C=C), 134.96 (C=C), 147.53 (Ar), 151.45 (ArCH=), 159.89 (C=N), 168.99 (C=O); IR (KBr) ν : 1733 (C=O), 1542, 1103, 993, 848, 753 cm^{-1} .

(Z)-4-(2-furylmethylene)-3-methylisoxazol-5(4H)-one (5g)

Yellow crystal: mp 240-242 °C (Lit [2k] mp 240-242 °C), $^1\text{H-NMR}$ (300 MHz, CDCl_3): δ 2.32 (s, 3H, CH_3), 7.12-7.18 (m, 1H, furyl), 7.85 (s, 1H, furylCH=), 8.11-8.16 (m, 1H, furyl), 8.60-8.67 (m, 1H, furyl); IR (KBr) ν : 1748 (C=O), 1616, 1590, 1318, 1292, 1220, 1176 cm^{-1} .

(Z)-4-(3-bromobenzylidene)-3-methylisoxazol-5(4H)-one (5h)

Yellow crystal: mp 141-143 °C; $^1\text{H-NMR}$ (300 MHz, CDCl_3): δ 2.31 (s, 3H, CH_3), 7.35 (s, 1H, ArCH=), 7.41 (t, J = 8.1 Hz, 1H, Ar), 7.71 (d, J = 7.8 Hz, 1H, Ar), 8.34 (d, J = 7.8 Hz, 1H, Ar), 8.46 (s, 1H, Ar); $^{13}\text{C-NMR}$ (300 MHz, CDCl_3): δ 11.60 (CH_3), 121.12 (Ar-Br), 122.89 (C=, inside of isoxazolone ring), 130.48 (Ar), 131.90 (Ar), 133.87 (Ar), 136.03 (Ar), 136.50 (Ar), 147.71 (ArCH=), 160.86 (C=N), 167.45 (C=O); IR (KBr) ν : 1729 (C=O), 1544, 1217, 1123, 871, 775 cm^{-1} .

(Z)-4-(4-(dimethylamino)benzylidene)-3-methylisoxazol-5(4H)-one (5i)

Red crystal: mp 206-209 °C (Lit [2k] mp 206-207 °C); $^1\text{H-NMR}$ (300 MHz, CDCl_3): δ 2.23 (s, 3H, CH_3), 3.15 (s, 6H, $\text{N}(\text{CH}_3)_2$), 6.71 (d, J = 9 Hz, 2H, Ar), 7.27 (s, 1H, ArCH=), 8.39 (d, J = 9 Hz, 2H, Ar); $^{13}\text{C-NMR}$ (300 MHz, CDCl_3): δ 11.71 (CH_3), 40.10 ($(\text{CH}_3)_2\text{N}$), 111.07 (Ar), 111.50 (C=, inside of isoxazolone ring), 121.51 (Ar), 137.62 (Ar), 149.26 (Ar), 154.22 (ArCH=), 161.59 (C=N), 170.12 (C=O); IR (KBr) ν : 1714 (C=O), 1557, 1380, 1196, 1095, 867, 765 cm^{-1} .

(Z)-4-(4-methylbenzylidene)-3-methylisoxazol-5(4H)-one (5j)

Lemon crystal: mp 129-131 °C (Lit [2j] mp 126-127 °C); $^1\text{H-NMR}$ (300 MHz, CDCl_3): δ 2.29 (s, 3H, CH_3), 2.45 (s, 3H, CH_3), 7.32 (d, J = 7.8 Hz, 2H, Ar), 7.40 (s, 1H, ArCH=), 8.29 (d, J = 7.8 Hz, 2H, Ar); $^{13}\text{C-NMR}$ (300 MHz, CDCl_3): δ 11.65 (CH_3), 22.07 (CH_3), 118.40 (C=, inside of isoxazolone ring), 129.88 (Ar), 134.14 (Ar), 145.73 (Ar), 149.96 (ArCH=), 161.22 (C=N), 168.21 (C=O); IR (KBr) ν : 1731 (C=O), 1594, 1114, 873, 777 cm^{-1} .

(Z)-4-(4-fluorobenzylidene)-3-methylisoxazol-5(4H)-one (5k)

Yellow crystal: mp 154-156 °C (Lit [2k] mp 153-155 °C); $^1\text{H-NMR}$ (300 MHz, CDCl_3): δ 2.23 (s, 3H, CH_3), 6.80 (d, J=8.1 Hz, 2H, Ar), 8.12 (s, 1H, ArCH=), 8.80 (d, J=8.1 Hz, 2H, Ar); IR (KBr) ν : 1768 (C=O), 1612, 1586, 1470, 1375, 1323, 1274 cm^{-1} .

(Z)-4-(3-fluorobenzylidene)-3-methylisoxazol-5(4H)-one (5l)

Yellow crystal: mp 142-144 °C (Lit [2n] mp 142-144 °C); $^1\text{H-NMR}$ (300 MHz, CDCl_3): δ 2.33 (s, 3H, CH_3), 7.20 (m, 1H, Ar), 7.33 (t, J = 7.6 Hz, 1H, Ar), 7.62 (m, 1H, Ar), 7.39 (s, 1H,

ArCH=), 9.00 (m, 1H, Ar); IR (KBr) ν : 1730 (C=O), 1682, 1590, 1524, 1431, 1255, 879 cm^{-1} .

(Z)-4-(4-nitrobenzylidene)-3-methylisoxazol-5(4H)-one (5m)

Orang crystal: mp 163-165 °C (Lit [2k] mp 164-166 °C); $^1\text{H-NMR}$ (300 MHz, CDCl_3): δ 2.21 (s, 3H, CH_3), 6.71-8.90 (m, 4H, Ar), 8.25 (s, 1H, ArCH=); IR (KBr) ν : 1778 (C=O), 1618, 1596, 1489, 1366, 1340, 1281 cm^{-1} .

(Z)-4-(4-ethoxybenzylidene)-3-methylisoxazol-5(4H)-one (5n)

Yellow crystal: mp 151-153 °C (Lit [2n] mp 150-152 °C); $^1\text{H-NMR}$ (300 MHz, CDCl_3): δ 2.33 (t, J = 7.2 Hz, 3H, EtO), 2.28 (s, 3H, CH_3), 4.16 (q, J = 7.2 Hz, 2H, EtO), 6.70 (d, J = 8.6 Hz, 2H, Ar), 7.34 (s, 1H, ArCH=), 8.44 (d, J = 8.6 Hz, 2H, Ar); IR (KBr) ν : 1735 (C=O), 1582, 1556, 1275, 890 cm^{-1} .

Acknowledgments

The authors gratefully appreciated the financial support of this work with the grant No. 02-2905/22092-1393/12/17 by the research council of Islamic Azad University branch of Mahabad.

References

1. a) Knecht, W.; Löffler, M. *Biochem. Pharmacol.* **1998**, *56*, 1259-1264. b) Suryawanshi, S. N.; Tiwari, A.; Chandra, N.; Ramesh.; Gupta, S. *Bioorg. Med. Chem. Lett.* **2012**, *22*, 6559-6562. c) Kafle, B.; Cho, H. *Bull. Korean Chem. Soc.* **2012**, *33*, 275-277. d) Changtam, C.; Hongmanee, P.; Suksamrarn, A. *Eur. J. Med. Chem.* **2010**, *45*, 4446-4457. e) Santos, M. M. M.; Faria, N.; Iley, J.; Coles, S. J.; Hursthouse, M. B.; Martins, M. L.; Moreira, R. *Bioorg. Med. Chem. Lett.* **2010**, *20*, 193-195. f) Conti, P.; Tamborini, L.; Pinto, A.; Sola, L.; Ettari, R.; Mercurio, C.; De Micheli, C. *Eur. J. Med. Chem.* **2010**, *45*, 4331-4338. g) Kano, H.; Adachi, I.; Kido, R.; Hirose, K. *J. Med. Chem.* **1967**, *10*, 411-418. h) Giovannoni, M. P.; Vergelli, C.; Ghelardini, C.; Galeotti, N.; Bartolini, A.; Piaz, V. D. *J. Med. Chem.* **2003**, *46*, 1055-1059. i) Srinivas, A.; Nagaraj, A.; Reddy, C. S. *Eur. J. Med. Chem.* **2010**, *45*, 2353-2358. j) Padmaja, A.; Rajasekhar, C.; Muralikrishna, A.; Padmavathi, V. *Eur. J. Med. Chem.* **2011**, *46*, 5034-5038. k) Padmaja, A.; Payani, T.; Reddy, G. D.; Padmavathi, V. *Eur. J. Med. Chem.* **2009**, *44*, 4557-4566. l) Prashanthi, Y.; Kiranmai, K.; Subhashini, N. J. P.; Shivaraj. *Spectrochim. Acta A.* **2008**, *70*, 30-35. m) Talley, J. J.; Brown, D. L.; Carter, J. S.; Graneto, M. J.; Koboldt, C. M.; Masferrer, J. L.; Perkins, W. E.; Rogers, R. S.; Shaffer, A. F.; Zhang, Y. Y.; Zweifel, B. S.; Seibert, K. *J. Med. Chem.* **2000**, *43*, 775-777. n) Karabasanagouda, T.; Adhikari, A. V.; Girisha, M. *Indian J. Chem. B* **2009**, *48*, 430-437. o) Kamal, A.; Bharathi, E. V.; Reddy, J. S.; Janaki, M.; Ramaiah, D.; Reddy, M. K.; Viswanath, A.; Reddy, T. L.; Shaik, T. B.; Pushpavalli, S. N.; Bhadra, M. P. *Eur. J. Med. Chem.* **2011**, *46*, 691-703. p) Lee, Y. S.; Park, S. M.; Kim, B. H. *Bioorg. Med. Chem. Lett.* **2009**, *19*, 1126-1128. q) Mao, J.; Yuan, H.; Wang, Y.; Wan, B.; Pak, D.; He, R.; Franzblau, S. G. *Bioorg. Med. Chem. Lett.* **2010**, *20*, 1263-1268. r) Tavares, A.; Arruda, B. C.; Boes, E. L.; Stefani, V.; Stassen, H. K.; Campo, L. F.; Bechtold, I. H.; Merlo, A. A. *J. Braz. Chem. Soc.* **2012**, *23*, 880-888.

- s) Zhang, X. H.; Wang, L. Y.; Zhan, Y. H.; Fu, Y. L.; Zhaia, G. H.; Wenc, Z. Y. *J. Mol. Struct.* **2011**, *994*, 371-378. t) Zhang, X. H.; Zhan, Y. H.; Chen, D.; Wang, F.; Wang, L. Y. *Dyes Pigments* **2012**, *93*, 1408-1415. u) Pu, S.; Li, H.; Liu, G.; Liu, W.; Cui, S.; Fan, C. *Tetrahedron* **2011**, *67*, 1438-1447. v) Liu, G.; Liu, M.; Pu, S.; Fan, C.; Cui, S. *Tetrahedron* **2012**, *68*, 2267-2275.
2. a) Zhang, Y. Q.; Ma, J. J.; Wang, C.; Li, J. C.; Zhang, D. N.; Zang, X. H.; Li, J. *Chin. J. Org. Chem.* **2008**, *28*, 141-144. b) Liu, Q.; Wu, R. T. *J. Chem. Res.* **2011**, *10*, 598-599. c) Liu, Q.; Zhang, Y. N. *Bull. Korean Chem. Soc.* **2011**, *32*, 3559-3560. d) Kiyani, H.; Ghorbani, F. *Elixir Org. Chem.* **2013**, *58A*, 14948-14950. e) Kiyani, H.; Ghorbani, F. *Heterocycl. Lett.* **2013**, *3*, 359-369. f) Kiyani, H.; Ghorbani, F. *Heterocycl. Lett.* **2013**, *3*, 145-153. g) Liu, Q.; Hou, X. *Phosphorus, Sulfur Silicon Relat. Elem.* **2012**, *187*, 448-453. h) Kiyani, H. *Org. Chem. Indian J.* **2013**, *9*, 97-101. i) Kiyani, H.; Ghorbani, F. *Open J. Org. Chem.* **2013**, *1*, 5-9. j) Zhang, Y. Q.; Wang, C.; Zhang, M. Y.; Cui, P. L.; Li, Y. M.; Zhou, X.; Li, J. C. *Chin. J. Org. Chem.* **2008**, *28*, 914-917. k) Cheng, Q. F.; Liu, X. Y.; Wang, Q. F.; Liu, L. S.; Liu, W. J.; Lin, Q.; Yang, X. *J. Chin. J. Org. Chem.* **2009**, *29*, 1267-1271. l) Saikh, F.; Das, J.; Ghosh, S. *Tetrahedron Lett.* **2013**, *54*, 4679-4682. m) Fozooni, S.; Gholam Hosseinzadeh, N.; Hamidian, H.; Akhgar, M. R. *J. Braz. Chem. Soc.* **2013**, *24*, 1649-1655. n) Chavan, A. P.; Pinjari, A. B.; Mhaske, P. C. **2014**, *J. Heterocyclic Chem.* doi: 10.1002/jhet.2293.
3. a) Singh, M. S.; Chowdhry, S. *RSC Adv.* **2012**, *2*, 4547-4592. b) Murthy, S. N.; Madhav, B.; Kumar, A. V.; Rao, K. R.; Nageswar, Y. V. D. *Helv. Chem. Acta* **2009**, *92*, 2118-2124. c) Jiang, B.; Wang, X.; Shi, F.; Tu, S. J.; Li, G. *Org. Biomol. Chem.* **2011**, *9*, 4025-4028. d) Wan, J. P.; Liu, Y. *RSC Adv.* **2012**, *2*, 9763-9777. e) Dömling, A.; Wang, W.; Wang, K. *Chem. Rev.* **2012**, *112*, 3083-3135. f) Ramón, D. J.; Yus, M. *Angew. Chem. Int. Ed.* **2005**, *44*, 1602-1634. g) de Graaff, C.; Ruijter, E.; Orru, R. V. A. *Chem. Soc. Rev.* **2012**, *41*, 3969-4009. h) Ugi, I. *Pure Appl. Chem.* **2001**, *73*, 187-191. i) Kumaravel, K.; Vasuki, G. *Curr. Org. Chem.* **2009**, *13*, 1820-1841. j) Chanda, A.; Fokin, V. V. *Chem. Rev.* **2009**, *109*, 725-748. k) Gu, Y. *Green Chem.* **2012**, *14*, 2091-2128. l) Siamala, M. *Org. Prep. Proced. Int.* **2009**, *41*, 1-68.
4. a) Setamdideh, D.; Khezri, B.; Esmaeilzadeh, S. *J. Chin. Chem. Soc.* **2012**, *59*, 1119-1124. b) Setamdideh, D.; Khezri, B.; Alipour-amjad, A. *J. Chin. Chem. Soc.* **2013**, *60*, 590-596. c) Sofighaderi, S.; Setamdideh, D. *Orient. J. Chem.* **2013**, *29*, 1135-1137. d) Setamdideh, D.; Sepehraddin, F. *J. Mex. Chem. Soc.* **2014**, *58*, 22-26. e) Azizi Asl, P.; Setamdideh, D. *J. Chin. Chem. Soc.* **2014**, *59*, 940-944. f) Setamdideh, D. *J. Mex. Chem. Soc.* **2014**, *58*, 230-234.

Kaolin Bleaching by Leaching Using Phosphoric Acid Solutions

Román A. Hernández Hernández,^{1*} Felipe Legorreta García,¹ Leticia E. Hernández Cruz,¹ Arnoldo Bedolla Jacuinde²

¹ Universidad Autónoma del Estado de Hidalgo, Área Académica de Ciencias de la Tierra y Materiales. Carretera Pachuca-Tulancingo, Km 4.5 s/n, Mineral de la Reforma, Hgo., México, C.P. 42184.

² Universidad Michoacana de San Nicolás de Hidalgo, Instituto de Investigaciones Metalúrgicas. Av. Francisco J. Mujica S/N Ciudad Universitaria, Morelia, Michoacán, México, C.P. 58000.

*angelitofox3@hotmail.com

Received October 3rd, 2013; Accepted August 20th, 2015.

Abstract. This paper presents a study of kaolin ore bleaching from the municipality of Agua Blanca of Iturbide, Hidalgo, México. This process was carried out using solutions of phosphoric acid as the leaching reagent for the iron dissolution process. It is well known that iron oxide is the major contaminant of clay minerals and silicate used in industry. These contents should be decreased, usually by 0.1%, to achieve a required whiteness index of 90% (ISO) or higher. The whitening improves its economic value, making it possible to use it as a high-quality raw material in industries such as ceramics and paper. For this purpose, we examined the effect of parameters such as the concentration of the leaching reagent (0.10 M, 0.50 M, 1 M, and 3 M), temperature (298-373 K), and pH level (1, 2 and 3). The experimental results showed that the studied variables have a great influence over the ability to obtain an iron dissolution percentage of more than 98% after 2 hours and 373 K.

Key words: Leaching, Phosphoric acid, Kaolin, Iron.

Resumen. En este trabajo se presenta un estudio para el blanqueo de mineral de caolín del municipio de Agua Blanca de Iturbide, Hidalgo (México), que se llevó a cabo utilizando soluciones de ácido fosfórico como reactivo de lixiviación para el proceso de disolución de hierro. Se sabe que el óxido de hierro es el principal contaminante de minerales arcillosos y silicatos utilizados en la industria. Estos contenidos se deben disminuir, por lo general 0.1% para alcanzar un índice de blancura requerida de 90% (ISO) o superior. Su blanqueamiento mejora el valor económico que le da la posibilidad de ser utilizados como materia prima de alta calidad en industrias como la cerámica y papel. Por esta razón hemos estudiado el efecto de los parámetros tales como concentración del reactivo de lixiviación (0.10 M, 0.50 M, 1 M y 3 M), temperatura (25 a 100 °C) y el pH (1, 2 y 3). Los resultados experimentales mostraron que las variables estudiadas tienen gran influencia en la obtención del porcentaje de disolución de hierro de más de 98% después de 2 h y temperatura de 100 °C.

Palabras clave: Lixiviación, Ácido fosfórico, Caolín, Hierro.

Introduction

The term kaolin is used to refer to white clays, whereby the principal mineral is kaolinite ($\text{Al}_2\text{Si}_2\text{O}_5(\text{OH})_4$). The Kaolin particles are usually hexagonal and 0.05-10 μm in diameter (0.5 μm on average). Since this mineral is a product of the decomposition of feldspars and micas present in pegmatite micaceous schist, it is usually accompanied by other minerals such as quartz, sulfur, feldspars, micas, and iron and titanium oxides, among others [1, 2]. The main uses of kaolin are: paper filling and coating (45%); refractories and ceramics (31%); fiberglass (6%); cement (6%); rubber and plastic (5%); paint (3%); and others (4%) [3].

Iron is the main contaminant in clay and kaolin minerals. In fact, the presence of this impurity in these minerals lowers their economic value and makes it impossible to use them in numerous traditional (i.e., the production of ceramic products and paper) and more advanced applications. The high quality of these industrial minerals is generally obtained via physical or chemical processes.

When one considers that conventional processes do not succeed in removing the aforementioned metal, it is under-

standable that numerous studies have focused on improving the dissolution process. These studies are generally carried out on synthetic iron oxide and, therefore, they do not consider the interactions with nonferrous minerals (for example, they do not take into consideration the presence of encapsulated iron), which cause a significant change in the dissolution process kinetics.

Several physical and chemical processes, such as sieving, magnetic separation [4], selective flocculation [5], leaching with chemicals like oxalic and other organic acids [6-11], organic acids in the presence of a fermented medium [12], leaching containing microbial-produced oxalic and hydrochloric acid [13], EDTA [14], sodium dithionate- H_2SO_4 mixtures [15], and so on, have been employed to lower the content of these impurities in the kaolin clays.

In this study, the application of phosphoric acid to bleach kaolin clays is reported for the first time. Furthermore, the residual solutions that have formed can be used to manufacture ceramics [16]; this is the primary reason why, in this paper, we elected to present the results we obtained once we tested the efficiency of H_3PO_4 when purifying kaolin clays. Furthermore, we also sought to optimize the process parameters, while exam-

ining the effects of temperature, pH, and concentration of the leaching agent on the recuperation percentages to obtain mineral kaolin with low iron contents.

Experiment

Reagents and Materials

The kaolin mineral sample was obtained from Agua Blanca Iturbide (Hidalgo, México), which had been previously reduced in size and classified by ASTM mesh. A complete chemical analysis by atomic absorption spectrophotometry is shown in Table 1. The iron content in the mineral was $0.70\% \pm 0.01\%$, reported as Fe_2O_3 . Mineral particles with an average size of $35\ \mu\text{m}$ were used in the leaching experiment. Phosphoric acid (reagent grade; J.T. Baker, Center Valley, PA, USA) was used as a leaching agent. The leaching system that was used consisted of a heating mantle, a 500 mL Pyrex glass reactor with a condenser, and magnetic stirring. A centrifuge was used (Model 228; Thermo Fisher Scientific, Waltham, MA, USA) for solid-liquid separation of the sample that was collected to quantify the dissolved iron. Iron was quantified using atomic absorption spectrophotometry (Optima 3000 XL; Perkin Elmer Inc., Waltham, MA, USA). To determine the mineral species present in the kaolin samples, X-ray diffraction patterns were determined using an Equinox 2000 diffractometer (I.N.E.L. Instrumentation Electronique, Artenay, France), with $\text{Cu K}\alpha$ radiation at 40 kV and 40 mA.

Experiment design

The leach solution was prepared by mixing known amounts of phosphoric acid (H_3PO_4 , reagent grade) with distilled water. Sulfuric acid was slowly added to adjust the pH to the required value. The liquor (volume 400 mL) was then transferred to a round flask (capacity: 0.50 L); to obtain different temperatures before adding the clay sample (40 g), a heating mantle controlled by a thermostat was used. The kaolin was suspended by

Table 1. Chemical Analysis of the kaolin sample.

Components	% Weight
SiO_2	54.30
Al_2O_3	43.10
Fe_2O_3	0.700
CaO	0.004
MgO	0.006
Na_2O	0.265
K_2O	0.349
TiO_2	0.418
LIO*	0.950

LIO* = Lost on Ignition.

magnetic stirring. In the leaching tests at 373 K, the reactor was equipped with a thermometer and a reflux condenser. All leaching tests were carried out at atmospheric pressure. Each reaction was conducted for 2 h and samples were taken out at 5, 15, 30, 60, 90, and 120 min for iron analysis. For each sample, 10 mL of liquor was withdrawn from the reactor into a 25 mL volumetric flask. This sample was vacuum filtered and then immediately centrifuged at 300 rpm for 15 min. A 5 mL aliquot of clear solution was collected to determine the total iron concentration. The analysis was performed using atomic absorption spectrometry. The solution pH level was controlled at a pH of 1.0, 2.0, or 3.0 using sulfuric acid. Experiments were performed in duplicate. The variables studied were the concentration of phosphoric acid, pH, and temperature.

Results and discussion

Mineralogical Analysis

X-ray diffraction analysis revealed the nature of the crystalline phases present in the mineral, as shown in Fig. 1. The study sample is mainly constituted by the kaolinite mineral with minor silica contributions, which were also detected as quartz and tridymite. Iron is considered to be an impurity and it is present as magnetite (Fe_3O_4), hematite (Fe_2O_3), titanium oxide-ferrous (Fe_2TiO_4), and greigite (Fe_3S_4).

A decrease in the peaks that correspond to magnetite and hematite was also shown for (a) natural kaolin mineral and (b) leached kaolin; according to this finding, we can observe that during the leaching process, it is possible to reduce the iron content.

Effect of Acid Concentration

To observe the effect of different phosphoric acid concentrations of 0.10, 0.50, 1.0, and 3.0 M, experiments were performed

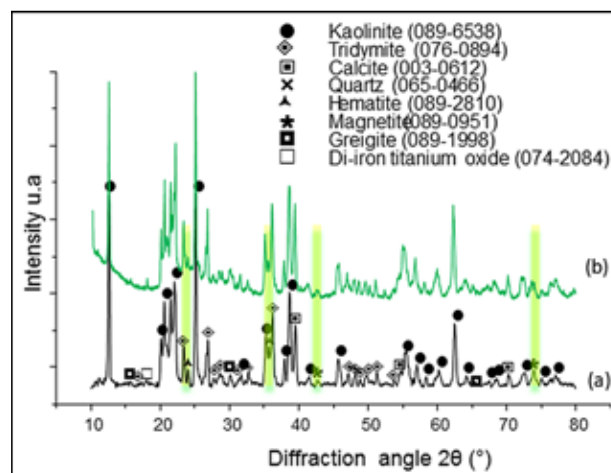


Fig. 1. X-ray diffractogram of: a) kaolin mineral and b) leached kaolin.

in the range of 298-373 K at a pH level of 1. Fig. 2 shows that increasing the phosphoric acid concentration increase the iron dissolution rate from kaolin clay. It was also observed that the iron leaching rate at 1.0 M is higher than at 0.10 M, where the iron dissolution rates were 98.65% and 19.81%, respectively. It was also observed that the curves showed (see Fig. 2) for 1.0 M and 3.0 M presented similar behavior trends and iron dissolution rates from the kaolin clays. Thus, we can conclude that this concentration range no longer affects the kinetics above 1.0 M at these conditions.

The results found in this study are also in accordance with those of another study [17], which reported a high efficiency rate of iron removal; however, unlike the methods used in this work, the other study was carried out on quartz sand using phosphoric acid.

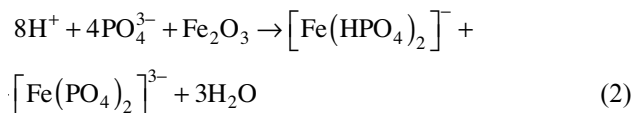
Hydrogen ions play an important role in the dissolution of iron oxides with inorganic acids. H_3PO_4 in solution provides H^+ , which reacts with iron oxide; the possible reaction according to Zhizhen et al [17] might be:



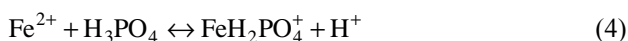
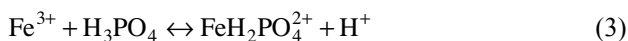
These hydrogen ions are absorbed on the surface by activating the iron mineral particle surface. The hydrogen ions are adsorbed on sites on the solid surface, creating surface-active centers on which the main reaction for dissolution takes place. According to adsorption theory, as the hydrogen ion concentration in the solution increases, the amount of adsorbed hydrogen ions also increases. An increase in the number of active centers results in a corresponding increase in the dissolution rate [14].

H_3PO_4 does not only provide more H^+ ions ($\text{PK}_{a1}=2.12$, where a_1 =first dissociation H^+), which will react with iron oxide, but the PO_4^{3-} ions that are produced during the course of H^+ ionization also have a larger complexing ability toward iron ions. All of these features constitute the highest leaching percentages of H_3PO_4 .

The possible reaction according Zhizhen et al [17] is the following:



Moreover, Al-Sogair et al [18, 19] proposed the following reactions of iron with phosphoric acid:



The iron content in the kaolin analysis that was performed after 2 h was 0.004 g, as determined by traditional metallurgical balance and atomic absorption spectrophotometry. The iron conversion was as follows: the reaction (1) takes place during iron dissolution. First, phosphoric acid dissociation occurs; following that, the dissolution of iron in the ore. Subsequently,

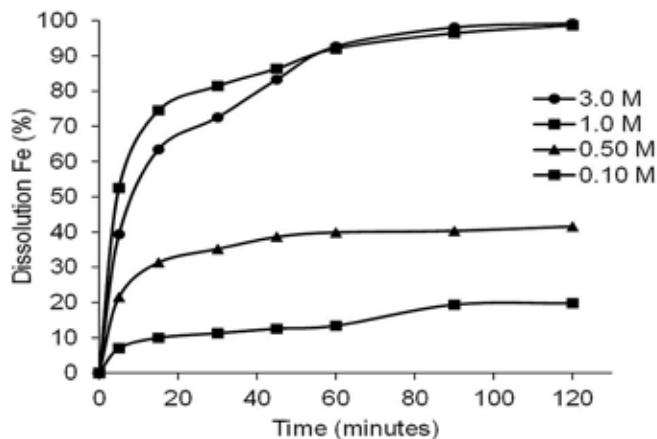


Fig. 2. Effect of phosphoric acid concentration on Fe dissolution from kaolin clay at 373 K, pH 1.0.

the formation of different iron phosphate complexes occurs, according to reactions (2), (3), and (4). These multiple synergisms of H_3PO_4 yield the best leaching results. The phosphate anion constitutes an important part of the mechanism [20]. The phosphate anion reacts strongly with both ferric and ferrous ion complexes, to such an extent that iron phosphates are only soluble when the anion is not completely dissociated. This is the principal reason for the successful bleaching of kaolin by phosphoric acid.

Effect of Reaction Temperature

In order to study the effect of temperature on iron dissolution, several experiments were carried out in the temperature range of 298-373 K in 1.0 M phosphoric acid solutions with a constant pH of 1. The typical rate curves are shown in Fig. 3. From this figure, it can be seen that the dissolution rate is highly sensitive to the reaction temperature. It can also be observed that the iron dissolution was very slow at temperatures in the range of 273-313 K, but this rate increased rapidly above 333 K. This indicates that a reasonable reaction rate can only be achieved at temperatures above 353 K. Therefore, iron dissolution using phosphoric acid could be thermally activated to improve the efficiency of this process.

Effect of pH

The effect of pH was studied through a series of tests performed at 373 K in a 3.0 M phosphoric acid solution and with pH values varying between 1 and 3. The results are presented in Fig. 4. The rate of iron dissolution is significantly affected by pH. The optimum dissolution rate is observed at a pH level of 1, whereas in less acidic solutions, the dissolution rate decreases.

To better explain the effect of pH on iron dissolution and the corresponding reactions, we developed distribution diagrams for Fe^{2+} and Fe^{3+} (see Figs. 5 and 6, respectively) using the Medusa software program (Chemical Equilibrium Dia-

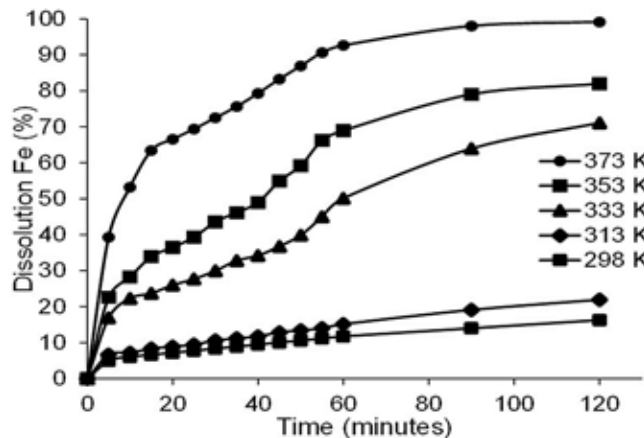


Fig. 3. Effect of temperature on Fe dissolution from kaolin clays, 1.0 M phosphoric acid, pH 1.0.

grams). Due to the lack of equilibrium data for other temperatures, we presented the diagrams at 298 K. The phosphate anion strongly complexes both ferric and ferrous ions; nevertheless, the iron phosphates are only soluble when the anion is not completely dissociated (pH < 2 and 4 for ferric and ferrous ions, respectively). This is the principal reason behind the successful bleaching of kaolin with phosphoric acid.

As stated above, increased temperature favors both iron dissolution and the formation of complexes (iron phosphate). When the kaolin mineral is added to a phosphoric acid solution, pH affects the speciation in the solution. In strong acid solutions (pH 1.0), the ferric iron ions are complexed as $[\text{FeH}_2\text{PO}_4^{2+}]$ (eq. 3), and as the pH level increases, the amount of these complex ions in the solution begins to decrease. Furthermore, with pH values higher than 2.0, most of the iron ions are in the form of solid $[\text{FeHPO}_4 \cdot 2\text{H}_2\text{O}]$, which is when water-insoluble tertiary phosphates tend to precipitate. From the aforementioned findings, it can be deduced that the complexation of iron ions

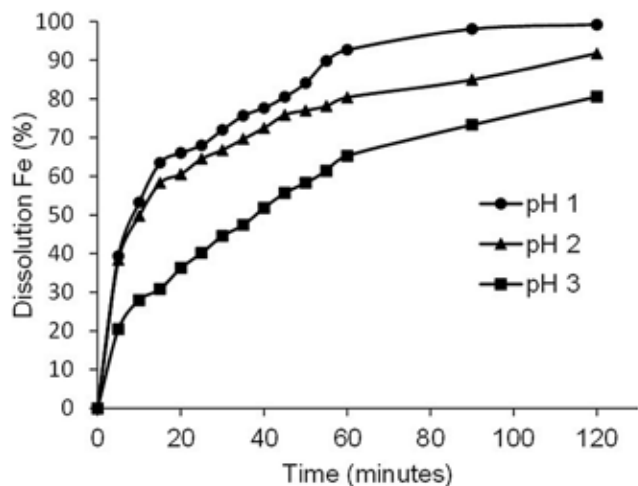


Fig. 4. Effect of pH on Fe dissolution from kaolin clays, 3.0 M phosphoric acid, 373 K.

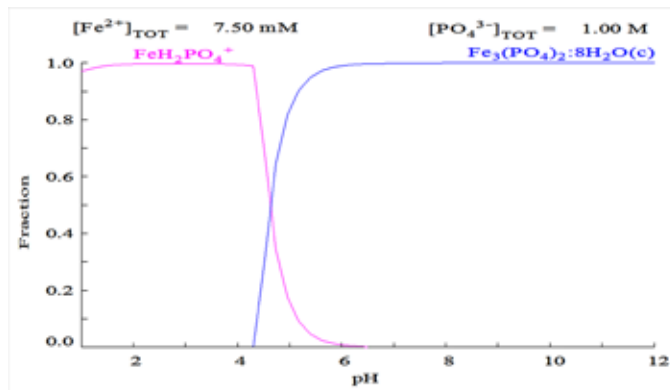


Fig. 5. Diagram species (Fe 7.5 mM) with 1.0 M phosphoric acid for Fe^{2+} .

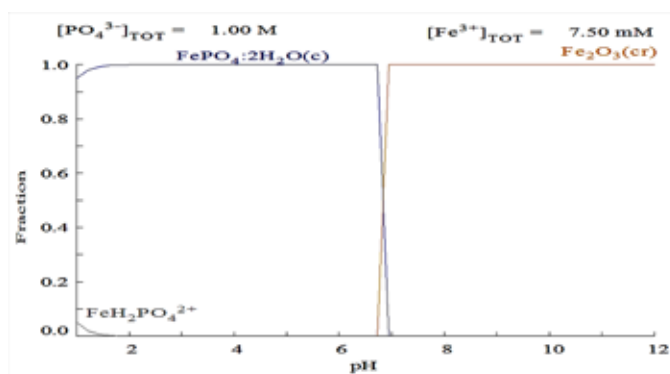


Fig. 6. Diagram species (Fe 7.5 mM) with 1.0 M phosphoric acid for Fe^{3+} .

must occur in strong acid solutions. Experimentally, this is found at pH values around 1.0-1.5.

Conclusions

The application of phosphoric acid to bleaching kaolin clays is reported for the first time. The experimental results obtained in this study showed that phosphoric acid is one of the best leaching reagents in the purification of iron impurities from kaolin clays, particularly due to the properties of H_3PO_4 itself (it is very soluble in water, it acts as a chelating agent, and it dissociates at relatively low pH values). Also, the phosphate anion reacts strongly with complexes of both ferric and ferrous ions; this is the principal reason underlying the successful bleaching of kaolin with phosphoric acid. It was also observed that the leach rate is influenced by both pH level and the reaction temperature. To be effective above 353 K, phosphoric acid must to be thermally activated. Moreover, the dissolution rate decreases with increasing pH; this is due to the formation of $[\text{FePO}_4 \cdot 2\text{H}_2\text{O}]$, which tend to precipitate. The best conditions for removal of iron were found to be a temperature of 373 K, a solid-to-liquid ratio of 10%, kaolin clays with an average particle size of 35 μm a pH of 1.0, and a phosphoric acid concentration of 3.0 M.

References

1. Avgustinik, A. In: *Cerámica*, Ed. Reverté S.A., Barcelona, 1983.
2. Norton, A. *Cerámica Fina*, Ed. Omega, Barcelona, 1983.
3. Murray, H. *Min. Miner.* **2002**, 64, 1-9.
4. Shoumkov, S.; Dimitrov, Z.; Brakalov, L. *Interceram*, **1987**, 36, 26-38.
5. Besraa, L.; Senguptaa, D.; Royb, S.; Ay, P. *International Journal of Mineral Processing*, **2002**, 66, 203-232.
6. Lee, S.; Tran, T.; Jung, B.; Kim, S.; Kim, M. *Hydrometallurgy*, **2007**, 87, 91-99.
7. Martínez-Luévanos, A.; Rodríguez-Delgado, M. G.; Uribe-Salas, A.; Carrillo-Pedroza, F. R.; Osuna-Alarcón, J. G. *Applied Clay Science*, **2011**, 51, 473-477.
8. Pantias, D.; Taxiarchou, M.; Paspaliaris, I.; Kontopoulos, A. *Hydrometallurgy*, **1996**, 42, 257-265.
9. Veglio, F.; Toro, L. *Int. J. Miner. Process.* **1993**, 39, 87-99.
10. Legorreta-García, F.; Salinas-Rodríguez, E.; Hernández-Cruz, L. E.; Hernandez-Hernández, R.A.; Cerecedo Sáenz E.; *European Scientific Journal.*, **2015**, 11, 12-23.
11. De Mesquita, L.; Rodrigues, T.; Gomes, S. *Miner. Eng.*, **1996**, 9, 965-971.
12. Hosseini, M.R.; Ahmadi A. *Applied Clay Science.*, **2015**, revised version submitted for publication.
13. Groudev, S. *Miner. Metall. Process.*, **1999**, 16, 19-28.
14. Borggaard, O. *J. Soil Sci.*, **1979**, 30, 727-734.
15. Ambikadevi, V.R.; Lalithambika, M. *Applied Clay Science*, **2000**, 16, 133-145.
16. Arun, S.; Wagh, Y.; Seung, Y. *Journal of the American Ceramic Society*, **2003**, 86, 1850-1855.
17. Zhizhen, Z.; Jingsheng, L.; Xiaoxia, L.; Houquan, H.; Lifan, Z.; Tiantian, X. *International Journal of Mineral Processing*, **2012**, 114, 30-34.
18. Al-Sogair, F.; Marafie, H. M.; Shuaib, N. M.; Youngo, H. B.; El-Ezaby, M. S. *J. Coord. Chem.*, **2002**, 55, 1097-1109.
19. Ueshima, M.; Fortin, D.; Kalin, M. *Geomicrobiology Journal*, **2004**, 21, 313-323.
20. Majima, H.; Awakura, Y.; Mishima, T.; *Met. Trans.* **1985**, 16B, 23-30.

Application of Wavelet and Genetic Algorithms for QSAR Study on 5-Lipoxygenase Inhibitors and Design New Compounds

Fatemeh Bagheban Shahri*, Ali Niazi and Ahmad Akrami

Department of Chemistry, Arak Branch, Islamic Azad University, Arak, Iran

Corresponding author. Email: f-bagheban@iau-arak.ac.ir, f.baghebanshahri@gmail.com

Fax: +98 86 34057336

Received January 1st, 2015; Accepted September 4th, 2015

Abstract. A quantitative structure-activity relationship (QSAR) modeling was carried out for the prediction of inhibitory activity of 1-phenyl[2H]-tetrahydro-triazine-3-one analogues as inhibitors of 5-lipoxygenase. Partial least squares (PLS) algorithm was employed to model the relationships between molecular descriptors and inhibitory activity of molecules using the genetic algorithm (GA) method as variable selection tool. Pre-processing methods such as wavelet transform (WT) were also used to enhance the predictive power of multivariate calibration methods. To evaluate the models applied in this study (PLS, GA-PLS and WT-GA-PLS), the inhibitory activities of several compounds, not included in the modeling procedure, were predicted. The results of models showed high prediction ability with root mean square error of prediction 0.194, 0.161 and 0.140 for PLS, GA-PLS and WT-GA-PLS, respectively. The WT-GA-PLS method was employed to predict the inhibitory activity of the new inhibitor derivatives.

Key words: 1-phenyl[2H]-tetrahydro-triazine-3-one analogues, genetic algorithms, wavelet transform, QSAR, PLS.

Resumen. Se realizó la modelación de una relación estructura-actividad (QSAR, por sus siglas en inglés) para la predicción de la actividad inhibitoria de análogos del 1-fenil[2H]-tetrahydro-triazina-3-ona como inhibidores de la 5-lipoxigenasa. Se utilizó el algoritmo de mínimos cuadrados parciales (PLS, por sus siglas en inglés) para simular las relaciones entre los descriptores moleculares y la actividad inhibitoria de moléculas, usando el método de algoritmos genéticos (GA, por sus siglas en inglés) como herramienta de selección de variables. También se utilizaron métodos de preprocesamiento como transformada de ondeleta (WT, por sus siglas en inglés) para incrementar el poder predictivo de los métodos de calibración multivariable. Para evaluar los modelos aplicados en este estudio (PLS, GA-PLS y WT-GA-PLS), se evaluaron las actividades inhibitorias de varios compuestos no incluidos en el proceso de modelación. Los resultados de los modelos mostraron una alta capacidad predictiva con un error cuadrático medio en la predicción de 0.194, 0.161 y 0.140 para PLS, GA-PLS y WT-GA-PLS, respectivamente. Se utilizó el método WT-GA-PLS para predecir la actividad inhibitoria de nuevos derivados inhibidores.

Palabras clave: Análogos del 1-fenil[2H]-tetrahydro-triazina-3-ona, algoritmos genéticos, transformada de ondeleta, QSAR, PLS.

Introduction

Lipoxygenases (LOs) are a class of widely occurring, non-heme iron-containing oxygenases that can be isolated from animals, higher plants, and fungi. Currently, three distinct mammalian LOs have been characterized, 5-LO, 12-LO, and 15-LO, which oxygenate arachidonic acid at specific carbon centers (C5, C12, and C15, respectively) [1]. The 5-lipoxygenase is the first dedicated enzyme in the biosynthetic pathway leading to the leukotrienes. Since leukotrienes have been implicated as important mediators in such diseases as asthma, psoriasis, ulcerative colitis, and rheumatoid arthritis, the inhibition of 5-lipoxygenase offers a potential approach in the therapy of such diseases [2]. In the present study, the inhibitory activity of 1-phenyl[2H]-tetrahydro-triazine-3-one analogues as inhibitors of 5-lipoxygenase were used to construct a mathematical model with structural information, so called a quantitative structure-activity relationship (QSAR).

QSAR is an important tool in Agrochemistry, Pharmaceutical Chemistry and Toxicology [3, 4]. QSAR models are mathematical equations, which relate chemical structure of a

compound to its physical, chemical, biological and technological properties. The main goal of the QSAR studies is to establish an empirical rule or function to relate the structural descriptors of compounds under investigation to bioactivities. This rule or function is then utilized to predict the same bioactivities of compounds which are not involved in the training set from their structural descriptors. Model development in QSAR studies comprises different critical steps as (1) descriptor generation, (2) data splitting to calibration (or training) and prediction (or validation) sets, (3) variable selection, (4) finding appropriate model between selected variables and activity and (5) model validation [5]. Since a large number of molecular descriptors are available for QSAR analysis, the most relevant descriptors should be selected. Many variable selection methods such as stepwise regression [6], simulated annealing [7] and genetic algorithms [8-10] are available. It has been shown that genetic algorithms (GAs) can be successfully used as a feature selection technique [11-13].

A GA is a stochastic method to solve optimization problems defined by a fitness criterion applying evolution hypothesis of Darwin and different genetic functions, i.e. crossover and

mutation. Leardi [14] demonstrated that GA, after suitable modifications, produces more interpretable results, since the selected variables are less dispersed compared to other methods. Among the investigation of QSAR, one of the most important factors affecting the quality of the model is the method to build the model. Many multivariate data analysis methods such as multiple linear regression (MLR) [15, 16] artificial neural network (ANN) [17] and partial least squares (PLS) [18] have been used in QSAR studies. MLR, as most commonly used chemometrics method, has been extensively applied to QSAR investigations. However, due to the collinearity between descriptors, MLR is unable to extract useful information from the data, and the over-fitting problem will occur as a consequence. The artificial neural network (ANN) offers satisfactory accuracy in most cases but tends to over fit the training data. The PLS method is based on the factor analysis which is originally suggested and chemically applied by Wold et al [19]. In order to enhance the predictive power of multivariate calibration methods, molecular descriptors are often corrected prior to the data analysis. One of the data preprocessing techniques is wavelet transform (WT) [20], which used to eliminate undesirable background effects and enhance the subsequent PLS regression model. In this study, the PLS, GA-PLS and WT-GA-PLS methods were proposed to model and predict the inhibitory activity of 1-phenyl[2H]-tetrahydro-triazine-3-one analogues as inhibitors of 5-Lipoxygenase.

Material and Computational Methods

Hardware and Software

The computations were made with the ASUS Personal Computer that was equipped with the Windows 7 operating system and MATLAB (Version 11.0, Math Work Inc.). All the required evaluations for GA variable selection and PLS modeling were carried out using the PLS program from PLS-Toolbox Version 4.0 and MATLAB from Eigenvector Research Inc. The calculations for data processing implemented in software using MATLAB Wavelet Toolbox and DWT technique. Kennard-Stones program was written in MATLAB according to the algorithm [21, 22]. ChemOffice package (Version 2013) was used to draw the molecular structure and optimization by the AM1. Descriptors were calculated using Dragon software (Milano Chemometrics and QSAR research group, <http://www.disat.unimib.it/chm/>). These descriptors are calculated using two-dimensional representation of the molecules and therefore geometry optimization is not essential for calculating these types of descriptors.

Data Set

The inhibitory activity values of 1-phenyl[2H]-tetrahydro-triazine-3-one analogues were taken from the literature [2]. The chemical structures of 1-phenyl[2H]-tetrahydro-triazine-3-one analogues (Fig. 1) and their corresponding inhibitory activity values have been listed in Table 1. In order to assure that train-

ing and prediction sets cover the total space occupied by the original data set, it was divided into parts of training and prediction set according to the Kennard-Stones algorithm [21, 22]. The Kennard-Stones algorithm is known as one of the best ways of building training and prediction sets, and it has been used in many QSAR studies. The Kennard-Stone algorithm selects a set of molecules in studied set of data, which are uniformly distributed over the space defined by the candidates. This is a classic technique to extract a representative set of molecules from a given data set. In this technique the molecules are selected consecutively. The first two objects are chosen by selecting the two farthest apart from each other. The third sample chosen is the one farthest from the first two objects, etc. Supposing that m objects have already been selected ($m < n$), the $(m + 1)^{\text{th}}$ sample in the calibration set is chosen using the following criterion:

$$\max(\min(d_{1r}, d_{2r}, \dots, d_{mr})) \{ \max(m < r \leq n) \} \quad (1)$$

Where, n stands for the number of samples in the training set, d_{jr} , $j=1, \dots, m$ are the squared euclidean distances from a candidate sample r , not yet included in the representative set, to the m samples already included in the representative set [23].

Molecular Descriptors

A major step in constructing QSAR model is the generation of the corresponding numerical descriptors of the molecular structures. Molecular descriptors define the molecular structure and physicochemical properties of molecules by a single number. To calculate different kinds of theoretical descriptors for each molecule, the Dragon (Milano Chemometrics and QSAR research group, <http://www.disat.unimib.it/chm/>) software was utilized. The Dragon is able to calculate different molecular descriptors such as constitutional, topological, molecular walk counts, BCUT, Galvez topol, Charge indices, 2D autocorrelations, charge, aromaticity indices, Randic molecular profiles, geometrical, RDF, 3D-MoRSE, WHIM, GETAWAY, functional

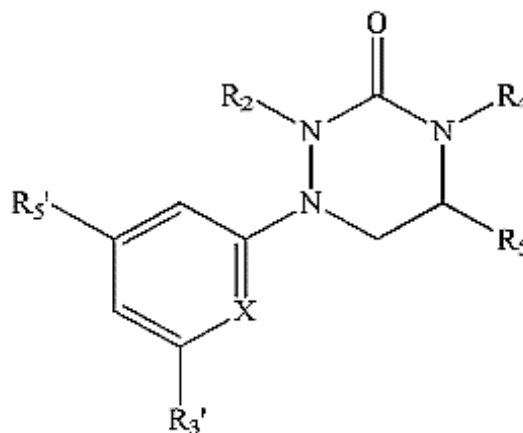


Fig. 1. Chemical structure of 1-phenyl[2H]-tetrahydro-triazine-3-one analogues.

Table 1. Structures and observed inhibitory activity of 5-Lipoxygenase of 1-phenyl[2H]-tetrahydro-triazine-3-one analogues.

No.	Substitution						log(1/IC ₅₀) obs ^a
	X	R ₃ '	R ₅ '	R ₂	R ₄	R ₅	
1	CH	H	H	H	H	CH ₂ OCH ₂ Ph	6.00
2	CH	H	H	H	H	Bu	5.82
3	CH	H	H	H	H	i-Pr	5.17
4	CH	H	H	H	H	Me(R)	5.17
5 ^b	CH	H	H	H	H	Me ₂	5.17
6	CH	H	H	H	H	Et	5.16
7 ^b	CH	H	H	H	H	Me	4.94
8	CH	H	H	H	H	CH ₂ OC ₂ H ₄ OMe	4.85
9 ^b	CH	H	H	H	H	Me(S)	4.85
10	CH	H	H	H	H	CO ₂ Me	4.70
11 ^b	CH	H	H	H	H	H	4.68
12	CH	H	OCH ₂ Ph	H	H	H	5.96
13	CH	H	Br	H	H	H	5.31
14	CH	H	Cl	H	H	H	5.20
15 ^b	CH	H	Et	H	H	H	4.89
16	CH	H	SMe	H	H	H	4.85
17 ^b	CH	H	Me	H	H	H	4.82
18	CH	H	CF ₃	H	H	H	4.77
19	CH	H	F	H	H	H	4.72
20 ^b	CH	H	CN	H	H	H	4.43
21 ^b	CH	H	OMe	H	H	H	4.33
22	CH	H	NO ₂	H	H	H	4.31
23	CH	H	NH ₂	H	H	H	3.75
24	CH	H	Br	H	H	Me	5.59
25	CH	H	Cl	H	H	Me	5.57
26 ^b	CH	H	F	H	H	Me	5.20
27 ^b	CH	H	Me	H	H	Me	4.72
28	CH	H	H	H	C(=O)-i-Pr	H	5.89
29	CH	H	H	H	C(=O)Et	H	5.59
30	CH	H	H	H	C(=O)Me	Me	5.48
31	CH	H	H	H	C(=O)Me	H	5.47
32	CH	H	H	H	OCH ₂ Ph	Me	5.37
33 ^b	CH	H	H	H	OH	Me	5.22
34	CH	H	H	H	OEt	Me	5.13
35	CH	H	H	H	OCH ₂ Ph	H	5.08
36	CH	H	H	C(=O)Et	C(=O)Et	H	4.90
37	CH	H	H	H	OMe	Me	4.65
38	CH	H	H	C(=O)Me	C(=O)Me	H	4.40
39	N	Br	H	H	H	Me	5.62
40	N	Br	H	H	H	H	5.46
41	N	Cl	H	H	H	Me	5.46
42 ^b	N	Me	H	H	H	Me	5.42
43	N	Me	H	H	H	H	5.26
44 ^b	N	OMe	H	H	H	Me	5.26

No.	Substitution						log(1/IC ₅₀)
	X	R ₃ '	R ₅ '	R ₂	R ₄	R ₅	
45	N	Cl	H	H	H	H	5.25
46	N	F	H	H	H	Me	5.18
47	N	F	H	H	H	H	5.04
48	N	OMe	H	H	H	H	5.02
49 ^b	N	H	H	H	H	Me	4.66
50	N	H	H	H	H	H	4.59
51	CH	H	Cl	H	C(=O)Me	H	5.89
52	CH	H	Cl	H	OH	Me	5.41
53 ^b	CH	H	F	H	OH	Me	5.16
54	CH	Me	Me	H	OH	H	5.08
55	CH	F	F	H	H	H	5.05
56 ^b	CH	Me	Me	H	H	H	4.92
57 ^b	N	Cl	H	H	H	H	5.48
58 ^b	CH	H	Cl	H	H	H	5.35
59 ^b	CH	H	H	H	H	H	4.77
60 ^b	CH	Cl	Me	H	H	H	5.48

^a Observed inhibitory activity.

^b The compounds selected as the test set.

groups, atom-centered fragments, properties and empirical. In this study, just GETAWAY (geometry, topology, and atom-weights assembly) and WHIM (weighted holistic invariant molecular) descriptors were used. A total number of 293 descriptors were calculated by Dragon for each molecule and 60×293 data matrix X was obtained. The rows and columns of this matrix are the number of molecules and molecular descriptors respectively.

Discrete Wavelet Transform

Transform-based methods are of fundamental importance in signal and image processing. Wavelet transform decomposes a signal into a set of basic functions. These basic functions are obtained from a single prototype wavelet called mother wavelet by dilations and shifting [20]. The discrete wavelet transform (DWT) is a linear transformation that operates on a data vector whose length is an integer power of two, transforming it into a numerically different vector of the same length. It is a tool which separates the data into different frequency components, and then studies each component with resolution matched to its scale. DWT [24] is computed with a cascade of filtering followed by a factor 2 sub-sampling (Fig. 2).

H and *L* denote high and low-pass filters respectively, ↓2 denotes sub-sampling. Outputs of these filters are given by equations (2) and (3):

$$a_{j+1}[p] = \sum_{n=-\infty}^{+\infty} l[n-2p] a_j[n] \quad (2)$$

$$d_{j+1}[p] = \sum_{n=-\infty}^{+\infty} h[n-2p] d_j[n] \quad (3)$$

The elements a_j are used for next step (scale) of the transform and the elements d_j , the wavelet coefficients, determine the output of the transform. $l[n]$ and $h[n]$ are coefficients of low and high-pass filters respectively. It can be assumed that on scale $j+1$ there is only half from number of a and d elements on scale j . These elements are called scaling function coefficients.

Results and discussion

Principal Component Analysis

Principal component analysis (PCA) was performed on the calculated structural descriptors to the whole data set (Table 1), for investigation the distribution in the chemical space, which shows the spatial location of samples to assist the separation of the data into training and prediction sets. PCA is a useful multi-

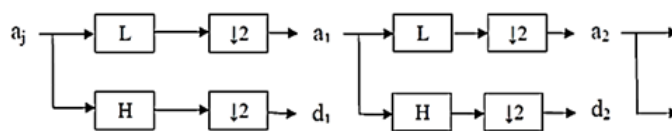


Fig. 2. DWT tree. (a) *H* and *L* denote high and low-pass filters respectively, (b) ↓2 denotes sub-sampling (c) a_1 and a_2 denote the approximation of the data and (d) d_1 and d_2 denote the detail of the data.

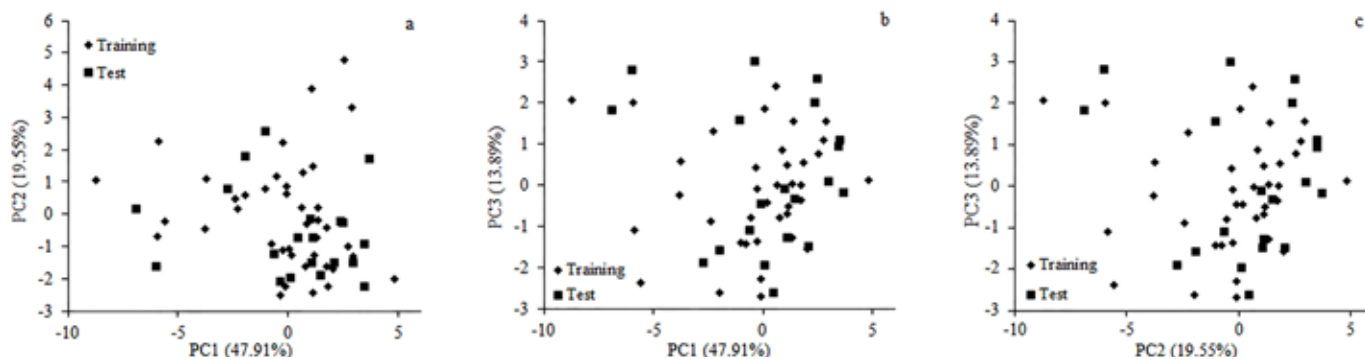


Fig. 3. Principal components analysis of the descriptors for the data set, (a) PC2 versus PC1, (b) PC3 versus PC1 and (c) PC3 versus PC2.

variate statistical technique in which new variables (called principal components, PCs) are calculated as linear combinations of the old ones. These PCs are sorted by decreasing information content so that most of the information is preserved in the first few PCs. An important feature is that the obtained PCs are uncorrelated, and they can be used to derive scores which can be used to display most of the original variations in a smaller number of dimensions. These scores can also allow us to recognize groups of samples with similar behavior. A total of 293 descriptors were initially calculated by PCA for the entire data set of 60 compounds. The total number of descriptors was reduced to 35 descriptors by eliminating the descriptors that were deemed insignificant (i.e. where the one-parameter correlation confinement with the activity is less than 0.1). The PCA results indicate that three PCs (PC1, PC2 and PC3) described 81.35% of the overall variances: 47.91%, 19.55% and 13.89% for PC1, PC2 and PC3, respectively (Fig. 3). As seen in Fig. 3, there is not a clear clustering between compounds. The data separation is very important in the development of reliable and robust QSAR models. The quality of the prediction depends on the data set used to develop the model. For regression analysis, the data set was separated into two groups, a training set (40 data) and a prediction set (20 data) according to the Kennard-Stones algorithm. As shown in Fig. 3, the distribution of the compounds in each subset seems to be relatively well-balanced over the space of the principal components.

PLS Modeling

The multivariate calibration is a powerful tool for modeling, as it extracts further information and allows building more robust models [25, 26]. The PLS method is used to establish relationships between the dependent variables of the activity matrix and the descriptors of the matrix as independent variables also that are called latent variables. Based on the inhibitory activity data (Table 1), the data was classified to training and prediction sets according to Kennard-Stones algorithm and the PLS model was run. The optimum number of factors to be included in the calibration model was determined by computing the root mean square error of calibration (*RMSEC*) from cross-validated models using a high number of factors (half the number of total

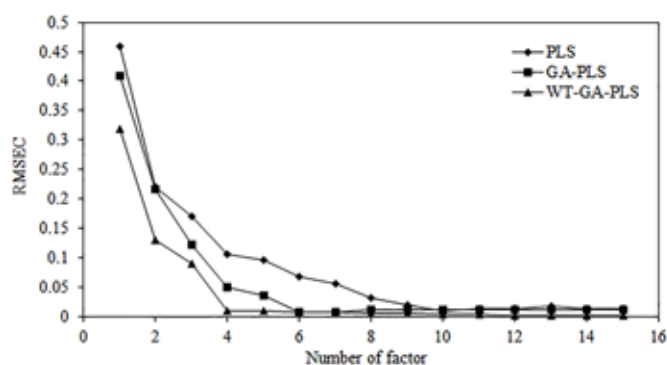


Fig. 4. Plot of *RMSEC* versus number of factors.

training set + 1). The cross-validation method was employed to eliminate only one compound at a time and then, PLS was employed to calibrate the remaining of the training set. The inhibitory activity of the left-out sample was predicted using this calibration. This process was repeated until each compound in the training set had been left out once. According to Haaland suggestion [26], the optimum number of factors selected. As it is shown in Fig. 4, the *RMSEC* is minimized when the number of factors is 10, thus, the optimum number of factors for the training set of PLS method was chosen to be 10. The data set was mean-centered, prior to the PLS analysis.

GA-PLS Modeling

As mentioned before, one of the problems is choosing the set of molecular descriptors. GAs as intelligent selection techniques [27], was utilized to achieve this objective. The parameters of genetic algorithms used in this study are as below: the probability of mutation 1% and 90% for crossover, number of runs is 100 and window size for smoothing is 3. Prior to performing the GA-PLS, all the descriptors were mean-centered. After running of GAs for variables, the selected descriptors were used to run PLS. Among the descriptors calculated, the most significant molecular descriptors were identified. Table 2 shows the calculated descriptors for each molecule, the *t* values for null hypothesis and their related *P* values [28]. The number of factors reduced to 6 upon the application of GA-PLS (Fig. 4). As

Table 2. The most significant molecular descriptors used in this study.

Notation	Descriptors	t value	P value
H2v	H autocorrelation of lag 2 / weighted by van der Waals volume	8.330	0.000
R2u	R autocorrelation of lag 2 / unweighted	6.169	0.000
R1u	R autocorrelation of lag 1 / unweighted	-6.613	0.000
P2u	2nd component shape directional WHIM index / unweighted	-4.575	0.000
R6U ⁺	R maximal autocorrelation of lag 6 / unweighted	-4.317	0.000
R7e	R autocorrelation of lag 7 / weighted by Sanderson electronegativity	-4.018	0.000

shown in Fig. 4, the *RMSEC* is minimized when the number of factors is 6, thus, the optimum number of factors for the training set of GA-PLS method was chosen to be 6. The present study shows that the GAs can be a good method for descriptor selection in analysis.

WT-GA-PLS Modeling

In order to enhance the predictive power of multivariate calibration methods, molecular descriptors are often corrected prior to the data analysis. In this case, wavelet transform was used as the processing method. When WT-GA-PLS is used the number of factors reduced to 4 (Fig. 4). Table 2 shows the calculated descriptors for each molecule, the *t* values for null hypothesis and their related *P* values. In order to evaluate the models applied in this study (PLS, GA-PLS and WT-GA-PLS), the inhibitory activities were tested with set of tests. The WT-GA-PLS method combines WPT, which performs feature extraction and de-noising, GA which optimizes variation and selection of the fitness values, as well as PLS, which provides calibration model and reduces the dimension of the data. To be successful in obtaining a reliable result by the WT-GA-PLS method, different parameters such as wavelet functions (Coiflet 1, 2...5, and Daubechies 6, 7, 8), decomposition level (*L* = 1–2) and the number of PLS factors were tested. In these investigations, Coiflet 3, *L* = 1 and number of PLS factors = 4 were selected as the optimal parameters.

Model Validation and Prediction of Inhibitory Activity

The predictive ability of these methods (PLS, GA-PLS and WT-GA-PLS) were investigated by prediction of inhibitory of 20 molecules (their structures are given in Table 1). The validation of predictive ability is another key step in the QSAR studies. Several statistical parameters have been used for the evaluation of the suitability of the developed QSAR models for prediction of the property of the studied compounds this include the root mean square error of prediction (*RMSEP*) and relative standard error of prediction (*RSEP*), validation through an external prediction set.

$$RMSEP = \sqrt{\frac{\sum_{i=1}^n (y_{i,pred} - y_{i,obs})^2}{n}} \quad (4)$$

$$RSEP(\%) = 100 \times \sqrt{\frac{\sum_{i=1}^n (y_{i,pred} - y_{i,obs})^2}{\sum (y_{i,obs})^2}} \quad (5)$$

where $y_{i,pred}$ is the predicted of the inhibitory activity using different model, $y_{i,obs}$ is the observed value of the inhibitory activity, and *n* is the number of compounds in the prediction set. The statistical parameters obtained by these methods are listed in Table 3.

Table 3 shows *RMSEP*, *RSEP* and the percentage error for prediction of inhibitory activity of 1-phenyl[2H]-tetrahydro-triazine-3-one analogues. As can be seen, the good results were achieved in WT-GA-PLS model with percentage error ranges from -5.844 to +4.512 % for inhibitory activity of 1-phenyl[2H]-tetrahydro-triazine-3-one analogues. Other statistical parameters have been used for the evaluation of the suitability of the developed models for prediction of the activity of the studied compounds this include cross validation coefficient (Q^2 and R^2) [29]. These parameters are defined as follows:

$$Q_{abs}^2 = 1 - \frac{\sum_Y (Y_{exp} - Y_{LOO})^2}{\sum_Y (Y_{exp} - \bar{Y}_{exp})^2} \quad (6)$$

$$R_{abs}^2 = 1 - \frac{\sum_Y (Y_{exp} - Y_{pred})^2}{\sum_Y (Y_{exp} - \bar{Y}_{exp})^2} \quad (7)$$

As seen in Table 3, these parameters show the good statistical qualities. The plots of the predicted inhibitory activity versus actual values are shown in Fig. 5 for each model. It is possible to see that WT-GA-PLS presents excellent prediction abilities when compared with other models.

Y-randomization Test

This is a widely used technique to ensure the robustness of a QSAR model. In this test, the dependent-variable vector, Y-vector, is randomly shuffled and a new QSAR model is developed using the original independent-variable matrix. The process is repeated three times and the average of the three measurements showed low R^2 values 0.226, 0.241 and 0.254 and Q^2 values 0.137, 0.152 and 0.170 for the PLS, GA-PLS and WT-GA-PLS, respectively. If all QSAR models obtained in the Y-randomization test have relatively high R^2 and Q^2 , it implies that an acceptable QSAR model cannot be obtained for the given data set by the current modeling method [30, 31].

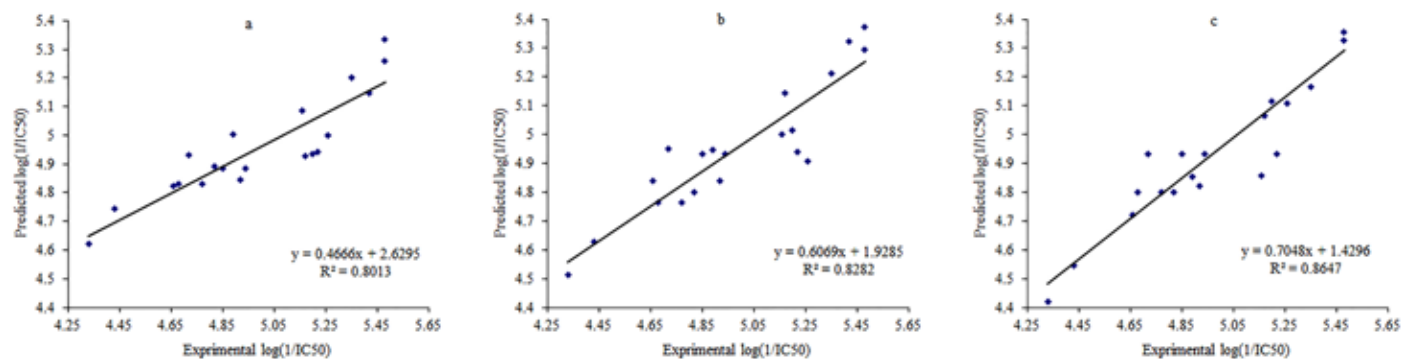


Fig. 5. Plots of predicted versus actual $\log(1/IC_{50})$, (a) PLS, (b) GA-PLS and (c) WT-GA-PLS.

Table 3. Observation and calculation values of $\log(1/IC_{50})$ using PLS, GA-PLS and WT-GA-PLS models.

No. of compounds (Table I)	Observation $\log(1/IC_{50})$	PLS		GA-PLS		WT-GA-PLS	
		Predicted	Error (%)	Predicted	Error (%)	Predicted	Error (%)
5	5.170	4.926	-4.702	5.144	-0.489	5.064	-2.050
7	4.940	4.883	-1.137	4.931	-0.182	4.930	-0.190
9	4.850	4.884	0.719	4.930	1.665	4.930	1.665
11	4.680	4.829	3.196	4.763	1.788	4.800	2.570
15	4.890	5.004	2.335	4.947	1.173	4.854	-0.736
17	4.820	4.892	1.510	4.80	-0.394	4.798	-0.452
20	4.430	4.745	7.112	4.627	4.467	4.545	2.598
21	4.330	4.620	6.713	4.511	4.196	4.418	2.036
26	5.200	4.935	-5.094	5.014	-3.559	5.115	-1.628
27	4.720	4.930	4.461	4.951	4.913	4.933	4.512
33	5.220	4.942	-5.312	4.937	-5.408	4.931	-5.536
42	5.420	5.149	-4.998	5.323	-1.787	5.424	0.086
44	5.260	5.001	-4.920	4.906	-6.726	5.106	-2.912
49	4.660	4.824	3.527	4.837	3.804	4.720	1.300
53	5.160	5.087	-1.399	5.001	-3.069	4.858	-5.844
56	4.920	4.846	-1.500	4.838	-1.666	4.820	-2.028
57	5.480	5.259	-4.025	5.295	-3.361	5.355	-2.279
58	5.350	5.202	-2.749	5.210	-2.614	5.164	-3.471
59	4.770	4.829	1.249	4.763	-0.132	4.800	0.635
60	5.480	5.333	-2.682	5.371	-1.978	5.327	-2.788
N. F. ^a		10		6		4	
R ²		0.652		0.759		0.818	
Q ²		0.536		0.691		0.744	
RMSEP		0.194		0.161		0.140	
RSEP (%)		3.882		3.229		2.807	

^a Number of factors.

Molecular Design

The role of computation in molecular design has grown steadily since the late 1960s [32, 33]. In the early days emphasis was on statistical and computational approaches aimed at quantify-

ing the relationship of chemical structure to biological properties. In addition, recent modeling by computational approaches has become a critical tool in the drug discovery process. As an application of proposed method, we investigated WT-GA-PLS model to predict the inhibitory activity of five new

Table 4. New structures of 1-phenyl[2H]-tetrahydro-triazine-3-one analogues and predicted $\log(1/IC_{50})$ by WT-GA-PLS.

Number of Design	Substitution						$\log(1/IC_{50})$ Calc. ^a
	X	R ₃ '	R ₅ '	R ₂	R ₄	R ₅	
1	N	H	Me	H	H	Me	4.931
2	N	Cl	H	H	H	F	5.450
3	CH	Br	Me	H	H	H	5.778
4	CH	H	Cl	H	OH	H	5.191
5	CH	Br	H	H	H	Me	5.860

^a Calculated by WT-GA-PLS model.

1-phenyl[2H]-tetrahydro-triazine-3-one analogues whose biological tests were not performed with them yet. Table 4 shows the chemical structure of five new compounds and their inhibitory activity calculated by this proposed method.

Conclusions

Using WT-GA-PLS, a QSAR model has been successfully developed for the prediction of inhibitory activity for 60 compounds. The results well illustrate the power of descriptors in prediction of inhibitory activity of 1-phenyl[2H]-tetrahydro-triazine-3-one analogues. The model could predict the inhibitory activity of 1-phenyl[2H]-tetrahydro-triazine-3-one analogues derivatives not existed in the modeling procedure accurately. The work is the first application of WT-GA-PLS for QSAR study and shows that descriptors are capable to recognize the physicochemical information and be can useful to predict the inhibitory activity of the new compounds.

Acknowledgments

The authors gratefully acknowledge the support to this work from, Islamic Azad University, Arak Branch, and research council.

References

1. Camargo, A. B.; Marchevsky, E.; Luco, J. M. *J. Agric. Food Chem.* **2007**, 55, 3096-3103.

2. Zhou, Y. P.; Jiang, J. H.; Lin, W. Q.; Zou, H. Y.; Wu, H. L.; Shen, G. L.; Yu, R. Q. *Eur. J. Pharm. Sci.* **2006**, 28, 344-353.

3. Ioele, G.; Luca, M. D.; Oliverio, F.; Ragno, G. *Talanta* **2009**, 79, 1418-1424.

4. Cui, W.; Yan, X. *Chemometr. Intell. Lab. Syst.* **2009**, 98, 130-135.

5. Ghasemi, J. B.; Ahmadi, S. H.; Brown, S. D. *Environ. Chem. Lett.* **2011**, 9, 87-96.

6. Hocking, R. R. *Biometrics.* **1976**, 32, 1-49.

7. Shen, Q.; Lu, Q. Z.; Jiang, J. H.; Shen, G. L.; Yu, R. Q. *Eur. J. Pharm. Sci.* **2003**, 20, 63-71.

8. Leardi, R. *J. Chemom.* **1994**, 8, 65-79.

9. Depczynski, U.; Frost, V. J.; Molt, K. *Anal. Chim. Acta.* **2000**, 420, 217-227.

10. Hibbert, D. B. *Chemom. Intell. Lab. Syst.* **1993**, 19, 277-293.

11. Leardi, R. *J. Chemom.* **2000**, 14, 643-655.

12. Leardi, R. *J. Chemom.* **2001**, 15, 559-569.

13. Ghasemi, J. B.; Niazi, A.; Leardi, R. *Talanta* **2003**, 59, 311-317.

14. Leardi, R.; Boggia, R.; Terrile, M. *J. Chemom.* **1992**, 6, 267-281.

15. Kompany-Zareh, M. *Acta Chim Slov.* **2003**, 50, 259-273.

16. Narasimhan, B.; Judge, V.; Narang, R.; Ohlan, R.; Ohlan, S. *Bio-org. Med. Chem. Lett.* **2007**, 17, 5836-5845.

17. Hemmateenejad, B.; Safarpour, M. A.; Taghavi, F. *J. Mol. Struct.* **2003**, 635, 183-190.

18. Niazi, A.; Jameh-Bozorghi, S.; Nori-Shargh, D. *Turk. J. Chem.* **2006**, 30, 619-628.

19. Joreskog, K. G.; Wold, H. *System Under Indirect Observations*, Amsterdam, North Holland, **1982**.

20. Blessie, A. A.; Nalini, J.; Ramesh, S. C. *Int. J. Comput. Sci. Issues.* **2011**, 8, 449-453.

21. Kennard, R. W.; Stones, L. A. *Technometrics.* **1969**, 11, 137-148.

22. Daszykowski, M.; Walczak, B.; Massart, D. L. *Anal. Chim. Acta.* **2002**, 468, 91-103.

23. Ahmadi, M.; Shahlaei, M. *Res. Pharm. Sci.* **2015**, 10, 307-325.

24. Mallat, S. A. *Wavelet Tour of Signal Processing*, Academic Press, San Diego, **1998**.

25. Ghasemi, J. B.; Niazi, A. *Talanta* **2005**, 65, 1168-1173.

26. Haaland, D. M.; Thomas, E. V. *Anal. Chem.* **1988**, 60, 1193-1202.

27. Niazi, A.; Leardi, R. *J. Chemom.* **2012**, 26, 345-351.

28. Cherkasov, A.; et al. *J. Med. Chem.* **2014**, 57, 4977-5010.

29. Tropsha, A. *Mol. Inf.* **2010**, 29, 476-488.

30. Tropsha, A.; Gramatica, P.; Vijay, K.G. *QSAR. Com. Sci.* **2003**, 22, 69-77.

31. Golbraikh, A.; Tropsha, A. *J. Mol. Graph. Model.* **2002**, 20, 269-276.

32. Richon, A. B. *Drug Discov. Today* **2008**, 13, 659-664.

33. Clark, D. E. *Exp. Opin. Drug Discov.* **2006**, 1, 103-110.

Cytotoxic Constituents from the Stem Bark of *Alvaradoa amorphoides*

Carlos Quintal-Novelo,¹ Luis W. Torres-Tapia,¹ Rosa Moo-Puc,² Sergio R. Peraza-Sanchez^{1,*}

¹ Centro de Investigación Científica de Yucatán (CICY), Calle 43 No. 130, Col. Chuburná de Hidalgo, Mérida, Yucatán, México 97200

² Unidad de Investigación Médica, Centro Médico Ignacio García Téllez, Instituto Mexicano del Seguro Social (IMSS), Calle 41 No. 439, Colonia Industrial, Mérida, Yucatán, México 97150

* Corresponding author. E-mail: speraza@cicy.mx; Centro de Investigación Científica de Yucatán (CICY), Calle 43 No. 130, Col. Chuburná de Hidalgo, Mérida, Yucatán, México 97200. Fax: (999) 981-3900, Tel. (999) 942-8330, Ext. 264.

Received February 9th, 2015; Accepted September 11th, 2015

Abstract. The chemical study of *Alvaradoa amorphoides* led to the isolation of four major constituents: chrysophanol (**1**), β -sitosterol (**2**), atraric acid (**3**), and 17-octadecen-6-ynoic acid (**4**). All compounds were evaluated on *in vitro* cytotoxic and antiproliferative assays. Atraric acid and 17-octadecen-6-ynoic acid showed cytotoxic activity. Additionally, compound **4** exhibited cytotoxic activity showing a certain degree of selectivity against cancer cell lines.

Key words: *Alvaradoa amorphoides*, cytotoxic activity, antiproliferative activity, acetylenic compound.

Resumen. De *Alvaradoa amorphoides* se aislaron cuatro compuestos: crisofanol (**1**), β -sitosterol (**2**), ácido atrárico (**3**) y el ácido 17-octadecen-6-inoico (**4**). Los compuestos fueron evaluados en los ensayos *in vitro* de actividad citotóxica y antiproliferativa. El ácido atrárico y el ácido 17-octadecen-6-inoico presentaron actividad citotóxica. Adicionalmente, el compuesto **4** mostró cierto grado de selectividad contra las líneas cancerígenas.

Palabras clave: *Alvaradoa amorphoides*, actividad citotóxica, actividad antiproliferativa, acetileno.

Introduction

According to the World Health Organization, cancer is one of the most important causes of death in the world. This disease caused 7.6 million deaths in 2008 [1]. In addition, it has been described drug resistance in cancer cells; therefore, the discovery of new, more effective and selective antineoplastic agents is one of the most important challenges in this area [2, 3]. According to the Food and Drug Administration (FDA), 40-45% of all anticancer drugs approved from 1940 to 2006 corresponded to natural products or derived from them [4]. One of the most important sources for finding new anticancer drugs is the plant kingdom [5].

The genus *Alvaradoa* (Pricramniaceae) is a natural source of compounds with potential activity against cancer, having been possible to isolate metabolites with cytotoxic activity. Phytochemical analysis of *A. haitiensis* concluded in the isolation of 10 anthracenone C-glycosides denominated alvaradoins E-N, and all compounds showed cytotoxic activity against KB cell line; furthermore, the compound alvaradoin E showed anti-leukemic activity on an *in vivo* model [6]. Regarding *A. amorphoides*, the stem bark is used in Mayan traditional medicine to treat skin disorders [7]. This species has only a few biological studies. Ankli et al. studied the dichloromethane and butanol leaf extracts, and they concluded that these extracts have cytotoxic activity against KB cell line [8]. Caamal-Fuentes et al. evaluated the methanol extract of the stem bark and this extract exhibited cytotoxicity against KB cells at $CC_{50} = 22.4 \mu\text{g mL}^{-1}$ [9]. It is worth noticing that there are no reports of compounds

isolated from the stem bark of this plant. In view of the above, the aim of this work was to isolate, purify, and identify the cytotoxic constituents of the stem bark of *A. amorphoides* through its evaluation in five cancer cell lines: KB, Hep-2, HeLa, PC3, and MCF-7, and a normal cell line (Hek-293), using the MTT colorimetric method for cytotoxic activity and SRB for the antiproliferative bioassay.

Results and discussion

The crude methanol extract from the stem bark of *A. amorphoides* was fractionated by liquid-liquid separation, affording the hexane fraction; both, methanol extract and hexane fraction were evaluated against the KB cell line, showing $CC_{50} = 23.0$ and $38.0 \mu\text{g mL}^{-1}$, respectively. The hexane fraction was subjected to successive chromatographic fractionation to afford four known compounds: chrysophanol (**1**), which is a common anthraquinone isolated from *Alvaradoa* species, included *A. amorphoides* [6,10,11]; β -sitosterol (**2**); atraric acid (**3**), which has previously been obtained from the stem bark of *Pygeum africanum* and being this the first report on its isolation from *A. amorphoides* [12]; and the acetylenic compound 17-octadecen-6-ynoic acid (**4**) [13,14]. The structures of compounds **1-4** were elucidated by IR, GC-MS, and NMR spectroscopic analyses and by comparison with the literature data (Figure 1). Compound **4** was originally isolated by Pearl *et al.* and it was identified by GC-MS by previously preparing its methyl derivative, the methyl 17-octadecen-6-ynoate [13]. Nevertheless,

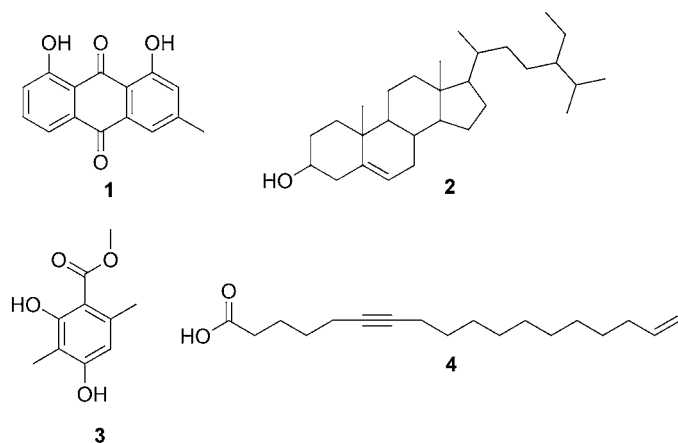


Figure 1. Compounds isolated from the stem bark of *A. amorphoides*.

this is the first time that compound **4** is isolated from the stem bark of *A. amorphoides* and the present work is contributing with the complete structural analysis of this molecule.

All compounds were evaluated against cancer cell lines (Tables 1 and 2). Compounds **3** and **4** showed cytotoxic activity (Table 1). The acetylenic-type compound (**4**) showed high selectivity against all tumor lines compared with the normal cell line. This high selectivity toward tumor cells is of great importance because the drugs used nowadays against cancer cause serious adverse effects. No reports exist about the biological activity of this enynoic acid. However, the 6-octadecynoic acid

(tariric acid) inhibits the growth of fluconazole-susceptible and resistant *Candida albicans* strain [15]. Acetylenic compounds have a great potential as possible anticancer agents [16]. None of the compounds showed antiproliferative activity.

The current study supports the ethnomedical use of *A. amorphoides* as a remedy for the treatment of cancer-like symptoms. This is the first time that the acetylenic compound 17-octadecen-6-ynoic acid (**4**) is isolated from the stem bark, and according to the cytotoxic bioassay, **4** should be considered as a potential anticancer agent. Taking into account its cytotoxic activity and its high selectivity towards tumor cells, the 17-octadecen-6-ynoic acid may be a lead for further studies on its mechanism of action in cancer cells.

Experimental

Purification by column chromatography (CC) was performed using silica gel 60 (0.040-0.063 mm, Merck, Darmstadt, Germany) and pre-coated silica gel plates (Merck, Kieselgel 60F₂₅₄, 0.25 mm) for preparative thin layer chromatography (PTLC). Gel permeation column chromatography was carried out using Sephadex LH-20 (Amersham Pharmacia Biotech AB, Sweden). Analytical TLC was performed on silica gel 60F₂₅₄ aluminum plates (E.M. Merck, 0.2 mm thickness). Detection of the components under UV/Vis light at 254 and 365 nm was performed on a Chromato-Vue® C-75 UV Viewing Cabinet. Visualization of components was carried out by using a solution of phospho-

Table 1. Cytotoxic activity of the compounds isolated from *A. amorphoides*.

Compound	Cell lines CC ₅₀ μg mL ⁻¹ (SI ^a)					
	Hep-2	HeLa	PC3	KB	MCF-7	Hek-293
1	---- ^b	----	----	----	----	----
2	----	----	----	----	----	----
3	28.52 (1.0)	25.22 (1.1)	44.41 (0.6)	17.74 (1.6)	45.10 (0.6)	30.13
4	17.75 (29.5)	23.33 (22.4)	23.47 (22.3)	24.45 (21.4)	25.32 (21.0)	532.7
Docetaxel	0.08	0.20	0.05	0.24	0.01	0.079

^a SI = Selectivity Index

^b ---- = CC₅₀ > 100 μg mL⁻¹

Table 2. Antiproliferative activity of the compounds isolated from *A. amorphoides*.

Compound	Cell lines IC ₅₀ μg mL ⁻¹ (SI ^a)					
	Hep-2	HeLa	PC3	KB	MCF-7	Hek-293
1	---- ^b	----	----	----	----	----
2	----	----	----	----	----	----
3	83.91 (0.5)	32.46 (1.4)	43.47 (1.0)	24 (1.9)	----	45.64
4	----	98.41 (3.6)	----	69.91 (5.1)	51.65 (6.9)	359.3
Docetaxel	0.05	0.03	0.04	0.04	0.01	0.05

^a SI = selectivity Index

^b ---- = IC₅₀ > 100 μg mL⁻¹

molybdc acid (20 g) and ceric sulfate (2.5 g) in 500 mL of sulfuric acid (5%), followed by heating. IR spectra were taken on KBr discs on a Nicolet Protégé 460 spectrophotometer. NMR experiments were recorded on a Bruker Avance 400 Ultra Shield spectrometer in CDCl_3 . Gas chromatograms and low-resolution mass spectra were obtained on an Agilent Technologies GC-MS instrument (models 6890N and 5975B) using the following chromatographic conditions: split injection; 1 mL sample at 1% concentration; Ultra 1 column (25 m \times 0.2 mm i.d.); flow rate 1.0 mLmin⁻¹ (helium as carrier gas); oven temperature program: T1 = 180 °C (3 min), T2 = 280 °C (15 min), gradient 10 °C/min; injector and detector (FID) temperature at 280 °C. High-resolution mass spectra were obtained on a JEOL GCMate mass spectrometer. All solvents of technical grade employed for chromatographic separations were distilled prior to use.

Plant Material

Alvaradoa amorphoides Liebm. (Picramniaceae) was collected in Mococho, Yucatan, Mexico in October 2010. The plant material was identified and authenticated by taxonomists from the Unit of Natural Resources of the Scientific Research Center of Yucatan (CICY). A voucher specimen was deposited at CICY's *U Najil Tikin Xiw* herbarium (P.Simá 2972).

Extraction and isolation

The dried and powdered stem bark of *A. amorphoides* (9.5 Kg) was extracted successively with methanol (3 \times 15 L) at room temperature for 72 h. The methanol extract was concentrated under reduced pressure resulting in 1.2 Kg of crude extract (12.6%). An aliquot of the methanol extract (226.4 g) was suspended in a solution of methanol-water 1:1 (1 L) and it was partitioned with hexane to obtain the hexane fraction (6.2 g). The hexane fraction was subjected to an initial fractionation by vacuum liquid chromatography (VLC), eluting with n-hexane, n-hexane:ethyl acetate (EtOAc) gradient mixtures, EtOAc, EtOAc:methanol (1:1), and methanol (MeOH), obtaining 21 fractions, which were pooled in 10 major fractions (A1-A10), according to their TLC profile. Fraction A8 (2.2 g) was passed through a column containing Sephadex LH-20, using MeOH for elution, yielding 38 fractions which were pooled in nine fractions (B1-B9) according to their TLC profile. Separation of B9 fraction (953 mg) on silica gel CC with gradient mixtures of hexane:EtOAc was carried out to obtain compound **1** (13.6 mg) and compound **2** (35.2 mg). Fraction B4 was loaded on a Sephadex CC and eluted with hexane:CHCl₃:methanol (2:1:1, v/v) to afford 21 fractions (C1-C21). Fraction C4 (245.8 mg) was subjected to flash CC, and eluted with hexane, hexane:EtOAc mixtures of increasing polarity, yielding compound **2** (49.0 mg). Fractions C5 and C6 were combined (292.6 mg), and then further purified by a silica gel column with hexane:acetone mixtures to give 76 fractions, which were pooled in 17 final fractions (D1-D17). Fraction D6 yielded compound **4** (13.5 mg). Fraction B5 (80 mg) was loaded on a silica gel CC and eluted with hexane, hexane:EtOAc mixtures of increasing po-

larity, yielding 14 major fractions (E1-E14). From fraction E3 compound **1** (5.3 mg) was obtained, fraction E8 yielded compound **3** (6.3 mg), and fraction E10 yielded compound **2** (10.6 mg).

Chrysophanol (1) [17]: yellow crystals; 18.9 mg; IR (KBr) ν_{max} 3400, 1674, 1625 cm⁻¹; ¹H NMR (CDCl_3 , 400 MHz) δ 12.10 (1H, s, OH-8), 11.99 (1H, s, OH-1), 7.80 (1H, dd, J = 1.1, 7.4 Hz, H-5), 7.66 (1H, d, J = 8.2 Hz, H-6), 7.63 (1H, d, J = 1.0 Hz, H-4), 7.27 (1H, dd, J = 1.1, 8.4 Hz, H-7), 7.08 (1H, d, J = 0.8 Hz, H-2); EI-MS (70 eV) m/z (rel. int.) = 254 [$\text{M}]^+$ (100).

β-Sitosterol (2). It was identified by comparison on TLC with an authentic sample and by means of GC-MS analysis.

Atraric acid (3): colorless needles; 6.3 mg; IR (KBr) ν_{max} 3402, 1625, 1306, 1274 cm⁻¹; ¹H NMR (CDCl_3 , 400 MHz) δ 12.05 (1H, s, OH-2), 6.21 (1H, s, H-5), 3.92 (3H, s, OMe-1'), 2.45 (3H, s, Me-6), 2.10 (3H, s, Me-3); EI-MS (70 eV) m/z (rel. int.) = 196 [$\text{M}]^+$ (40), 164 (60), 136 (100).

17-Octadecen-6-ynoic acid (4): yellow oil (13.5 mg); IR (KBr) ν_{max} 3075, 2925, 2841, 2208, 1707 cm⁻¹; ¹H NMR (CDCl_3 , 400 MHz) δ 1.26-1.37 (12H, m, H-10 – H-15), 1.46 (2H, quintet, J = 7.6 Hz, H-9), 1.53 (2H, quintet, J = 7.3 Hz, H-4), 1.73 (2H, quintet, J = 7.7 Hz, H-3), 2.03 (2H, q, J = 7.5 Hz, H-16), 2.12 (2H, m, H-8), 2.17 (2H, m, H-5), 2.37 (2H, t, J = 7.4 Hz, H-2), 4.92 (1H, ddt, J = 10.2, 2.0, 1.0 Hz, Ha-18), 4.99 (1H, dd, J = 17.1, 2.0 Hz, Hb-18), 5.80 (1H, ddt, J = 16.9, 10.2, 6.6 Hz, H-17); ¹³C NMR (CDCl_3 , 100 MHz) δ 18.3 (C-5), 18.8 (C-8), 23.8 (C-3), 28.3 (C-4), 28.8 (C-9), 28.8, 29.0, 29.0, 29.0, 29.3, 29.4, 33.3 (C-16), 33.7 (C-2), 79.2 (C-6), 80.7 (C-7), 114.0 (C-18), 139.2 (C-17), 179.1 (C-1); HRCI-MS (direct probe) m/z 278.2353 (calcd for C₁₈H₃₀O₂, m/z 278.2398).

Cell culture

The cytotoxic and antiproliferative activities of the extracts, fractions, and compounds were evaluated against six cell lines: laryngeal carcinoma (Hep-2, ATCC CCL-23), cervix adenocarcinoma (HeLa, ATCC-CCL-2), prostate adenocarcinoma (PC-3, ATCC-CRL-1435), nasopharyngeal carcinoma (KB, ATCC-CCL-17), breast adenocarcinoma (MCF-7, ATCC-HTB-22), and a human embryonic kidney cell line (Hek-293, ATCC-CRL-1573), from the American Type Culture Collection (ATCC). All were cultured in Dulbecco's Modified Eagle Medium (DMEM; Gibco) and supplemented with 10% heat-inactivated fetal bovine serum (FBS; Gibco), 100 UmL⁻¹ penicillin (InVitro), 100 μgmL⁻¹ streptomycin (InVitro), 2.5 μgmL⁻¹ amphotericin B (InVitro) in a 5% CO₂ humidified atmosphere at 37 °C. Dilution of stock solutions was made in culture medium yielding final extracts and compound concentrations of 3.125, 6.25, 12.5, 25, and 50 μgmL⁻¹ with a final DMSO concentration of 0.01%. This concentration of DMSO has no effect on the growth of cells.

Cytotoxicity and antiproliferative assays

The cytotoxicity and antiproliferative assays were carried out according to a procedure described in the literature [18,19]. We used the MTT method for cytotoxicity assay and SRB for the antiproliferative assay. The experiments were performed in triplicate and the concentrations that killed 50% of the cells (CC_{50}) or inhibited 50% of the cells (IC_{50}) were calculated by GraphPad Prism 4 software.

Acknowledgments

This research was financed by CONACYT (Project No. 156755). Carlos Quintal-Novelo is grateful to CONACYT for the scholarship No. 211980. The authors wish to thank Paulino Sima-Polanco, from the Unit of Natural Resources (CICY), for the collection and identification of plant material. The authors are grateful to Dr. Andrew James for English review of the paper.

References

- Jemal A., Bray F., Center M. M., Ferlay J., Ward E., Forman D. *CA. Cancer J. Clin.* **2011**, 61, 69-90.
- Gottesman, M. *Annu. Rev. Med.* **2002**, 53, 615-627.
- Thomas, H.; Coley, H. M. *Cancer Control* **2003**, 10, 159-165.
- Newman, D. J.; Cragg, G. M. *J. Nat. Prod.* **2007**, 70, 461-477.
- Cragg, G. M.; Newman, D. J. *J. Ethnopharmacol.* **2005**, 100, 72-79.
- Phifer, S. S.; Lee, D.; Seo, E. K.; Kim, N. C.; Graf, T. N.; Kroll, D. J.; Navarro, H. A.; Izydore, R. A.; Jimenez, F.; García, R.; Rose, W. C.; Fairchild, C. R.; Wild, R.; Soejarto, D. D.; Farnsworth, N. R.; Kinghorn, A. D.; Oberlies, N. H.; Wall, M. E.; Wani, M. C. *J. Nat. Prod.* **2007**, 70, 954-961.
- Osadao, R., *El Libro del Judío o Medicina Doméstica, Descripción de las Virtudes de las Yervas Medicinales de Yucatán*. Additional notes of Dr. Andrew Heath de Zapata, Mérida, Yucatán, México, **1834**, 20-255.
- Ankli, A.; Heinrich, M.; Bork, P.; Wolfram, L.; Bauerfeind, P.; Brun, R.; Schmid, C.; Weiss, C.; Bruggisser, R.; Gertsch, J.; Wasescha, M.; Sticher, O. *J. Ethnopharmacol.* **2002**, 79, 43-52.
- Caamal-Fuentes, E.; Torres-Tapia, L. W.; Sima-Polanco, P.; Peraza-Sanchez, S. R.; Moo-Puc, R. *J. Ethnopharmacol.* **2011**, 135, 719-734.
- Soto de Villatoro, B.; Giral Gonzalez, F.; Polonsky, J.; Baskevitch-Varon, Z. *Phytochemistry* **1974**, 13, 2018-2019.
- Harding, W.; Henry, G.; Lewis, P.; Jacobs, H.; McLean, S.; Reynolds, W. *J. Nat. Prod.* **1999**, 62, 98-101.
- Schleich, S.; Papaioannou, M.; Baniahmad, A.; Matusch, R. *Planta Med.* **2006**, 72, 547-551.
- Pearl, M. B.; Kleiman, R.; Earle, F. R. *Lipids.* **1973**, 8, 627-630.
- Minto, R. E.; Blacklock, B. J. *Prog. Lipid Res.* **2008**, 47, 233-306.
- Li, X. C.; Jacob, M. R.; ElSohly, H. N.; Nagle, D. G.; Smillie, T. J.; Walker, L. A.; Clark, A. M. *J. Nat. Prod.* **2003**, 66, 1132-1135.
- Dembitsky, V. M. *Lipids* **2006**, 41, 883-924.
- García-Sosa, K.; Villareal-Álvarez, N.; Lübben, P.; Peña-Rodríguez, L. M. *J. Mex. Chem. Soc.* **2006**, 50, 76-78.
- Denizot, F.; Lang, R. *J. Immunol. Methods* **1986**, 89, 271-277.
- Skehan, P.; Storeng, R.; Scudiero, D.; Monks, A.; McMahon, J.; Vistica, D.; Warren, J. T.; Bokesch, H.; Kenney, S.; Boyd, M. R. *J. Natl. Cancer Inst.* **1990**, 82, 1107-1112.

Removal of Direct Dyes with Alginic Acid

Juan Antonio Lozano-Alvarez,¹ Virginia-Francisca Marañón-Ruiz,^{2*} Juan Jáuregui-Rincón,¹ Iliana Medina-Ramírez,³ Claudio Frausto-Reyes⁴ and Rogelio Salinas-Gutiérrez⁵

¹ Departamento de Ingeniería Bioquímica, Universidad Autónoma de Aguascalientes, Av. Universidad 940 Cd. universitaria, Aguascalientes, México, C.P. 20131.

² Departamento de Ciencias de la Tierra y de la Vida, Centro Universitario de los Lagos, Universidad de Guadalajara. Av. Enrique Díaz de León # 1144, Col. Paseos de la Montaña, Lagos de Moreno, Jalisco, México, C.P.47460.

³ Departamento de Química, Universidad Autónoma de Aguascalientes, Av. Universidad 940 Cd. universitaria, Aguascalientes, México, C.P. 20131.

⁴ Centro de Investigaciones en óptica, Unidad Aguascalientes, Prol. Constitución 607, Fracc. Reserva Loma Bonita Aguascalientes, México, C. P. 20200.

⁵ Departamento de Estadística, Universidad Autónoma de Aguascalientes, Av. Universidad 940 Cd. universitaria, Aguascalientes, México, C.P. 20131.

* To whom correspondence should be addressed. Mail Adress: vmaranon@culagos.udg.mx
Telephone: 52 (474) 7424314 Ext. 66585. Fax: 52 (474) 7423678.

Received July 27,2015; Accepted November 10, 2015

Abstract. The interaction of Alginic acid with three direct dyes (Direct blue 1, Direct red 81, and Direct black 22) was studied. It was found that as a result of this interaction formation of adducts after addition of calcium ion, facilitates their removal from aqueous solution. Our results suggest a relationship among physico-chemical properties of each dye and its removal efficiency. The main mechanisms involved in dye removal are electrostatic interactions, hydrogen bonding and hydrophobic interactions.

Key words: Alginic acid, direct dyes, electrostatic interactions, hydrogen bonding, hydrophobic interactions.

Resumen. La interacción del ácido alginico con tres colorantes directos (azul directo 1, rojo directo 81 y negro directo 22) fue estudiada. Se encontró que como resultado de esta interacción, la formación de aductos tras la adición del ion calcio, facilita su remoción de solución acuosa. Nuestros resultados sugieren una relación entre las propiedades fisicoquímicas de cada colorante y su eficiencia de remoción. Los principales mecanismos involucrados en la remoción de colorantes son las interacciones electrostáticas, puentes de hidrógeno e interacciones hidrofóbicas.

Palabras clave: Ácido alginico; colorantes directos; interacciones electrostáticas; puentes de hidrógeno; interacciones hidrofóbicas.

Introduction

It is well known that suitable dyes to be used for the textile industry should have the highest physical and chemical stability [1]. However, these properties cause considerable environmental problems when these compounds are discharged into water receptors. It has been reported that approximately ten to fifteen percent of applied dye remains in the liquor resulting from dyeing process, in addition more than 100,000 different dyes and pigments are produced worldwide with a total annual production of 700,000 metric tons per year [2], as a consequence the water pollution by these substances represents a complex challenge to resolve.

Direct dyes can be applied to different substrates (materials) such as leather, cotton, silk, cellulose and wool. This group of dyes contain in their structure, different functional groups such as azo, sulfonate, amino, nitro, and others that make a wide variety of colors possible. Due to its complex chemical structure, these compounds are difficult to metabolize by organisms encountered in the environment and when transformed

through anaerobic treatments, the products generated (aromatic amines) are mutagenic and carcinogenic [3-5].

Different strategies have been used to remove direct dyes from aqueous solution, among them, advanced oxidation processes [6-13], coagulation/flocculation [14], electrochemical processes [15,16], extraction [17], inclusion in polymeric materials such as β -cyclodextrin-based polymers, and calix(n)renes derivatives [18-23], bacterial biodegradation [24-26], decolorization with fungi and their purified enzymes [27-30], and adsorption [31-33]. However, each method has its own limitations and drawbacks such as high cost of the material used in dye removal, cost of confinement of residual products, and the high energy demand of the processes, among others.

Adsorption is an economic option that can be applied to remove direct dyes. In recent years, low cost materials such as baggase pith, rice husk, maize cob and sunflower stalks have been evaluated for the treatment (dye removal) of polluted waters [34]. Although these substrates have an acceptable capacity to remove different dyes, their adsorption efficiency is very variable, since it depends on several factors, such as, the source

of residue, the harvest season, and the treatments applied to the low cost adsorbents used in the dye removal.

Lately, it has been demonstrated that biopolymers can be used for the removal of dyes from polluted waters. Several polymers have been evaluated, among them, chitosan, chitin, cellulose, guar gum, tamarind gum, locust bean gum, wheat and corn starch, dextrin, carrageenan, pectin, alginic acid and xanthan have shown good removal capacity and high biodegradability [35-40].

Alginic acid (ALG) is a polymer produced by brown seaweed (Phaeophyceae) and bacterium (*Azotobacter vinelandii*). It is widely used in the food industry as a stabilizer, thickener and gelling agent. Its structure consists in a linear chain of $\beta(1\rightarrow4)$ -D-mannuronate (M) and $\alpha(1\rightarrow4)$ -L-guluronate (G) [41]. Lozano-Alvarez *et al.* [39] reported that this polymer can be effectively used for the removal of disperse yellow 54 (DY54) from aqueous medium using the ALG and separating the ALG-DY54 adduct by acidification. It was also reported that the experimental data of the adsorption isotherms of dye/alginic acid can be best adjusted to the Zimm-Bragg model. The aim of this work is to study the performance of this biopolymer as removal agent when the adduct ALG-Dye is separated from the aqueous solution as calcium alginate gel as a consequence of the addition of calcium ion. In the same sense, we intend to expand our understanding of the interactions among different direct dyes (direct blue 1 (DB1), direct red 81 (DR81), and direct black 22 (DB22) and this polymer, taking into consideration the physicochemical properties of each dye molecule such as molecular weight, size, aggregation capacity,

number and nature of functional groups which determine the differences observed in their removal efficiency with this biopolymer. In this paper, we report a careful examination of these properties of direct dyes and relate them to their interaction with ALG biopolymer, aiming to improve the efficiency of this polymer to remove direct dyes from aqueous solution.

Results and Discussion

Sorption studies

The removal of direct dyes by ALG was evaluated. First, the removal capacity of this polymer was studied as a function of pH and ionic strength values. Fig. 1 shows the graphics corresponding to the removal efficiencies for the following systems: (a) ALG-DB1 (Ca), (b) ALG-DR81 (Ca) and (c) ALG-DB22 (Ca) taking into consideration, different pH and ionic strength values. Fig. 1a shows that pH influences considerably the removal capacity of ALG, observing higher removal efficiencies at high pH values. Fig. 2 represents the chemical structures of dyes used in this study, it can be seen from this figure that these direct dyes have considerable structural differences. Due to its chemical structure, DB1 molecules possess a negative charge at high pH values. Despite the fact that an increase of the pH value results in a higher repulsion between DB1 and ALG molecules, the deprotonation of guluronate (in the polyGGGGG and mixed MGMGM regions of ALG) is favored and the affinity of these regions for the Ca^{+2} increases.

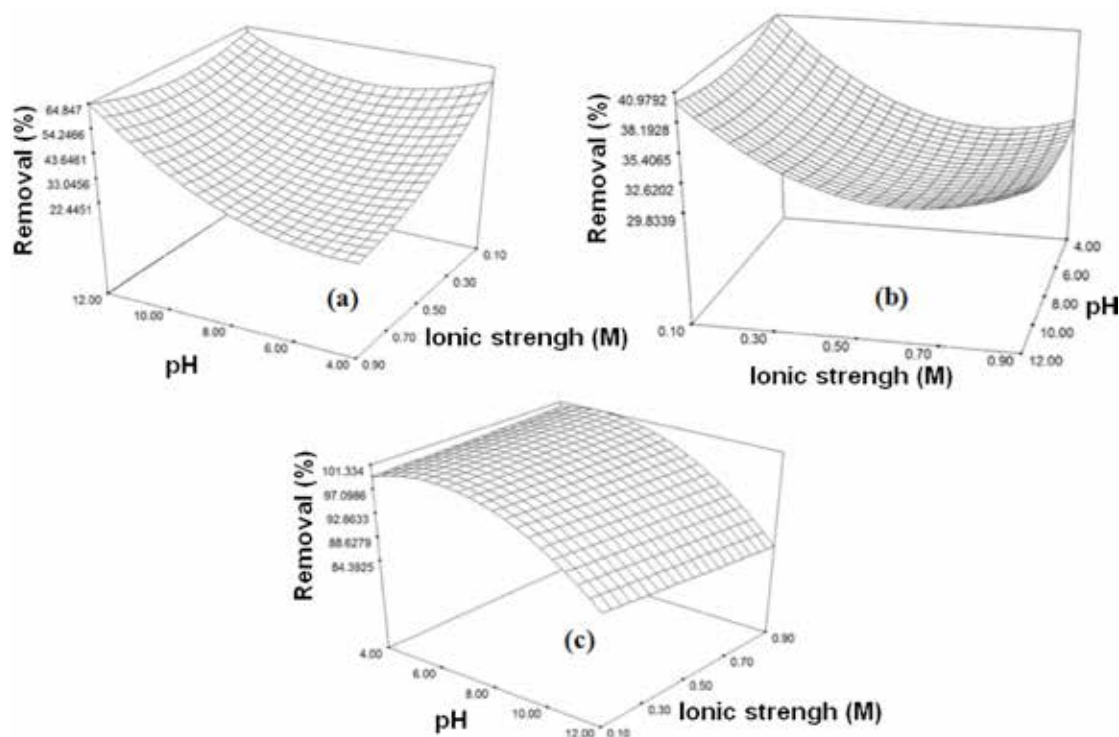


Fig. 1. Graphical representation of Removal efficiency as a function of pH and ionic strength for the following systems: (a) ALG-DB1 (Ca), (b) ALG-DR81 (Ca), and (c) ALG-DB22 (Ca).

In this sense, Donati *et al.* [42] have reported that the main residues involved in the formation of calcium alginate gel ALG (Ca) were the guluronate groups in the ALG molecules (poliGGG regions), nevertheless it was found that the “mixed regions” formed by mannuronate and guluronate in alternate form (MGMGMG) also participate in the gel formation. As a consequence, we propose that there is a decrease in the repulsion between ALG-DB1 adducts when the gel is formed. In addition it is known that the poli mannuronate sequences (poliMMMM) and the MGMGMG are more flexible than the poliGGG moieties [41], and consequently we propose that when the ALG-DB1 (Ca) gel is formed the spaces between poliMMMM and MGMGMG “capture” the DB1 molecules and DB1 clusters adsorbed to the ALG molecular surface.

We previously reported [39] that high values of ionic strength promote the formation of disperse yellow 54 (DY54) aggregates in aqueous solution which increased the Van der Waals and hydrophobic interactions between this dye and the ALG molecules. In this sense Oakes and Dixon [43] have proposed that an increase in the number of aromatic rings favors the phenomenon of dye aggregation (by π - π stacking) and as can be seen in fig. 2, DB1 has two phenyl and two naphthyl rings, which contribute to form greater DB1 aggregates that can bind to ALG. In addition, the functional groups attached to the

DB1 molecule (such as amino, sulfonate, methoxy and keto) can interact with the hydroxyl and carboxyl groups of ALG bio-polymer through hydrogen bonding. All these contributions resulting in a considerable increase of removal efficiency (64 % at pH =12 and ionic strength I=0.9M).

On the other hand, at lower pH values the effect of ionic strength on the removal efficiency of DB1 is greater than that observed at high pH values. Although there is a decrease in the repulsion between ALG and DB1 molecules, the presence of a high salt concentration hinder the approach between these chemical species, which results in lower removal efficiencies of this dye as can be seen in fig. 1a.

Fig. 1b shows schematically the effect of pH and ionic strength on the removal efficiency of the DR81 dye by ALG. Interestingly the effect of the pH is not as strong as that observed with DB1. The structure of DR81 (Fig. 2b) indicates that this dye possesses a negative charge in a wide pH range which explains why this dye is affected less than that observed with DB1. The DR81 molecule has two sulfonate groups that have a negative charge at almost any pH value, and the hydroxyl group can be deprotonated at high pH values increasing the negative charge of this dye. However, from Fig 1b it can easily be inferred that this last deprotonation step does not have a strong effect on the removal efficiency.

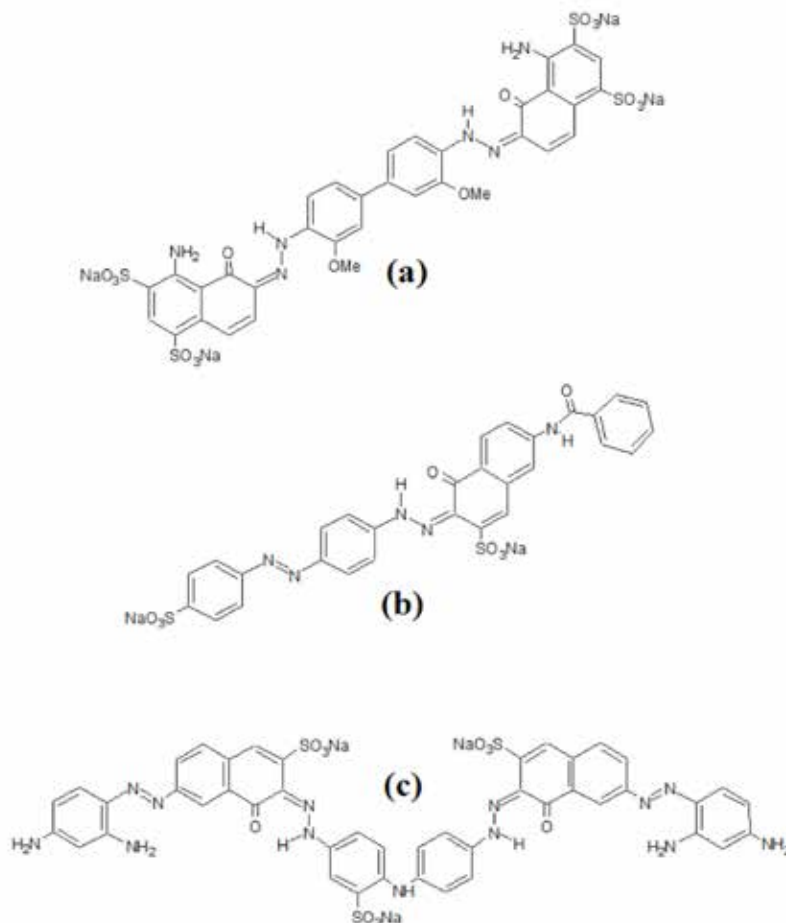


Fig. 2. The structure of Direct dyes: (a) Direct blue 1 (DB1), (b) Direct red 81 (DR81), and (c) Direct black 22 (DB22).

On the other hand, this figure also shows that the ionic strength causes a considerable effect on dye's removal. This result suggests a possible hydrogen bonding and electrostatic interactions between DR81 and the ALG. The amide bond might be broken at acidic and/or basic pH values, resulting in the formation of a dye molecule with an amine group that modifies the "removal efficiency profile" of the dye. This chemical modification of the dye, leads to coulombic interactions of the dye with the ALG polymer, but also, the presence of sodium chloride, decreases the efficiency of dye removal due to the excess of Cl^- and Na^+ ions which interact with the amino groups (in DR81) and carboxyl groups (in ALG) respectively. Conversely, a low ionic strength ($I=0.1\text{M}$) does not reduce ALG-DR81 interactions, resulting in a higher removal (41 % at $\text{pH}=4.0$ and $I=0.1\text{M}$). Although we encountered similarities in the mechanism involved in ALG-Direct dye (DB1 and/or DR81) interactions, also, some differences were encountered which are due to the smaller size and molecular weight of DR81, that can be reflected in a lower removal percentage.

Fig. 1c illustrates the influence of pH and ionic strength on the removal efficiency for the system ALG-DB22 (Ca). It is observed that the pH has a deeper effect than the ionic strength on the removal efficiency of this dye; in this sense, removal efficiencies of DB22 by ALG up to 99% can be achieved at low pH values ($\text{pH}=4$). With regard to the functional groups that integrate the complex chemical structure of DB22 (shown in Fig. 2c), such functional groups will be ionized as a function of the solution pH value, in particular, at $\text{pH}=4$, DB22 presents a charge with a positive value (+2) as a result of the net sum of the three sulfonate groups (each one possesses a charge of -1) and the five amino groups (contributing with an approximate charge of +5). In the same order, the ALG molecule contains guluronate and mannuronate monomers which have one carboxylate group per residue. The pK_a values of mannuronate and guluronate groups are $\text{pK}_{a_M}=3.38$ and $\text{pK}_{a_G}=3.65$ respectively [44], this means that these groups are partially deprotonated at a $\text{pH}=4$ (approximately, ten percent of the carboxyl groups are ionized), in consequence there is a little attraction among ALG molecules and DB22. UV-Vis studies (see spectroscopic section) suggest a high tendency of DB22 molecules to form H aggregates due to the presence of aromatic rings (phenyl and naphthyl), high size and elevated molecular weight. This results in the adsorption of these aggregates onto the molecular surface of the ALG molecule. Interestingly the aggregation phenomenon observed in this dye is strong enough to be almost unaffected by the ionic strength. To corroborate this mechanism, solubility studies were conducted (a more elaborated discussion can be found in the IR studies section) and our results indicated a strong interaction among DB22 and ALG since this dye cannot be separated from the biopolymer after successive ethanol additions.

On the other hand, an increase in pH will favor the deprotonation of amino and hydrazone groups attached to the DB22 molecules and the ionization of carboxyl groups from ALG molecule. As a consequence a greater repulsion between DB22 and the ALG is manifested as lower removal efficiency.

Removal Isotherms

Zimm and Bragg [45], originally proposed their theory to model the conformational transitions in proteins. Later, their theory was used in an adapted form to describe the binding of dyes and surfactants to polypeptides [46,47]. Our group [48], reported on the application of the Zimm-Bragg theory to ALG-Dye and XANT-Dye systems; It was found a respectable relationship between the experimental data and the theoretical isotherms resulting from this model.

The Zimm-Bragg theory takes into account that two processes are responsible for the aggregates formation: nucleation and aggregation. The first process (nucleation which is represented by K_u) consists in the tendency of one dye molecule to bind to a site adjacent to another one already occupied by other dye molecule on the polymer surface. The K_u magnitude is determined by the equation 1:

$$K_u = DD / (ED)(D), \quad \text{Eq. (1)}$$

Where DD refers to two adjacent sites occupied by two Dye molecules and E indicates an empty site onto the biopolymer. The Cooperativity parameter U is defined as follows:

$$U = \frac{(DD)(EE)}{(DE)^2}, \quad \text{Eq. (2)}$$

This parameter is related with the aggregation process of dye molecules bounded to the polymer. The binding coefficient (β) defined as the fraction of polymer sites occupied by dye molecules divided by the total potential sites of binding, is defined by the equation 3 showed below, where both parameters K_u and U are included.

$$\beta = \frac{1}{2} \left\{ 1 + \frac{s-1}{\left[(1-s)^2 + \left(\frac{4s}{u} \right) \right]^{\frac{1}{2}}} \right\}, \quad \text{Eq. (3)}$$

With $s=K_u C_{eq}$, where C_{eq} is defined as the concentration of free dye molecules that remain in aqueous solution at equilibrium state. The parameter K_u and U are obtained from the equations 4 and 5 respectively:

$$C_{eq}(in\beta = 0.5) = 1/K_u, \quad \text{Eq. (4)}$$

$$\left[\frac{d\beta}{\log C_{eq}} \right]_{in\beta = 0.5} = U^{1/2} / 4, \quad \text{Eq. (5)}$$

Applying the equations (4) and (5) to the experimental isotherm, the K_u and U values can be obtained. By using these values as the starting ones to perform an optimization process, the theoretical parameters of K_u and U that fit with the experimental data for each system are achieved.

In Fig. 3 is represented the experimental data and theoretical isotherms obtained from equation (3) by the optimization

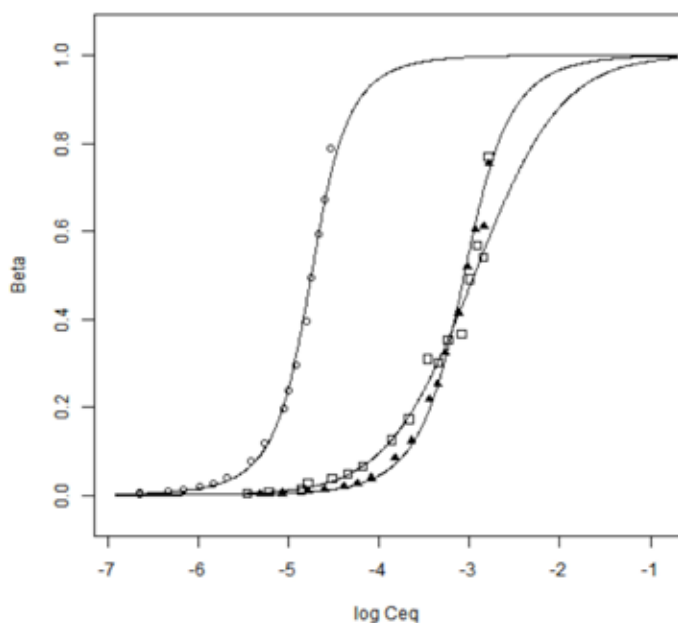


Fig. 3. Experimental data and theoretical Isotherms obtained from equation 3 for the following systems: Open squares (ALG-DB1 (Ca)), closed triangles (ALG-DR81 (Ca)) and open circles (ALG-DB22 (Ca)). The continuous line represents the theoretical Zimm-Bragg Isotherm for each system.

process and table 1 summarizes the K_u and U values encountered for all systems.

From Fig. 3 and table 1 it can be seen that the K_u and U values follow the order $DB22 > DR81 > DB1$. As mentioned before, the removal efficiency is a contribution of different factors that can be reflected in the K_u and U values. The molecular weight and size are considered as important parameters, because as bigger molecules are removed by ALG, then higher mass removal is achieved as compared to the same number of dye molecules with a smaller size and molecular weight. In this sense, within the molecules under study in this work, the largest and heaviest dye is DB22 ($MW=1083.97 \text{ g mol}^{-1}$); besides, the aggregation capacity and net charge of this molecule, also influence on the K_u and U values. Jáuregui Rincón et al. [48] reported the high aggregation capacity shown by this dye due to the presence of aromatic rings and different functional groups such as sulfonate, amino, azo, keto and hydrazone which results in a net charge (in this case positive for DB22) that can be attracted by a molecule with an opposite charge (ALG). In addi-

tion, these functional groups have the ability to interact through hydrogen bonds with ALG. All these contributions result in higher nucleation and cooperativity values ($K_u = 55,936 \text{ mol Kg}^{-1}$ and $U = 4.1981$) for the system ALG-DB22 (Ca).

It was found that K_u and U parameters were slightly higher in the ALG-DR81 (Ca) system than the values observed for the ALG-DB1 (Ca) product (ALG-DR81 (Ca): $K_u = 1,142.1 \text{ mol Kg}^{-1}$ and $U = 2.8409$; ALG-DB1(Ca): $K_u = 887.48 \text{ mol Kg}^{-1}$ and $U = 0.81076$). Although the size and molecular weight of DB1 are greater parameters than those corresponding to DR81, it is important to note that the removal isotherms were carried out at a $\text{pH} = 4$ and $\text{pH} = 12$ for DR81-ALG (Ca) system and ALG-DB1 (Ca) respectively and this caused a higher negative charge in the DB1 molecules (approximately -4) than the DR81 dye (-2) (see Fig. 2). As a result of this difference in negative charge, we propose that there is a minor repulsion between the DR81 and ALG molecules than that resulting from the DB1 and ALG. Notwithstanding the addition of calcium ions which decreases the repulsion between the ALG and the dyes, it seems to be that it is not enough to favor a higher nucleation and aggregation in the DB1 molecules. From the R^2 values, one can conclude that the Zimm-Bragg model describes in a good manner the experimental values in the three systems, despite the existence of moderate average relative error values due to experimental uncertainties arising from the high viscosity and slight turbidity of the solutions of each system.

Recently it was reported the K_u and U values of the ALG-DY54 (Ca) system (where DY54 denotes disperse yellow 54 dye) [48]. In our work, it was found that $K_u = 685 \text{ mol Kg}^{-1}$ and $U = 200$, which implicates a lower nucleation capacity than the dyes used in this work, this can be attributed to a lower molecular weight and size of the DY54 molecules. In addition the basic pH, at which removal experiments were performed ($\text{pH}=11.4$), favored the repulsion forces between both the ALG and DY54 molecules. Conversely the high value of the cooperativity constant exceeds the values obtained for DB22, DR81, and DB1 compounds, it was reported that a dye precipitation in conjunction with the formation of a calcium hydroxide powder increased dramatically the value of this parameter. Interestingly from these results we can deduce that the ALG biopolymer has the capacity to reduce the dye concentration in an aqueous phase but also has the ability to remove insoluble materials such as $\text{Ca}(\text{OH})_2$, cellulose, and kaolin as was reported recently [49-51].

Table 1. Parameters obtained when Zimm-Bragg model is applied to experimental data of ALG-Dye (Ca) systems.

System	ALG-DB1(Ca)	ALG-DR81(Ca)	ALG-DB22(Ca)
$K_u (\text{mol Kg}^{-1})$	887.48	1,142.1	55,936.0
U	0.8107	2.8409	4.1981
R^2	0.9499	0.9903	0.9941
ARE ^a	11.343	8.3392	14.2290

a: Average relative error.

Spectroscopic studies

UV-Visible studies

Analysis of the interaction of ALG polymer and direct dyes was followed by means of UV-Vis spectroscopy. In Fig. 4 it can be easily seen the influence of the pH value and the absorption spectrum of DB1 in aqueous solution. It is observed that in the pH range from 4 to 9, the absorption maximum of DB1 keeps constant; however, when pH is raised (pH = 12), a shift in the absorption maximum of the solution is observed (from $\lambda=618$ nm at pH=9 to $\lambda=584$ nm at pH=12). This change is due to a deprotonation of the dye molecule and it indicates that the hydrazone tautomer of DB1 predominates in aqueous solution, the spectrum obtained at pH=12 corresponds to the common anion as was found by Abbot *et al.* [52].

It was reported a natural tendency of different dyes to form H aggregates and it was also found that structural characteristics such as molecular weight, size, and the presence of different chemical groups favor this aggregation phenomenon [43, 53-57]. In order to investigate the aggregation capacity of DB1 at a pH=12, the spectra of this dye were acquired at different concentration values (1-500 ppm). Our results are represented in Fig. 5. From this figure we can see that the maximum absorption ($\lambda=584$ nm) does not change as a function of concentration. Abbot *et al.* [58] reported that DB1 has the ability to form dimers and trimers at ionic strength values similar to those used in this study. Besides, it was also reported that at pH 13, this dye forms the “common anion” and the planarity of this new chemical specie is similar to the hydrazone form of the DB1 at pH=7.0 [52]. From here, we can discuss that in our study, DB1 forms the common anion at pH=12 and that such anion does not have additional tendency to form aggregates when the concentration of the dye is increased. At this pH value the negative charge from this common anion promotes a considerable repulsion force between dye molecules, decreasing the aggregation capacity of this dye. However, these results do not exclude the existence of H aggregates before the pH was adjusted to a

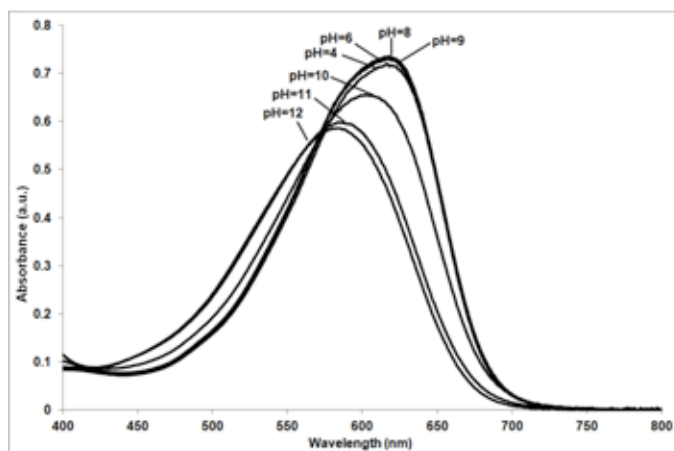


Fig. 4. UV-Visible absorption spectrum of DB1 in an aqueous solution at different pH values.

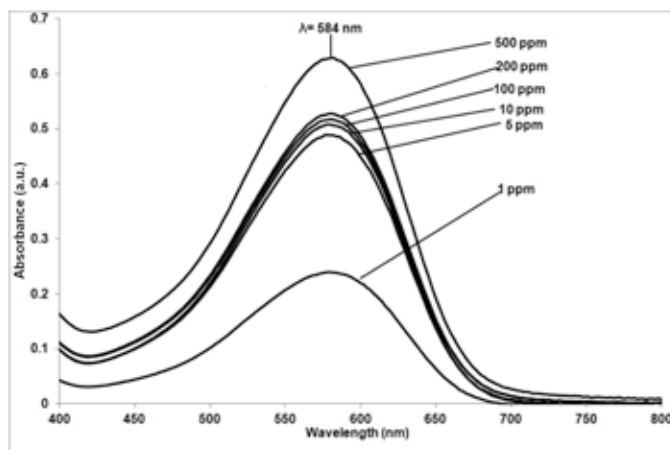


Fig. 5. UV-Visible absorption spectrum of DB1 in an aqueous solution at different concentration values (pH = 12.0).

pH=12 and it is possible that DB1 aggregates involving “common anions inside them” still remain at this pH value and the UV-Visible studies only reveal that these anionic forms of DB1 do not form additional aggregates when the concentration of DB1 is increased.

Additionally the absorption electronic spectra of DB1 solutions at different concentrations were obtained in the presence of ALG (1% w/v) in an aqueous environment at a pH=12 (Fig. 6). As can be seen in this figure, the presence of ALG causes a shift from 584 nm (in the absence of ALG) to 578 nm at concentration values of DB1 as low as 5 mgL^{-1} , these results indicate that ALG promotes the aggregation of DB1 molecules.

Pal and Mandal [36] found that potassium alginate induced a large blue shift ($\Delta\lambda = 125$ nm) when interacted with 1,9-dimethylmethyleneblue (DMB) in aqueous solution, such displacement of λ_{max} was explained as a strong tendency of DMB to form H aggregates in the presence of ALG in its potassium salt form. This research group attributes H aggregate formation of DMB to its planar structure which favors the π - π stacking between dye molecules. As was mentioned before the presence

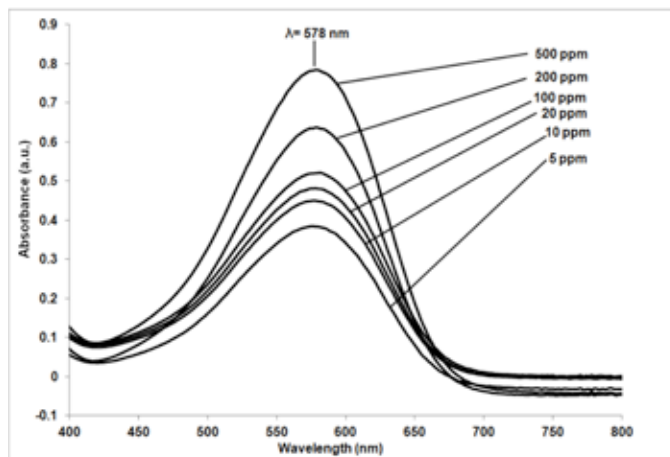


Fig. 6. UV-Visible absorption spectrum of DB1 at different concentration values in the presence of ALG (1 % w/v, pH = 12.0).

of aromatic rings in the dye molecules promotes H aggregation and it was even found that naphthyl rings were more effective in the π - π stacking between adjacent dye molecules than phenyl rings. Although the DB1 molecules are found as “common anionic forms”, they have a planar geometry and both phenyl and naphthyl rings attached to DB1 dye favor the subsequent formation of H aggregates. In addition to the hydrogen bonding interaction between the functional groups attached to DB1 (amino, sulfonate, methoxy and hydrazone) and hydroxyl and carboxyl groups from ALG, we propose the existence of Yoshida’s interactions [59] between the polysaccharide hydroxyl groups and the aromatic rings of DB1 molecules which results in the experimental blue shift of $\Delta\lambda=6$ nm. This displacement suggests a little rearrangement in the DB1 molecules, from an unstable form (soluble common anion) to a more stable chemical species, probably trimers of DB1 in their anionic form adsorbed to ALG surface but with a lesser overlapping than that observed in neutral conditions reported by Abbot *et al.* [58]. After the addition of calcium ion (as chloride salt) to ALG-DB1 complex in an aqueous medium, it was observed a new hypsochromic shift from 578 to 560 nm (Fig. 7). The addition of the calcium ion causes a reduction in the repulsion forces acting between ALG and DB1 molecules and promotes a conformational change in the ALG molecules when the calcium alginate is formed, providing a better overlapping in DB1 adjacent molecules “trapped” in the network. This change is manifested in the DB1 electronic absorption spectrum as a displacement from $\lambda_{\max}=578$ nm to $\lambda_{\max}=560$ nm. From these results we can infer that DB1 molecules have a low tendency to aggregate at basic conditions (pH=12) and the presence of the ALG and calcium ions in the ALG-DB1 (Ca) adduct reinforces the π - π stacking interactions in the DB1 molecules.

In the fig. 8 it is depicted the electronic absorption spectra of DR81 (1×10^{-5} M) at different pH values. From this figure, it can be seen that λ_{\max} is located at $\lambda_{\max}=512$ nm in the pH range from 2 to 8. When pH is increased, a shift in λ_{\max} (from 512 nm

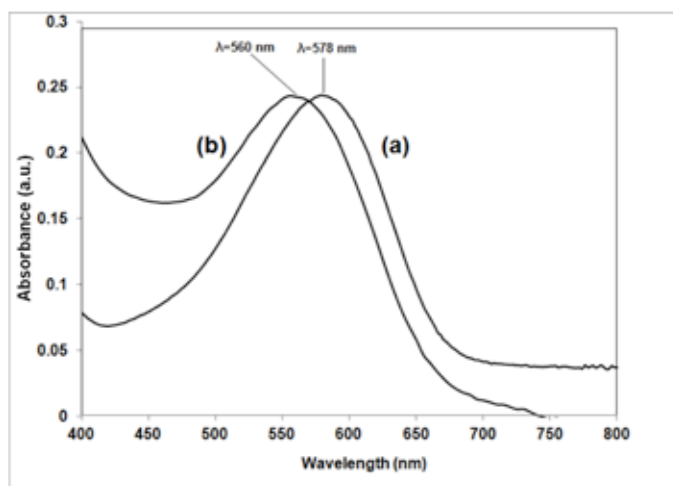


Fig. 7. UV-Visible absorption spectrum of: (a) ALG-DB1 (200 mg L^{-1} of dye concentration, pH = 12), and (b) ALG-DB1 (Ca) gel (same conditions and 5% w/v of calcium chloride solution was added).

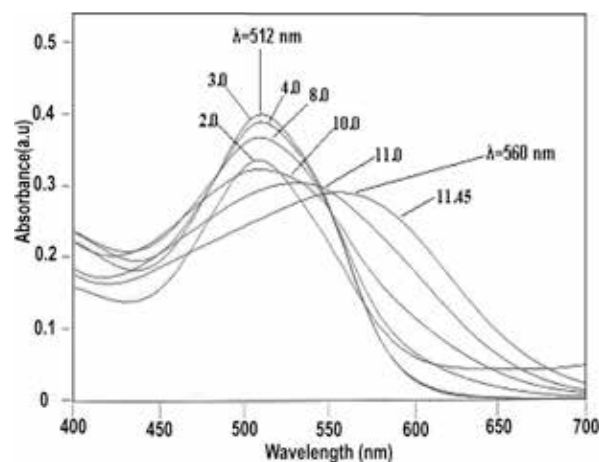


Fig. 8. UV-Visible absorption spectra of DR81 (1×10^{-5} M) at different pH values.

to 560 nm) is observed when the pH is located at pH = 11.4. This shift occurred as a consequence of the deprotonation of the hydrazone form of this dye suggesting the presence of this tautomeric form in aqueous solution.

Fig. 9 shows the spectra of DR81 at different concentration values (5 – 100 mg L^{-1} , pH = 4), a slight shift from 512 nm (5 mg L^{-1}) to 509 nm (100 mg L^{-1}) was observed when the concentration of this dye was increased. This small decrease in λ_{\max} was not as big as that observed in DB1, suggesting that at acidic conditions the aggregation ability of DR81 is lower than that observed with DB1. In addition, it was observed similar spectra of DR81 (data not shown), when solutions with the same dye content in the presence of ALG (1% w/v) were obtained, suggesting that ALG molecule does not have any influence in an additional formation of DR81 aggregates, due to repulsion forces among this biopolymer and DR81 and the presence of weaker interactions experimented by both the ALG and DR81 molecules.

On the other hand, it was found that the addition of calcium chloride to ALG-DR81 resulted in a gel formation and a blue shift from $\lambda_{\max}=509$ nm to $\lambda_{\max}=505$ nm was observed (data not

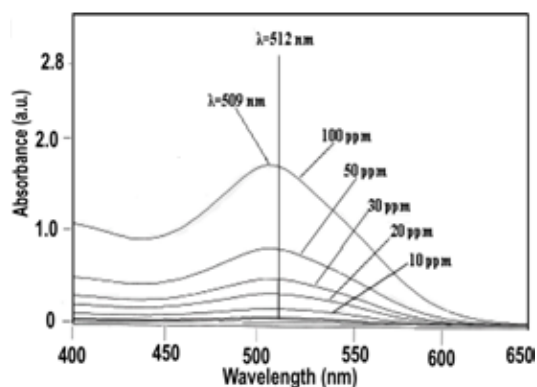


Fig. 9. UV-Visible absorption spectrum of DR81 in an aqueous solution at different concentration values (5 – 100 mg L^{-1} , pH = 4.0).

shown). We propose that in an analogous manner to ALG-DB1(-Ca) system, the formation of the gel induced by Ca^{+2} decreases the coulombic repulsions between DR81 and ALG molecules and it is allowed that the region MGMGM and poliMMMM act in a similar way as was proposed before with the DB1 dye, but in a lesser extent. This difference in “calcium induction shift” can be qualitatively measured by the $\Delta\lambda$, that can be defined as the difference in nanometers between λ_{max} found in the ALG-Dye system without Ca^{+2} and after the addition of this ion, which has a value of $\Delta\lambda=18$ nm in the ALG-DB1 (Ca) adduct and $\Delta\lambda=4$ nm for ALG-DR81 (Ca) system. The differences observed in the $\Delta\lambda$ values can be interpreted in terms of overlapping efficiency in both dyes, namely, in aqueous environment at basic pH values the DB1 molecules cannot form aggregates but adsorption to the ALG molecule surface induces a little overlapping between aromatic rings belonging to adjacent DB1 molecules, furthermore the formation of the ALG-DB1 (Ca) gel promotes this interaction (π - π stacking) and a newer hypsochromic shift is observed. On the other hand, we do believe that DR81 molecules are already stacked and in consequence they are forming H aggregates in an acidic aqueous solution, then an increase in the dye concentration only promotes a small aggregation.

From Fig. 2(c), it can be seen that the DB22 molecule has both, azo and hydrazone tautomeric forms and in consequence this dye can show the properties of these two tautomers. It was reported the electronic absorption spectra of DB22 at different pH values [48], and it was found that in the pH range of 2-8.3 the spectra were similar (with a $\lambda_{\text{max}}=467$ nm) suggesting that there was not a possible deprotonation step, but an increase in the basicity to pH = 10.4 caused a red shift to $\lambda_{\text{max}}=590$ nm which revealed the presence of “common anion” coming from the azo and hydrazone tautomers of DB22 dye. Based on UV-Visible data, it was discovered that DB22 forms H aggregates as a consequence of its great molecular weight and size, high number of naphthyl and phenyl rings, which affect the aggregation ability of this dye. In spite of the presence of sulfonate groups attached to the DB22 molecule, this compound has a higher ability to form H aggregates because these groups are oriented in such manner that the repulsion between them is minimal and the stability of DB22 aggregate is remained. UV-Visible spectra of DB22 showed that this biopolymer does not cause any influence in the DB22 spectrum in aqueous medium, this is in accordance with the experimental results observed with the DR81. The basic structural components of ALG molecules are the guluronate and mannuronate residues which are partially ionized and the DB22 molecule has a positive charge (approximately +2 at pH=4.0), the adsorption of DB22 aggregates did not cause any change in the electronic structure of the dye. These findings suggest that the DB22 “clusters” are highly stable and only can be disaggregated by deep changes in pH (basic pH values) due to formation of the common anion from both azo and hidrazone forms of this dye. We evaluated the effect of addition of calcium ion to the aqueous solution of ALG-DB22 complex (pH=4.0) by UV-Visible spectroscopy (data not shown); as observed for the previously discussed sys-

tems, a “blue shift” was observed in the absorption electronic spectrum of DB22 from $\lambda_{\text{max}}=467$ nm to $\lambda_{\text{max}}=452$ nm in the ALG-DB22 (Ca) adduct, resulting a shift $\Delta\lambda=15$ nm which suggests an additional rearrangement of the aggregates formed by DB22 molecules into the network produced in the gel. Braccini and Perez [41] have proposed that the gel formation of calcium alginate is carried out in two sequential steps: (1) the ALG dimer formation caused by calcium ions and (2) the subsequent interactions between these dimers. When the first step is performed, the dimers have diminished their negative net charge (the egg box model reviewed by Braccini and Perez includes four guluronate residues by each calcium ion, resulting in a net charge of -2 which is lower than -4 encountered in ALG without Ca^{+2}). In consequence, the repulsion among the sulfonate groups included in the DB22 molecules adsorbed into the ALG is decreased and the aggregation of the DB22 molecules on the surface of the dimers of ALG- Ca^{+2} is favored. Afterwards, the second step involves an unspecific interaction mainly mediated by the electrostatic interactions between the ALG dimers and as a consequence a stable network of calcium alginate is formed. In addition, we propose an “entrapment or capturing mechanism” of the DB22 “clusters” in the regions of poliMMMM and MGMGM sequences which have a weak affinity in the bonding of Ca(II), their flexibility allow to “trap” some aggregates of the DB22 into the gel as a consequence, a high removal efficiency value is obtained.

Infrared and Raman studies

In order to have a better knowledge of the systems that are formed within the ALG (Ca) gel, we analyze these adducts by

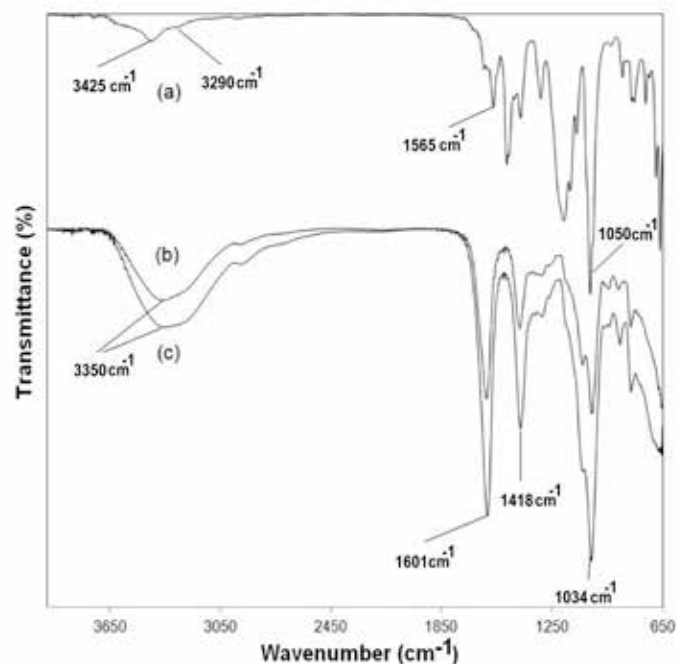


Fig. 10. FT-IR spectra of: (a) the DB1 dye, (b) calcium alginate ALG (Ca), and (c) the ALG-DB1 (Ca) adduct.

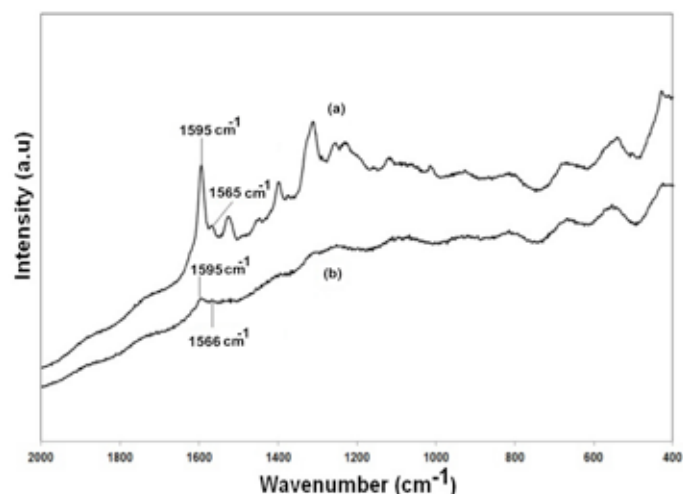


Fig. 11. Raman spectra of: (a) the DB1 dye, (b) and the ALG-DB1 (Ca) adduct.

Infrared (IR) and Raman spectroscopy. Infrared and Raman spectra of the DB1 dye, calcium alginate and ALG-DB1 (Ca) adduct, are depicted in figs. 10 and 11 respectively, and their data are contained in table 2.

The FT-IR spectrum of DB1 shows the typical symmetrical and asymmetrical vibrations of a primary amine located at 3425 cm^{-1} and 3290 cm^{-1} respectively, supporting the presence of the amino group in this dye (see also fig. 2). The signal located at 1565 cm^{-1} is assigned to $\nu(\text{C}=\text{N})$ from the hydrazone tautomer and the one at 1045 cm^{-1} refers to $\nu(\text{C}-\text{O})$ derived from methoxy groups attached to DB1 molecule. These bands may be theoretically found in the FT-IR spectrum of the ALG-DB1(Ca) spectrum (Fig. 10 c), however the presence of a broad band centered at 3350 cm^{-1} corresponding to hydrogen bonding “band” prevents to detect the typical amino vibration signals (see table 2). In the same manner, the peak corresponding to $\nu(\text{C}=\text{N})$ does not appear in the spectrum of ALG-DB1 (Ca) because this signal is

overlapped with the asymmetrical vibration peak $\nu_{\text{as}}(\text{COO})$ located at 1601 cm^{-1} in the ALG-DB1 (Ca) adduct, and as can be seen in the table 2, the $\nu(\text{C}-\text{O})$ stretching signal suggesting the presence of the methoxy groups from DB1 is immersed in the signal of the ALG (Ca) spectrum that possesses a similar peak due to the presence of the C-O bonds from the sugar residues in its structure (see fig. 10b). From the figs. 10b and 10c, it can be affirmed that these spectra are very similar and it was necessary to obtain the Raman spectra of these compounds to confirm the presence of DB1 in the ALG-DB1 (Ca) compound.

In fig. 11 the Raman spectra of DB1 (11a) and ALG-DB1 (Ca) adduct (11b) are depicted. Unfortunately the Raman spectrum of ALG (Ca) showed a high fluorescence and it was not possible to make a peak assignment from it. Despite the low amount of DB1 in the compound ALG-DB1 (Ca), it can be observed two peaks located at 1595 cm^{-1} and 1566 cm^{-1} which were assigned to the stretching $\nu(\text{C}=\text{C})$ from phenyl rings and $\nu(\text{C}=\text{N})$ from the hydrazone tautomer respectively in accordance with Abbot et al. [60,61], confirming the presence of this dye in the ALG-DB1 (Ca) adduct (see table 2).

Table 3 summarizes the principal FT-IR and Raman signals found in the spectra of the ALG (Ca), DR81, and ALG-DR81 (Ca) compounds. The FT-IR data suggest that the main peaks of the DR81 spectrum are immersed into the spectrum of the ALG-DR81 (Ca) adduct as a result to the similarity in vibration frequencies of their functional groups. For instance the hydrogen bonding region is overlapping the band corresponding to $\nu(\text{NH})$ from DR81 in its hydrazone form and the $\nu(\text{C}=\text{O})$ from the amido group of this dye was overlapped with the broad asymmetrical vibration of the carboxylate from the ALG (Ca) compound. On the other hand, Raman signals indicate the presence of DR81 in the ALG-DR81 (Ca) adduct without ambiguity. The peak located at 1595 cm^{-1} and those found in the range $1117\text{--}1135\text{ cm}^{-1}$ were assigned to $\nu(\text{C}=\text{C})$ from the phenyl rings and $\nu(-\text{SO}_3)$ from the sulfonate groups respectively. Moreover the presence of the peaks at 1564 cm^{-1} and 1444 cm^{-1} were attributed to the hydrazone and azo tautomers respectively in

Table 2. FT-IR and Raman data of ALG (Ca), DB1, and ALG-DB1 (Ca) compounds.

FT-IR Signals	ALG (Ca)	DB1	ALG-DB1 (Ca)	Observations
$\nu(\text{OH})$	3350 cm^{-1}		3350 cm^{-1}	Suggests the presence of hydrogen bonding.
$\nu_{\text{asym}}(\text{COO})$	1602 cm^{-1}		1601 cm^{-1}	
$\nu_{\text{sym}}(\text{COO})$	1420 cm^{-1}		1418 cm^{-1}	
$\nu(\text{C}-\text{O})$		1045 cm^{-1}	1034 cm^{-1}	Signal of DB1 is overlapped by ALG (Ca) signal.
$\nu(\text{C}=\text{N})$ from hydrazone tautomer		1565 cm^{-1}	It is not detectable	
$\nu_{\text{asym}}(\text{NH})$		3425 cm^{-1}	Not observable	Broad hydrogen bonding band prevents detection of this signal.
$\nu_{\text{sym}}(\text{NH})$		3290 cm^{-1}	Not observable	The same as above.
Raman Signal				
$\nu(\text{C}=\text{N})$ from hydrazone tautomer		1565 cm^{-1}	1566 cm^{-1}	This signal confirms the presence of DB1 in ALG-DB1 (Ca).
$\nu(\text{C}=\text{C})$ from phenyl rings		1595 cm^{-1}	1595 cm^{-1}	This signal confirms the presence of DB1 in ALG-DB1 (Ca).

Table 3. FT-IR and Raman data of ALG (Ca), DR81, and ALG-DR81 (Ca) compounds.

FT-IR Signals	ALG (Ca)	DR81	ALG-DR81 (Ca)	Observations
$\nu(\text{OH})$	3440 cm^{-1}	3444 cm^{-1}	3442 cm^{-1}	Hydrogen bonding still exists in ALG-DR81 (Ca).
$\nu_{\text{asym}}(\text{COO})$	1618 cm^{-1}		1620 cm^{-1}	A slightly change in vibration frequency.
$\nu_{\text{sym}}(\text{COO})$	1424 cm^{-1}		1424 cm^{-1}	Without changes
$\nu(\text{C}=\text{O})$		1602 cm^{-1}	1620 cm^{-1}	Signal of DR81 is overlapped by $\nu_{\text{as}}(\text{COO})$ signal from ALG (Ca) in ALG-DR81 (Ca).
Raman Signal				
$\nu(\text{C}=\text{C})$ from phenyl rings		1595 cm^{-1}	1595 cm^{-1}	This signal confirms the presence of DR81 in ALG-DR81 (Ca).
$\nu(\text{C}=\text{N})$ from hydrazone form		1563 cm^{-1}	1564 cm^{-1}	This signal suggests the presence of hydrazone form in ALG-DR81 (Ca) compound.
$\nu(\text{N}=\text{N})$ from azo tautomer		1443 cm^{-1}	1444 cm^{-1}	This signal suggests the presence of azo form in ALG-DR81 (Ca) compound.
$\nu(-\text{SO}_3^-)$		1133 and 1117 cm^{-1}	1135 and 1120 cm^{-1}	Both signals suggest and confirm the presence of DR81 in ALG-DR81 (Ca).

accordance with Silverstein and Milton [62], Armstrong *et al.* [63] and Biswas and Umaphathy [64]. These results indicate that DR81 is found in the ALG-DR81 (Ca) adduct in both tautomeric forms.

Table 4 shows the compilation of the principal FT-IR and Raman signals found in the spectra of the ALG (Ca), DB22, and ALG-DB22 (Ca) compounds. From the FT-IR data it can be seen that some signals were overlapped in a similar way that occurred in the ALG-DR81 (Ca) system, mainly the presence of

peaks from the ALG (Ca) compounds prevent the detection of the DB22 signals in the spectrum data of ALG-DB22 (Ca). The symmetrical and asymmetrical vibrations of the amino group attached to DB22 ($\nu_{\text{as}}(\text{NH})=3,380 \text{ cm}^{-1}$ and $\nu_{\text{s}}(\text{NH})=3260 \text{ cm}^{-1}$) are immersed in the broad hydrogen bonding band observed in the ALG-DB22 (Ca) system. In the same manner, the bands located at 1622 cm^{-1} and 1626 cm^{-1} assigned to $\nu(\text{C}=\text{O})$ from the hydrazone tautomer of the DB22 are overlapped with the asymmetrical vibration of the carboxylate group from ALG

Table 4. FT-IR and Raman data of ALG (Ca), DB22 and ALG-DB22 (Ca) compounds.

FT-IR Signals	ALG (Ca)	DB22	ALG-DB22 (Ca)	Observations
$\nu(\text{OH})$	3450 cm^{-1}	3444 cm^{-1}	3350 cm^{-1}	Hydrogen bonding still exists in ALG-DB22 (Ca).
$\nu_{\text{asym}}(\text{COO})$	1632 cm^{-1}		1621 cm^{-1}	A slight change in vibration frequency.
$\nu_{\text{sym}}(\text{COO})$	1439 cm^{-1}		1434 cm^{-1}	A slight change in vibration frequency.
$\nu(\text{C}-\text{O})$	1032 cm^{-1}		1037 cm^{-1}	A slight change in vibration frequency.
$\nu_{\text{asym}}(\text{NH})$		3380 cm^{-1}	Not observable	Broad hydrogen bonding band prevents the detection of this signal.
$\nu_{\text{sym}}(\text{NH})$		3260 cm^{-1}	Not observable	Same as above.
$\nu(\text{C}=\text{O})$		1626 and 1622 cm^{-1}	1621 cm^{-1}	Signal of DB22 is overlapped by $\nu_{\text{as}}(\text{COO})$ signal from ALG (Ca) in ALG-DB22 (Ca).
Raman Signal				
$\nu(\text{C}=\text{C})$ from phenyl rings		1608 cm^{-1}	1609 cm^{-1}	This signal confirms the presence of DB22 in ALG-DB22 (Ca).
$\nu(\text{C}=\text{N})$ from hydrazone tautomer		1554 cm^{-1}	1554 cm^{-1}	This signal suggests the presence of the hydrazone form in ALG-DB22 (Ca) compound.
$\nu(\text{N}=\text{N})$ from azo tautomer		1423 cm^{-1}	1420 cm^{-1}	This signal suggests the presence of the azo form in ALG-DB22 (Ca) compound.
$\nu(\text{C}=\text{C})$ from naphthyl rings		1240 cm^{-1}	1241 cm^{-1}	This signal confirms the presence of DB22 in ALG-DB22 (Ca).
$\nu(-\text{SO}_3^-)$		1166 cm^{-1}	1170 cm^{-1}	Same as above.

(Ca) in the ALG-DB22 (Ca) adduct, which made it difficult the assignment of these characteristic peaks of the DB22. Unlike the FT-IR data, the Raman signals show the presence of the DB22 in the ALG-DB22 (Ca) adduct. The (C=C) vibrations from the phenyl and naphthyl rings from DB22 were detected at 1609 cm^{-1} and 1241 cm^{-1} respectively and the presence of the sulfonate groups was observed as a peak found at 1170 cm^{-1} in the ALG-DB22 (Ca) compound. In the same way, the presence of two peaks located at 1554 cm^{-1} and 1420 cm^{-1} suggest that DB22 exist as hydrazone and azo tautomers in the ALG-DB22 (Ca) (see fig. 2).

On the other hand, we performed some solubility tests of all the ALG-Dye (Ca) products with ethanol and interestingly encountered that the amount of dye released to the ethanol phase followed this order: DB1~DR81>DB22. In this sense the ALG-DB1 (Ca) and ALG-DR81 (Ca) released similar amounts of the respective dye, in contrast only traces of DB22 was encountered when ethyl alcohol was added to the ALG-DB22 (Ca). These results in conjunction with the sorption and spectroscopic studies suggest that the affinity between these dyes and the alginate molecule is different and is dependent on the structural features such as molecular weight, size, number, and nature of functional groups attached to the dye molecules of these three dyes, suggesting the main interactions involved in their removal with the ALG biopolymer. In the case of DB1 the presence of two phenyl and two naphthyl rings promotes the formation of H aggregates which interact with ALG through hydrophobic interactions and the functional groups such as amino, sulfonate, methoxy and keto form hydrogen bonds with the hydroxyl and carboxyl groups of the ALG molecule (see fig. 2). In the case of DR81 dye, the molecular weight, size and number of aromatic rings are lower than that observed with DB1, but the interactions observed with ALG are similar than those found in the system ALG-DB1 (Ca) but in lesser extent. It is important to mention that both systems, the ALG-DB1 (Ca) and ALG-DR81 (Ca) exerted some degree of repulsion with ALG, as in consequence lower removal efficiencies were observed.

In the opposite case, the presence of different functional groups attached to DB22 molecule (amino, sulfonate, azo and hydrazone tautomers) resulted in a positive charge in the molecules of this dye under the experimental conditions, in despite of the low deprotonation of ALG molecules, DB22 molecules and aggregates were attracted to ALG molecules. In addition, the DB22 dye has the higher molecular weight of all three dyes and posses two naphthyl and four phenyl rings favoring the aggregation phenomenon, thus hydrophobic interaction between the aggregates formed and the ALG molecules can be expected. All these findings result in the higher removal efficiency observed for this system. Furthermore the entrapment ability of the ALG polymer when jellified as a calcium salt and the decrease effect in the repulsion between ALG and dyes enhanced the removal efficiency in all of the in all of the systems.

In conclusion the study of the removal of three direct dyes (direct blue 1, direct red 81, and direct black 22) with alginic acid showed considerable differences in the values of dye re-

moval efficiencies, finding the following order: ALG-DB22 (Ca)> ALG-DB1 (Ca) > ALG-DR81 (Ca). These findings suggest a relationship among physical chemical features of each dye and its removal efficiency. The main factors involved in this removal process were the aggregation capacity, the charge of each dye molecule resulting from the presence of different functional groups and the capacity of interact with ALG molecule through electrostatic interactions, hydrogen bonding and hydrophobic interactions. In addition, ALG polymer "traps" both aggregates and dye molecules when a gel is formed after the addition of calcium salt to polymer-dye adduct solution.

Moreover, more experimental work need to be done to find a deeper knowledge among the direct dye structure and its removal efficiency from aqueous solution using ALG, due to environmental importance of the direct dyes.

Experimental

Materials and Methods

Chemicals. The dyes DB1 and DR81 was purchased from Sigma-Aldrich and were used as received. DB22 was purchased as commercial mixture (Mardupol Co.). The purified DB22 dye was obtained by column chromatography (silica gel 60) using methanol as reported by Jáuregui-Rincón *et al.* [48]. Alginic acid (as sodium salt) was obtained from Sigma-Aldrich and was used without further purification. All solvents used were HPLC grade and were from J.T. Baker. Potassium bromide (spectrophotometric grade) and silica gel 60 (230-400 mesh) were supplied by Merck.

UV-Visible studies. Spectra of the dyes in an aqueous solution were obtained in a Thermospectronic spectrophotometer (model Genesis 2) at different conditions:

- Effect of pH: The different values of the dye solution were adjusted from acidic to basic values at a concentration of $1 \times 10^{-5}\text{ M}$.
- Effect of Dye Concentration in the absence and presence of the Biopolymer: The dye concentration was increased from $5 - 100\text{ mg L}^{-1}$ at fixed values of pH and ionic strength corresponding to each dye in an aqueous solution in the presence of 1% (w/v) and in the absence of ALG to study the effect of this biopolymer on the dye aggregation phenomenon.
- Effect of gelling agent: This procedure includes that described in b, but an additional step corresponding to the gel formation of ALG-Dye (Ca) product resulting from the addition of calcium chloride (5% w/v) to ALG-Dye solution.

In the cases of b and experiments, the pathlength of original cells was changed to adjust the absorbance to the detection limit of spectrophotometer, as a consequence, the response of the absorbance is not linear with the concentration values.

Optimization of dye removal conditions. The procedure used to determine the optimal conditions of dye removal was performed according to Jáuregui-Rincón *et al.* [48]. Briefly, each dye was dissolved in water and the concentration was adjusted to 250 ppm. An aliquot of this solution (40 mL) was added to a 50 mL solution of the biopolymer (1%). The pH of the samples was adjusted by using HCl and NaOH solutions. Three different pH values were evaluated: 4, 8, and 12. For each pH value, solutions with different ionic strength were prepared with the addition of sodium chloride crystals. The ionic strength values ($I = 0.1M, 0.5M$ and $0.9M$) were adjusted with a Corning Conductimeter checkmate II. The final volume of all samples was 100 mL and the final concentration of the dyes was 100 ppm (all samples were carried out in triplicate). Samples were cap sealed and shaken (200 rpm) for 24 h at 27 °C in dark conditions.

Calcium chloride (30 mL of 5% w/v solution) was added to each sample in order to induce gel formation. Once the gel was formed, distilled water was added to complete final volume of 200 mL. All samples were kept at room temperature (27 °C) for 24 h. The supernatant was centrifuged at 9000g for 20 min and free dye concentration was determined by UV-Vis spectroscopy.

Application of Zimm-Bragg model to experimental Isotherms

The parameters of the Zimm-Bragg model for each system were obtained from experimental data and through the R statistical software [65]. The reported parameters in this investigation are optimal in the sense they minimize the sum of relative errors given by the equation 6:

$$L(K_u, u) = \sum_{i=1}^n \left(\frac{\beta - \hat{\beta}_i}{\beta_i} \right)^2, \quad (6)$$

where β_i is the i -th observed value and $\hat{\beta}_i$ represents the i -th theoretical value in the Zimm-Bragg model.

The optimization process was conducted in the R software by defining the loss function $L(K_u, U)$ and by using the proposed values from experimental data as initial values.

IR and Raman studies. A sample powder of the pure dyes was used to obtain their corresponding Raman spectra. The analyzed powders (ALG-Dye (Ca) products) were isolated and purified as follows: The product was obtained from the last point of Removal isotherm (which contains the dye in the highest concentration in the gel). The product was separated by filtration, washed (five times with distilled water), dried (at 50 °C during 60 h) and grounded. A MicroRaman system (Renishaw 1000) was used for Raman analysis (2000–400 cm^{-1} range) and all samples were used without additional treatment.

For FT-IR the samples were analyzed (in a Perkin Elmer 1600 series) with potassium bromide pellets using transmission mode (systems including DR81 and DB22 dyes) and ATR mode

(with a Thermo scientific Nicolet iS10, using a Germanium window) for DB1 systems in the 4000–650 cm^{-1} .

Acknowledgements

We gratefully acknowledged the support for this project by Consejo Nacional de Ciencia y Tecnología, México (CONA-CyT, GRANT No.9502). The authors wish to thank Dr. Carlos Peña-Malacara (Instituto de Biotecnología de la Universidad Nacional Autónoma de México) for the molecular weight determination of the biopolymer used in this work.

References

- Teng, T.T.; Low, L.W. in: *Advances in Water Treatment and Pollution*. Sharma, S. K. and Sanghi, R. Eds. Springer, Dordrecht, **2012**, 65-93.
- McMullan, G.; Meehan, C.; Conneely, A.; Kirby, N. *Appl. Microbiol. Biotechnol.* **2001**, *56*, 81-87.
- Van der Zee, F.P.; Lettinga, G.; Field, J.A. *Chemosphere* **2001**, *44*, 1169-1176.
- Junnarkar, N.; Srinivas-Murthy, D.; Bhatt, N.S.; Madamwar, D. *World J. Microb. & Biot.* **2006**, *22*, 163-168.
- Mondal, P. K.; Chauhan, B. in: *Environmental Chemistry for a Sustainable World, Volume 2: Remediation of Air and Water Pollution*. Lichtfouse, E., Schwarzbauer, J. and Robert D. Ed; Springer, Dordrecht, **2012**, 255-275.
- Tosik, R.; Wiktorowski, S. *Sci. Eng.* **2001**, *23*, 295-302.
- Shu, H.Y.; Chang, M.C. *J. Hazard. Mater.* **2005**, *121*, 127-133.
- Salama, T.M.; Ali, I.O.; Hanafya, A.I.; Al-Meligy, W.M. *Mater. Chem. Phys.* **2009**, *113*, 159-165.
- Isaev A.B.; Aliev, Z.M.; Adamadzieva, N.A. *Russ. J. Appl. Chem.* **2012**, *85*, 765-769.
- Ong, S.A.; Min, O.M.; Ho, L.N.; Wong, Y.S. *Water Air Soil Pollut.* **2012**, *223*, 5483–5493.
- Genuino, H.C.; Hamal, D.B.; Fu, Y.J.; Suib, S.L. *J. Phys. Chem. C* **2012**, *116*, 14040-14051.
- Pereira, L.; Alves, M. In: *Environmental Protection Strategies for Sustainable Development, Strategies for Sustainability*. Malik, A.; Grohmann, E. Ed; Springer, Dordrecht, **2012**, 111-162.
- Ong, S.A.; Min, O.M.; Ho, L.N.; Wong, Y.S. *Environ. Sci. Pollut. Res.* **2013**, *20*, 3405–3413.
- Yang, Z.; Lu, X.; Gao, B.; Wang, Y.; Yue, Q.; Chen, T. *J. Mater. Sci.* **2014**, *49*, 4962–4972.
- Socha, A.; Sochocka, E.; Podsiadły, R. Sokolowska, J. *Color. Technol.* **2006**, *122*, 207–212.
- Aquino, J.M.; Rodrigo, M.A.; Rocha-Filho, R.C.; Sáez, C.; Cañizares, P. *Chem. Eng. J.* **2012**, *184*, 221-227.
- Horng, J.Y.; Huang, S.D. *Environ. Sci. Technol.* **1993**, *27*, 1169-1175.
- Yilmaz, E.; Memon, S.; Yilmaz, M. *J. Hazard. Mater.* **2010**, *174*, 592-597.
- Arslan, M.; Sayin, S.; Yilmaz, M. *Water Air Soil. Pollut.* **2013**, *224*, 1527-1536.
- Yilmaz-Ozmen, E.; Erdemir, S.; Yilmaz, M.; Bahadir, M. *Clean* **2007**, *35*, 612-616.
- Akceylan, E.; Bahadir, M.; Yilmaz, M. *J. Hazard. Mater.* **2009**, *162*, 960-966.

22. Kazakova, E.K.; Morozova, J.E.; Mironova, D.A.; Konovalov, A.I. *J. Incl. Phenom. Macrocycl. Chem.* **2012**, *74*, 467–472.
23. Kamboh, M.A.; Akoz, E.; Memon, S.; Yilmaz, M. *Water Air Soil Pollut.* **2013**, *224*, 1424–1433.
24. Senan, R.C.; Abraham, T.E. *Biodegradation* **2004**, *15*, 275–280.
25. Parikh, A.; Madamwar, D. *Biotechnol. Lett.* **2005**, *27*, 323–326.
26. Arun-Prasad, A.S.; Satyanarayana, V.S.V.; Bhaskara-Rao, K.V. *J. Hazard. Mater.* **2013**, *262*, 674–684.
27. Reyes, P.; Pickard, M.A.; Vazquez-Duhalt, R. *Biotechnol. Lett.* **1999**, *21*, 875–880.
28. Liu, W.; Chao, Y.; Yang, X.; Bao, H.; Qian, S. *J. Ind. Microbiol. Biotechnol.* **2004**, *31*, 127–132.
29. Ramsay, J.A.; Mok, M.H.W.; Luu, Y.S.; Savage, M. *Chemosphere* **2005**, *61*, 956–964.
30. Guerrero, E.; Aburto, P.; Terrés, E.; Villegas, O.; González, E.; Zayas, T.; Hernández, F.; Torres, E. *J. Porous Mater.* **2013**, *20*, 387–396.
31. Arami, M.; Limaee, N.Y.; Mahmoodia, N.M.; Tabrizi, N.S.J. *Hazard. Mater. B* **2006**, *135*, 171–179.
32. Aravindhan, R.; Fathima, N. N.; Rao, J. R.; Nair, B. U. *Colloids Surf. A Physicochem. Eng. Asp.* **2007**, *299*, 232–238.
33. Ferrero, F.; Periolatto, M. *Clean Techn. Environ. Policy* **2012**, *14*, 487–494.
34. Sanghi, R.; Bhattacharya, B. *Color. Technol.* **2002**, *118*, 256–269.
35. Annadurai, G. *Bioprocess Biosyst. Eng.* **2000**, *23*, 451–455.
36. Pal, M.K.; Mandal, N. *Biopolymers* **1990**, *29*, 1541–1548.
37. Blackburn, R.S. *Environ. Sci. Technol.* **2004**, *38*, 4905–4909.
38. Nasr, M.F.; El-Ola, S.M.A.; Ramadan, A.; Hashem, A.I. *Polym-Plast. Technol. Eng.* **2006**, *45*, 335–340.
39. Lozano-Alvarez, J. A.; Jáuregui-Rincón, J.; Mendoza-Díaz, G.; Rodríguez-Vázquez, R.; Frausto-Reyes, C. *J. Mex. Chem. Soc.* **2009**, *53*, 59–70.
40. Singh, V.; Malviya, T.; Sanghi, R. In: *Advances in Water Treatment and Pollution Prevention*. Sharma, S. K.; Sanghi, R. Eds. Springer, Dordrecht, **2012**, 377–403.
41. Braccini, I.; Perez, S. *Biomacromolecules* **2001**, *2*, 1089–1096.
42. Donati, I.; Holtan, S.; Mørch, Y.A.; Borgogna, M.; Dentini, M.; Skjåk-Bræk, M. *Biomacromolecules* **2005**, *6*, 1031–1040.
43. Oakes, J.; Dixon, S. *Rev. Prog. Color.* **2004**, *34*, 110–128.
44. Maurstad, G.; Danielsen, S.; Stokke, B.T. *J. Phys. Chem. B* **2003**, *107*, 8172–8180.
45. Zimm, B.H.; Bragg, J.K. *J. Chem. Phys.* **1959**, *3*, 526–535.
46. Schwarz, G.; Balthasar, W. *Eur. J. Biochem.* **1970**, *12*, 461–467.
47. Satake, I.; Yang, J.T. *Biopolymers* **1976**, *15*, 2263–2275.
48. Jáuregui-Rincón, J.; Lozano-Alvarez, J.A.; Medina-Ramírez, I. In: Elnashar, M. Ed. *Biotechnology of Biopolymers*, Intech, Croatia, **2011**, 165–190.
49. Lindstrom, T.; Christer, S. *J. Colloid. Interf. Sci.* **1976**, *55*, 69–72.
50. Singh, R.P.; Tripathy, T.; Karmakar, G.P.; Rath, S.K.; Karmakar, N.C.; Pandey, S.R.; Kannan, K.; Jain, S.K.; Lan, N.T. *Curr. Sci.* **2000**, *78*, 798–803.
51. Retes-Pruneda, J.L.; Davila-Vazquez, G.; Medina-Ramírez, I.; Chavez-Vela, N.A.; Lozano-Alvarez, J.A.; Alatrístre-Mondragon, F.; Jauregui-Rincon, J. *Environ. Technol.* **2014**, *35*, 1773–1784.
52. Abbott, L.C.; Batchelor, S.N.; Jansen, L.; Oakes, J.; Lindsay-Smith J.R., Moore, J.N. *New J. Chem.* **2004**, *28*, 815–821.
53. Monahan, A.R.; Blossey, D.F. *J. Phys. Chem.* **1971**, *75*, 1227–1233.
54. Reeves, R.L.; Maggio, M.S.; Harkaway, S.A.A. *J. Phys. Chem.* **1979**, *83*, 2359–2368.
55. Hamada, K.; Mitshuishi, M.; Ohira, M.; Miyazaki, K. *J. Phys. Chem.* **1993**, *97*, 4926–4929.
56. Tiddy, G.J.T.; Mateer, D.L.; Ormedrod, A.P.; Harrison, W.J.; Edwards, D.J. *Langmuir* **1995**, *11*, 390–393.
57. Ferus-Camelo, M.; Greaves, A.J. *Color. Technol.* **2002**, *118*, 15–19.
58. Abbot, L.C.; Batchelor, S.N.; Oakes, J.; Lindsay-Smith, J.R., Moore, J.N. *J. Phys. Chem. B* **2004**, *108*, 13726–13735.
59. Yoshida, Z.I.; Osawa, E.; Oda, R. *J. Phys. Chem.* **1964**, *68*, 2895–2898.
60. Abbott, L.C.; Batchelor, S.N.; Oakes, J.; Lindsay-Smith, J.R.; Moore, J.N. *J. Phys. Chem. A* **2004**, *108*, 10208–10218.
61. Abbott, L.A.; Batchelor, S.N.; Oakes, J.; Gilbert, B.C.; Whitwood, A.C.; Lindsay-Smith, J.R.; Moore, J.N. *J. Phys. Chem. A* **2005**, *109*, 2894–2905.
62. Silverstein, R.; Milton, R. *Spectrometric Identification of Organic Compounds*. Fifth ed. John Wiley & sons, USA, 1991, 127.
63. Armstrong, D.R.; Clarkson, J.; Smith, W.E. *J. Phys. Chem.* **1995**, *99*, 17825–17831.
64. Biswas, N.; Umapathy, S. *J. Phys. Chem. A* **2000**, *104*, 2734–2745.
65. Core, R. T. R: A language and Environment for statistical computing. R Foundation for Statistical Computing, Vienna, Austria, **2013**, <http://www.R-project.org>.

Editorial Policy

The *Journal of the Mexican Chemical Society (J. Mex. Chem. Soc.)*, former *Revista de la Sociedad Química de México (Rev. Soc. Quím. Méx.)*, since 1957 is devoted to facilitate the advancement of our understanding of chemistry. It will publish original contributions of research in all areas of the theory and practice of chemistry in its broadest context, as well as critical reviews in areas where the author has significant scientific contributions. The language of submission and publication is English. Papers are submitted on the understanding that the subject matter has not been previously published or submitted for publication elsewhere. Editors, referees and authors have to follow and maintain the ethical standards widely accepted in chemical research (see for example: the ACS guidelines of the RSC guidelines). Authors must accept full responsibility for the accuracy, content and selection of the data presented. All papers are sent to referees who recommend the Editor on the acceptance or rejection of the script. Referee's names are not disclosed, but their comments are forwarded to the authors. Authors submitting a manuscript do so on the understanding that if it is accepted for publication, copyright of their article is transferred to the *Sociedad Química de México*.

General Guidelines for Manuscript Preparation

Authors are encouraged to send contributions via *on-line submission* and should register at www.jmcs.org.mx to obtain an access login and password. Once logged into the electronic system, the authors can easily follow the instructions and they are asked to submit the proper files (ms word and pdf). The authors may track their manuscript through the system. The authors also may send contributions in electronic form as MS Word file to editor.jmcs@gmail.com. On submitting their manuscripts authors are encouraged to supply a cover letter suggesting the names and e-mail addresses of at least four potential referees. The cover letter may include the name of a member of the Editorial Board or the Advisory Editorial Board for manuscript assignment. All pages of the manuscript should be consecutively numbered. Accepted manuscripts should be resubmitted as MS Word file and separate files of the artwork in .TIFF, .JPG or PostScripts formats. Black and white photographs must be scanned with a resolution of no less than 600 dpi. It is advisable to provide illustrations (figures, schemes, charts, tables, graphics) in the actual size at which they should appear in the printed version and should be designed to fit in one- or two-columns format. The journal will publish a graphical abstract which includes the title and the author list, and illustrates the content of the paper in a pictorial form. The graphical abstract is limited to 9.0 cm wide and 4.5 cm tall, and authors may examine recent issues for appropriate examples. Page 1 should contain the article title (brief and informative), author(s) name(s) (first names and surnames, do not use initials for names, the corresponding author(s) should be indicated with an asterisk, use superscripts to indicate different addresses), complete affiliation(s) (the corresponding author's mailing address, phone number, fax number or e-mail address should be included). Page 2 should contain an abstract (both in English and Spanish, about 80 words) and five to eight key words in both languages.

A suggested organization of an article is: *Introduction, Results and Discussion, Experimental, Acknowledgements and References*. All the sections of the paper must be presented with the utmost conciseness and clarity. The measurements and data should be given in the International Units System (SI), and abbreviations should be used consistently through the text. Avoid reiteration of information. The discussion should present only the new results and relate them to existing knowledge in the field, and a paragraph summarizing the principal conclusion of the article is recommended. Complete X-ray data should be deposited at the Cambridge Crystallographic Data Centre or to Fachinformationszentrum Karlsruhe (FIZ), which will provide codes for each data set, which are then cited in a reference in the manuscript. If a representation of the crystal structure is to be included, it should be accompanied by pertinent crystallographic data, method of collection, and methods of structure

solution and refinement. The experimental section must contain all the information necessary for reproducibility. Convincing evidence to confirm the identity of a compound should be provided. All new compounds should be fully characterized with relevant and detailed spectroscopic data. For physical and spectroscopic data, the following general style must be used:

(3S)-7-Hydroxy-2',3',4',5',8-pentamethoxyisoflavan (1). Amorphous powder: mp 125-126°C; $[\alpha]_D + 3.12$ (c 0.320, MeOH); UV (MeOH) λ_{max} (log ϵ) 218 (3.91); 284 (2.89) nm; CD (c 0.0136, MeOH): $[\theta]_{210} -2.699$, $[\theta]_{226} 0.4130$, $[\theta]_{256} -0.8567$, $[\theta]_{265.5} -0.6865$; IR (CHCl₃) ν_{max} 3530, 2939, 2840, 1603, 1494, 1193, 1040 cm⁻¹; ¹H NMR (CDCl₃, 500 MHz) δ 6.72 (1H, dd, $J_{5,6} = 8.5$, $J_{4\alpha,5} = 1.0$ Hz, H-5), 6.53 (1H, dd, $J_{5,6} = 8.5$ Hz, H-6), 6.40 (1H, s, H-6'), 5.80 (1H, brs, OH), 4.39 (1H, ddd, $J_{2\beta,2\alpha} = 10.5$, $J_{2\beta,3\beta} = 3.5$, $J_{2\beta,4\beta} = 1.0$ Hz, H-2 β), 4.05 (1H, dd, $J_{2\alpha,3\beta} = J_{2\alpha,4\beta} = 10.5$ Hz, H-2 α), 3.95 (3H, s, CH₃O-C-3'), 3.92 (3H, s, CH₃O-C-8), 3.89 (3H, s, CH₃O-C-4'), 3.83 (3H, s, CH₃O-C-2'), 3.79 (3H, s, CH₃O-C-5'), 3.61 (1H, dddd, $J = 10.5$, 3.5, 5.5, 10.5 Hz, H-3), 2.96 (1H, ddd, $J_{4\alpha,4\beta} = 16.0$, $J_{4\alpha,3\beta} = 10.5$, $J_{4\alpha,5} = 1.0$ Hz, H-4 α), 2.90 (1H, ddd, $J = 16.0$, $J_{3\beta,4\beta} = 5.5$, $J_{2\beta,4\beta} = 1.0$ Hz, H-4 β); ¹³C NMR (CDCl₃, 125 MHz, assignments by APT and HMQC) δ 149.67 (C-5'), 147.60 (C-7), 147.15 (C-3'), 147.12 (C-8a), 145.50 (C-2'), 141.95 (C-4'), 134.80 (C-8), 128.90 (C-1'), 124.20 (C-5), 115.00 (C-4a), 107.10 (C-6), 70.28 (C-2), 61.89 (OCH₃-C-4'), 61.51 (OCH₃-C-2'), 61.00 (OCH₃-C-3'), 60.90 (OCH₃-C-8), 56.25 (OCH₃-C-5'), 31.84 (C-3), 31.32 (C-4); EIMS *m/z* (rel. int.): 376 [M]⁺ (73), 224 (100), 209 (42), 152 (16), 151 (38), 121 (14). *Anal.* C 63.65%, H 6.68%, calcd for C₂₀H₂₄O₇, C 63.82%, H 6.43%.

For computational results, pertinent data such as force field parameters and equations should be included, to allow readers to repeat and reproduce the calculations. References to the literature should be noted in the text in order of appearance with numerals between brackets and should coincide with entries in the References section. It is not recommended to include bibliography of difficult access (theses, abstracts of meetings, unpublished material, technical reports, work in press, etc.) as references. The style and punctuation should rigorously conform to the format in the following examples:

1. Kingsbury, J. S.; Corey, E. J. *J. Am. Chem. Soc.* **2005**, *127*, 13813-13815
2. Vanden Berghe, D. A.; Vlietinck, A. J., in: *Methods in Plant Biochemistry*, Vol. 6, Hostettmann, K., Ed., Academic Press, London, **1991**, 47-70.
3. Lehn, J.-M. *Supramolecular Chemistry*. VCH, Ed. Weinheim, **1995**.
4. Kadin, S.B. *US patent* 4,730,004 **1988**. (CA 110, P23729y)
5. <http://www.jmcs.org.mx>, accessed in January, 2005
6. Sheldrick, G. M. *SHELXL-93. Program for Crystal Structure Refinement*. University of Göttingen, Germany. 1993.

Journal abbreviations, technical terms and nomenclature should be those used by *Chemical Abstracts*. Figures and tables must not be included in the body of the text. Tables and figures with their respective legends, each on an individual page, should be added after references.

The electronic system will allow the correction of the galley proofs *on line*. For the manuscripts submitted directly to editor.jmcs@gmail.com, the galley proof of the accepted papers in PDF format are sent to the corresponding author. Corrected galley proofs should be returned within 48 h by fax, email or courier mail. If edition errors are published, a correction should be sent by the author to the Editor for publication in the following issue.

The author will cover to *Sociedad Química de México* the cost per page corresponding to the technical edition and printing, and two issues of the Journal (ca. \$ 200.00 MN per page). The author may request by an explanatory letter the exemption of payment. The *Sociedad Química de México* is a non profit association and the acceptance of the articles for publication in the Journal is solely based on academic grounds.



Sociedad Química de México, A.C.

Barranca del Muerto 26, Col. Crédito Constructor, Del. Benito Juárez, C.P. 03940, Mexico City
Phone: +5255 56626837; +5255 56626823
Contact: soquimex@sqm.org.mx
www.sqm.org.mx